Technische Universität München

Wissenschaftszentrum Weihenstephan für Ernährung, Landnutzung und Umwelt

The role of B cells and the gut microbiome in the development of Non-Alcoholic Steatohepatitis (NASH)

Eleni Kotsiliti

Vollstänger Abdruck der von der Fakultät Wissenschaftszentrum Weihenstephan für Ernährung, Landnutzung und Umwelt der Technische Universität München zur des akademischen Grades eines

Doktors der Naturwissenschaften (Dr. rer. nat.)

genehmigten Dissertation.

Vorsitzender: Prof. Dr. Martin Klingenspor

Prüfer der Dissertation: **1.** Prof. Dr. Dirk Haller

2. Prof. Dr. Mathias Heikenwälder

3. Prof. Dr. Samuel Huber

Die Dissertation wurde am 23.05.2019 bei der Technische Universität München eingereicht und durch die Fakultät Wissenschaftszentrum Weihenstephan für Ernährung, Landnutzung und Umwelt am 17.10.2019 angenommen

Table of contents

1. Summary

Obesity leads to metabolic syndrome, type 2 diabetes, steatosis and steatohepatitis, making hepatocellular carcinoma (HCC) the fastest growing cancer in the U.S.A. and Europe. In a long-term choline-deficient high-fat diet (CD-HFD) mouse model we demonstrated that dietary induced CD8+ T and NKT cells interact with hepatocytes to induce non-alcoholic fatty liver disease (NAFLD), with its severe pathology non-alcoholic steatohepatits (NASH) and eventually NASH-to-HCC transition. Recently, B cells are considered to be important mediators and players in innate and adaptive immune responses associated with metabolic diseases. From our published studies it has become apparent that the lymphocytes are crucial for NASH and NASH-induced HCC, however the exact role of B cells remains unclear.

Long term CD-HFD diet was given to mice lacking mature B cells ($JH^{-/-}$) and mice lacking mature B cells apart from IgA^{+} B cells in the lamina propria (µMT). Feeding experiments were performed in mice with a differential secretion of immunoglobulins ($AID^{-/-}$, AIDg23s and IgMi). To deplete $CD20^{+}$ B cells, wild type (C57BL/6J) and µMT CD-HFD were treated with anti-mouse CD20mAb (clone 5D2, Genentech) intraperitoneally.

CD-HFD $JH^{-/-}$ mice showed absence of steatosis, liver inflammation/damage and fibrosis. Contrary, the CD-HFD µMT were steatotic, inflamed but not fibrotic. The αCD20 treated mice, wild type and µMT CD-HFD, showed absence of steatosis, liver inflammation and fibrosis. Finally, the CD-HFD mice lacking immunoglobulins demonstrated a steatotic and inflamed hepatic profile with the $AID^{-/-}$ to lack fibrosis, contrary to AIDg23s. IgMi CD-HFD mice were obese without developing NASH or fibrotic phenotype.

It has been shown that the microbiota are playing a role in inducing obesity, systemic inflammation and metabolic disease. The human intestinal lumen is occupied by a rich diversity of gut bacteria that under healthy conditions, along with the gut IgA^{+} B cells, maintain the gut homeostasis.

Long-term CD-HFD was given to mice and they were administrated a wide spectrum antibiotic cocktail that wiped out 99% of the gut bacteria. The antibiotics were given either prophylactically, during the whole feeding period, or therapeutically, the last two feeding months. Both experimental groups showed abrogation of NASH and

hepatic fibrosis while the mice were obese. Long-term CD-HFD was given also to germ free mice. The mice were obese and did develop NASH and hepatic fibrosis.

Our data illuminate new mechanistic aspects of the role of B cells in NASH development and fibrosis and also show that modulation of the microbiome is a key factor to NASH development but sterile inflammations suffices to induce NASH.

2. Zusammenfassung

Fettleibigkeit führt zu metabolischem Syndrom, Typ-2-Diabetes, Steatose und Steatohepatitis, was zur Folge hat, dass das hepatozelluläre Karzinom (HCC) zur am schnellsten wachsenden Krebsart in den USA und Europa geworden ist. In einem Langzeit-Mausmodell mit Cholin-defizienter Hochfettdiät (CD-HFD) konnten wir zeigen, dass durch die Nahrung induzierte CD8+ T- und NKT-Zellen mit Hepatozyten interagieren um eine nichtalkoholische Fettlebererkrankung (NAFLD) zu induzieren, den schwerwiegenderen Phänotyp der alkoholischen Steatohepatits (NASH) und schließlich den Übergang von NASH zu HCC. Seit kurzem gelten B-Zellen als wichtige Vermittler und Akteure bei angeborenen und adaptiven Immunreaktionen im Zusammenhang mit Stoffwechselerkrankungen. Aus unseren veröffentlichten Studien geht hervor, dass die Lymphozyten für NASH und NASH-induzierte HCC von entscheidender Bedeutung sind, die genaue Rolle von B-Zellen bleibt jedoch unklar.

Langzeit-CD-HFD-Diät wurde Mäusen verabreicht, denen reife B-Zellen ($JH^{-/-}$) fehlten und Mäusen, denen reife B-Zellen außer IgA+ B-Zellen in der Lamina Propria (µMT) fehlten. Fütterungsversuche wurden auch an Mäusen mit unterschiedlicher Sekretion von Immunglobulinen ($AID^{-/-}$, AIDg23s and IgMi) durchgeführt. Um die CD20+ B-Zellen zu depletieren, wurden Wildtyp (C57BL/6J) und µMT CD-HFD Mäuse intraperitoneal mit Anti-Maus CD20mAb (Klon 5D2, Genentech) behandelt.

CD-HFD $JH^{-/-}$-Mäuse zeigten weder Steatose, noch Leberentzündung/-schädigung oder Fibrose. Im Gegensatz dazu waren die CD-HFD µMT Mäuse steatotisch und entzündet aber nicht fibrotisch. Die mit αCD20 behandelten Mäuse, Wildtyp und µMT CD-HFD Mäuse zeigten weder Steatose, noch Leberentzündung oder Fibrose. Schließlich zeigten die CD-HFD-Mausmodelle mit fehlenden Immunglobulinen ein steatotisches und entzündetes Leberprofil, wobei die $AID^{-/-}$ Mäuse, im Gegensatz zu den AIDg23s Mäusen, keine Fibrose zeigten. IgMi CD-HFD-Mäuse waren fettleibig, ohne NASH oder einen fibrotischen Phänotyp zu entwickeln.

Es wurde bereits gezeigt, dass die Darmflora eine Rolle bei der Entstehung von Fettleibigkeit, systemischen Entzündungen und Stoffwechselkrankheiten spielt. Das menschliche Darmlumen ist von einer reichen Vielfalt an Darmbakterien besetzt, die zusammen mit den IgA+ B-Zellen des Darms die Darmhomöostase aufrechterhalten.

Mäusen denen eine Langzeit-CD-HFD verabreicht wurde, bekamen ein Breitspektrumantibiotika-Cocktail verabreicht, der 99% der Darmbakterien auslöschte. Die Antibiotika wurden entweder prophylaktisch während der gesamten Fütterungsperiode oder therapeutisch in den letzten beiden Fütterungsmonaten gegeben. Beide Versuchsgruppen zeigten eine Aufhebung von NASH und Leberfibrose, obwohl die Mäuse fettleibig waren. Langzeit-CD-HFD wurde auch strikt keimfreien Mäusen verabreicht. Diese Mäuse waren fettleibig und entwickelten NASH und Leberfibrose.

Unsere Daten heben neue mechanistische Aspekte der Rolle von B-Zellen bei der NASH-Entwicklung und Fibrose hervor und zeigen auch, dass die Modulation der Darmflora ein Schlüsselfaktor für die NASH-Entwicklung ist, aber sterile Entzündungen ausreichen, um NASH zu induzieren.

3. Abbreviation list

T2DM	type 2 diabetes mellitus
PAI- 1	plasminogen activator inhibitor 1
CRP	C-reactive protein
SAA	serum amyloid A
TNF	tumour necrosis factor
IL	interleukin
MΦ	macrophages
JNK	c-JUN N-terminal kinase
NF-κB	nuclear factor-kappa B
NLRP3	NLR family pyrin domain-containing 3
MHO	metabolically healthy obesity
CSCs	cancer stem cells
NAFLD	non-alcoholic fatty liver disease
BW	body weight
NK	natural killer
NASH	non-alcoholic steatohepatitis
HCC	hepatocellular carcinoma
TG	triglyceride
PNPLA3	patatin-like phospholipase domain-containing 3
NAS	NAFLD Activity Score
CD-HFD	choline-deficient high fat diet
ND	normal chow diet
NKT	natural killer T
LTβR	lymphotoxin-β receptor
MYC	avian myelocytomatosis viral oncogene homolog
MCD	methionine choline-deficient diet
MDSC	myeloid-derived suppressor cell
NKp3	natural killer cell p30-related protein
DAMP	damage-associated molecular patter
TLR	toll-like receptor
PAM	pathogen-associated molecular pattern
LPS	lipopolysaccharide
KC	Kupffer cell
HSC	hepatic stellate cell
MAPK	mitogen-activated protein kinase
ERK1	extracellular signal–regulated kinase 1
IRF3	interferon regulatory factor 3
TGF-β	transforming growth factor-β
PDGF	platelet-derived growth factor
CDAA	choline-deficient amino-acid-defined
Ig	immunoglobulin
MDA	malondialdehyde
Ab	antibody
PDL1	programmed death ligand 1
ALT	alanine transaminase
PUFA	polyunsaturated fatty acid
TZD	thiazolidinedione
PPAR	peroxisomal proliferator activated receptor
RAAS	renin-angiotensin-aldosterone system
ACE	angiotensin-converting enzyme
HFD	high fat diet
RELMβ	resistin-like molecule β
CFU	colony forming units
FMT	faecal microbiota transplant
FAO	Food and Agriculture Organization of the United Nations
WHO	World Health Organization
GLP-1	glucagon-like peptide-1
FDA	Food and Drug Administration
BM	bone marrow
PB	plasmablast
PC	plasma cell
ASC	antibody-secreting cell

MZ	marginal zone
TI	T-cell independent
TD	T-cell dependent
Ag	antigen
GC	germinal centre
APC	antigen presenting cell
DCs	dendritic cells
CSR	class-switch recombination
SHM	somatic hypermutation
L	light
H	heavy
V	variable
C	constant
J	joining
Dh	diversity
RSS	recombination signal sequence
RAG	recombination activation gene
BCR	B cell receptor
AID	activation-induced cytidine
GALT	gut-associated lymphoid tissue
ILCs	innate lymphoid cells
APRIL	a proliferation-inducing ligand
BAFF	B cell-activating factor
FAE	follicle-associated epithelium
MHCII	major histocompatibility complex class II
ECM	extracellular matrix
HSC	hepatic stellate cell
ALD	alcoholic liver disease
MyD88	myeloid differentiation factor 88
SLO	secondary lymphoid organ
MALT	mucosa-associated lymphoid tissue
mIg	membrane-bound immunoglobulin
ITAM	immunoreceptor tyrosine activation motif
ER	endoplasmic reticulum
LP	lamina propria
SI	small intestine
FACS	flow cytometry
IHC	immunohistochemistry
(NAS)	Non-Alcoholic Fatty Liver Disease activity score

4. Introduction

4. A. Obesity

4. A.1. Epidemiology

The pandemic of obesity [1,2] poses a grave threat to people's health in a global scale **(fig. 1)**. Excess weight gain occurs due to energy imbalance and during 2011-2014 approximately 35% of adults, having a body mass index (BMI) ≥30 kg/m^2, and 17% of children and adolescents were affected by obesity in the U.S.A [3]. Obesity is associated with several major co-morbidities and therefore the overall disease burden is increasing. Since 1980, the global age-standardized prevalence of obesity has nearly doubled from 6.4 % in 1980 to 12.0 % in 2008 with half the increase occurring between 2000 and 2008 [4,5]. The causes of obesity, biological and social, may vary considerably by sex or gender [6-10]. In the latter half of the 20th century in developed countries, there has been a shift towards sedentary occupations for both women and men combined with infrequent or reduced physical activity during free time [10]. This trend has been observed in the U.S.A and Europe alike [11,12]. In developed countries intake of (animal-source) dairy foods and high-energy alcoholic beverages may affect gender disparities in obesity [10]. On the other hand, the developing countries are undergoing a nutritional transition due to multiple factors that affect negatively energy intake and energy expenditure [10,13-15].

a. Percentage of obese adults, 1975

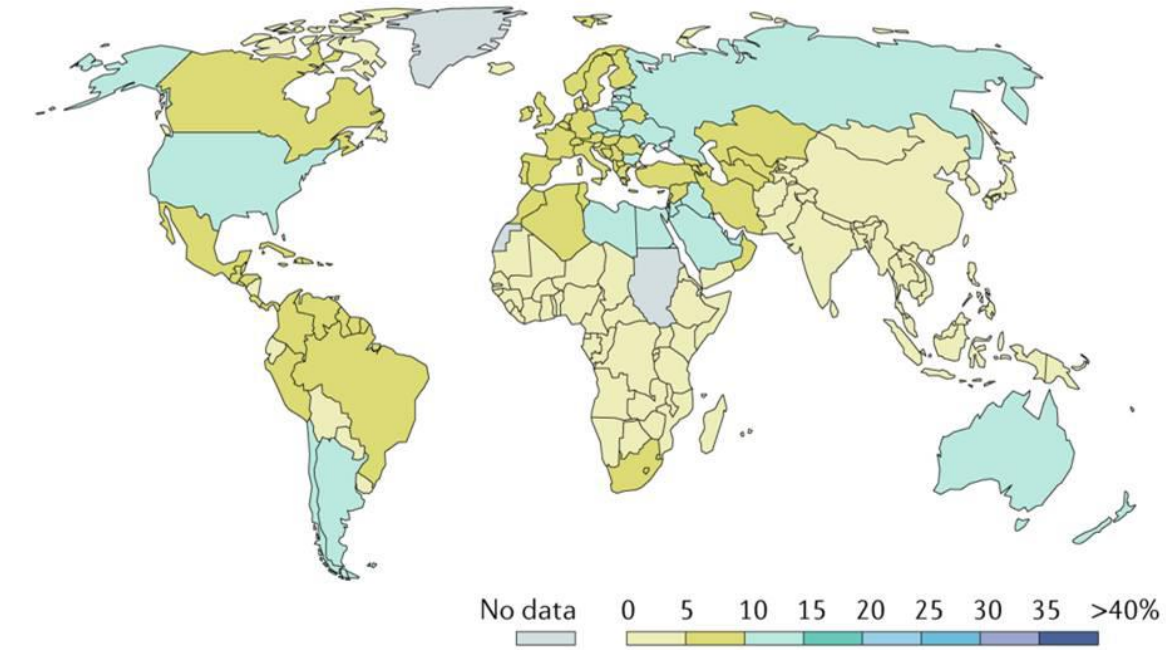

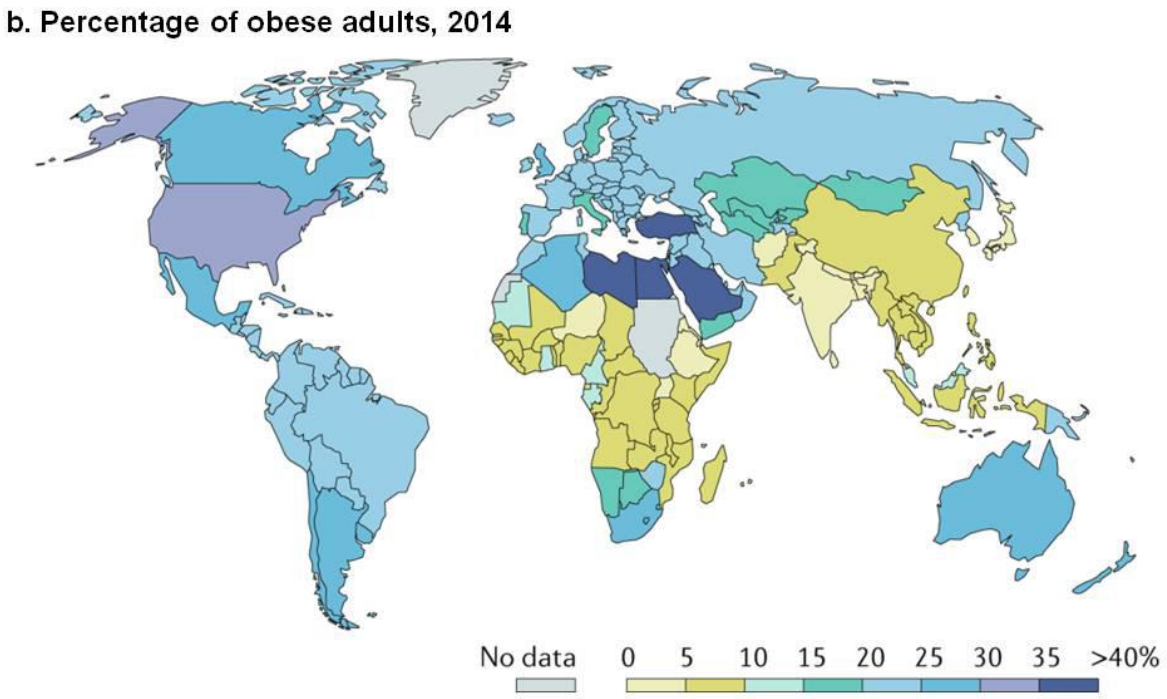

Figure 1. Percentage of obese adults worldwide in **a.** 1975 and **b.** 2014. The number of adults with obesity increased substantially between 1975 and 2014. (Adapted from Blüher M, *Nature Reviews Endocrinology*, 2019[16])

4. A.2. Obesity and Inflammation

Obesity is associated with insulin resistance, hyperglycaemia, dyslipidaemia and hypertension, which together are termed as metabolic syndrome [17,18]. These metabolic disorders increase the risk of development of type 2 diabetes mellitus (T2DM) and cardiovascular diseases and contribute to high rates of mortality and morbidity [17,18]. Systemic markers of inflammation increased in obesity and T2DM include white blood cell counts and plasma levels of coagulation factors (fibrinogen and plasminogen activator inhibitor 1 (PAI- 1)), acute-phase proteins such as C-reactive protein (CRP) and serum amyloid A (SAA) and pro-inflammatory cytokines (tumor necrosis factor (TNF)-a, interleukin (IL)-1b and IL-6. These markers are reduced when the patients lose weight and increase their physical activity [19-24].

It is well established that adipose tissue, liver, muscle and pancreas are sites of inflammation in presence of obesity and T2DM [18]. Infiltration of macrophages (MΦ) into these tissues results to the production of pro-inflammatory cytokines [25]. The cytokines act in an autocrine and paracrine manner to promote insulin resistance by interfering with insulin signaling in peripheral tissues through activation of the c-JUN N-terminal kinase (JNK) and nuclear factor-kappa B (NF-κB) pathways [26]. These

pathways are activated in multiple tissues in obesity and T2DM and have a central role in promoting tissue inflammation [18]. IL-1b is one of the major pro-inflammatory cytokines produced by MΦs and it has been shown to be a key contributor to the pathogenesis of T2DM by activating NF-κB pathways and the generation of other inflammatory mediators, such as TNFa and IL-1b itself [27]. Accumulating evidence give to NLR family pyrin domain-containing 3 (NLRP3) inflammasome a central role in obesity-induced insulin resistance [28-30]. The NLRP3 inflammasome acts as a sensor of metabolic danger during obesity, such as high levels of glucose [31], saturated free fatty acids [32,33], lipid intermediates including ceramides [30] and uric acid [34].

Nevertheless, data from several studies suggest that some obese people are not insulin resistant [35-38]. This group of obese individuals do not display the typical metabolic disorders associated with obesity and are at lower risk of developing T2DM and cardiovascular diseases. This phenotype is referred as metabolically healthy obesity (MHO) and may account for around 30% of the obese population [39]. The MHO phenotype is characterized by differentiated body fat distribution with lower visceral fat and greater subcutaneous fat [40], decreased fat deposition in the liver [41] and by a less inflammatory profile with lower levels of circulating inflammatory markers [40,42] compared to the unhealthy obese phenotype. It has been reported that the visceral adipose tissue of MHO phenotype is associated with lower activation of the NLRP3 inflammasome in infiltrating MΦs [28]. Along the same lines, the AdTG leptin-deficient *ob/ob* mouse, which has higher circulating concentrations of adiponectin than its *ob/ob* littermate, was found to become obese but remains insulin sensitive [43]. Moreover, it exhibits increased subcutaneous adipose tissue mass, low fat content of the liver and the skeletal muscle, increased adipogenesis, reduced infiltration of MΦs in adipose tissue and low systemic inflammation [43].

4. A.3. Obesity and Cancer Risk

Evidence suggest that individuals who are overweight (BMI 25.0–29.9 kg/m^2) or who are obese (BMI ≥30 kg/m^2) are at increased risk of developing several types of cancer [44-46]. Preclinical studies point to the direction that chronic inflammation associated with obesity, as well as the unique nature of cancer stem cells (CSCs) derived from adipose tissue in obese individuals, might contribute to the increased cancer risk of such patients [47-49]. The main factors that are considered to connect

obesity and cancer are the insulin–IGF-1 axis, sex hormones, and the adipocyte-derived cytokines (adipokines) [45,46]. Tumors invade stromal compartments that are rich in adipose tissue, and adipocytes function as endocrine cells to critically shape the tumor microenvironment and contribute to tumor development and progression [45,46]. Adipose tissue within the tumor microenvironment actively contributes to tumor growth and metastasis by functioning as an endocrine organ and acting as an energy reservoir for embedded cancer cells [50-52]. Excessive adiposity is specifically associated with increased risk of multiple malignancies including non–Hodgkin lymphoma, esophageal adenocarcinoma, and cancers of the colon, liver, pancreas, gallbladder, kidney, uterine endometrium, and breast [53,54]. However, cancer risk in obesity is different between ethnic groups; African Americans appear rather susceptible to cancer, in contrast to Hispanics who appear to be relatively protected while the association of increased BMI with breast cancer is particularly strong in Asia-Pacific populations [55,56].

4. B. Non-Alcoholic Fatty Liver Disease (NAFLD)

4. B.1. The Liver

In both humans and mice the liver is a vital organ for nutrient processing, protein production, energy homeostasis and detoxification. Lipids, peptides, carbohydrates and nutrients are transported to the liver through gut-derived portal venous blood, and then pass through sinusoidal lining cells before finally being taken up and metabolized by hepatocytes. The human liver is consisted of four separate lobes, it occupies the right upper quadrant of the abdomen and it accounts for approximately 2% of total body weight (BW). The murine liver weighs approximately the 6% of the BW and it extends in the entire subdiaphragmatic space. Like the human, it consists of four lobes and despite the fact that lobar patterns are species-specific, the basic lobular subunits are highly conserved in structure and function. Mixed arterial and portal venous blood enters the lobule via structures known as triads; triads are composed of arterioles, venules, bile ductules and lymphatics. Nutrients and macromolecules are freely exchanged between hepatocytes and plasma across sinusoids lined by fenestrated endothelium. Resident cells that include hepatic stellate cells, Kupffer cell, MΦs, T and natural killer (NK) cells, maintain immune surveillance [57].

4. B.2. Epidemiology of NAFLD

NAFLD is a spectrum of liver disease characterized by macrovesicular fatty infiltration (steatosis), inflammation, and hepatocytes ballooning injury. It has become the most common cause of liver disease and abnormal liver function test in industrialized countries [58,59] with a prevalence of 20 to 33% [60,61]. Within the next 20 years NAFLD will become the major cause of liver related morbidity and mortality as well as a leading indication for liver transplantation. NAFLD is more common in men than in women, with a prevalence 30–40% in men and 15–20% in women, and is higher in T2D patients, occurring up to 70% [62]. The highest rates of prevalence are reported from South America (31%) and the Middle East (32%), followed by Asia (27%), the USA (24%) and Europe (23%), whereas NAFLD is less common in Africa (14%) [63]. In addition, taking under account that the obesity rate in children is rising [64], the risk for paediatric NAFLD is higher, especially in the developed countries [63]. It has been recently reported that NAFLD prevalence is higher in obese children and adolescences (mean prevalence 34.2%) than in the general population (7.6%) and that prevalence is higher on average in males compared with females and increases incrementally with greater BMI [65]. Approximately 30% of patients with simple steatosis will eventually develop non-alcoholic steatohepatitis (NASH) [66,67], 15–25% of NASH patients will progress to cirrhosis and 30–40% of cirrhotic patients will die due to liver related complications [68]. NASH is also considered the major cause of cryptogenic cirrhosis [69]. NASH-associated cirrhosis can decompensate into subacute liver failure [70], progress to hepatocellular carcinoma (HCC) [71], and reoccur post transplantation [72]. NASH is considered the second most common indication for liver transplantation in the USA after chronic hepatitis C, and is still growing [63].

NAFLD can occur also in the absence of obesity, termed as “lean NAFLD”, and it can develop in 10-20% of Americans and Europeans [59,73]. Lean NAFLD includes a heterogeneous spectrum of disease arising from different etiologies, such as environmental or genetic causes, with many physicians to argue that it is more benign in nature than NAFLD in individuals who are obese. Factors that might be associated to lean NAFLD are increased visceral obesity (as opposed to general obesity), high fructose and fat intake and genetic risk factors, including congenital defects of metabolism [63]. Most of the lean NAFLD patients have normal weight but are metabolically obese. This group is described in at least 5% of the population in

the West and it consists of individuals who are non-obese, frequently sedentary, and who have impaired insulin sensitivity, increased cardiovascular risk and increased hepatic lipid levels [74]. Compared with patients who have NAFLD and are overweight or obese, lean NAFLD patients are younger and have a lower prevalence of the metabolic syndrome (2–48% versus 22–64% in patients who are overweight or obese) [73,75].

4. B.3. Risk factors

It has become apparent that the progression of NAFLD from steatosis to NASH and fibrosis is not linear [63] **(fig. 2)**. NAFLD grows exponentially as the stage of fibrosis increases [76-78]. Furthermore it has been reported that Hispanic individuals are more susceptible than white patients, whereas the lowest susceptibility is observed in black individuals [79] placing genetic susceptibility amongst the potential risk factors. Romeo et al revealed that there is a highly significant association with increased hepatic triglyceride (TG) levels for the patatin-like phospholipase domain-containing 3 (*PNPLA3*) gene [80]. More studies have identified genes related to NAFLD pathogenesis and progression with their relative importance to vary between the different populations and lifestyle choices [79]. Therefore socioeconomic and environmental factors such as dietary habits and activity, are important and must be considered [63]. Moreover, epigenetic factors may contribute to the heritable effect on disease risk. For example it has been reported the remodeling of DNA methylation at genes related to fibrosis in male mice [81] with the same methylation profile to have been observed in NASH patients [81,82].

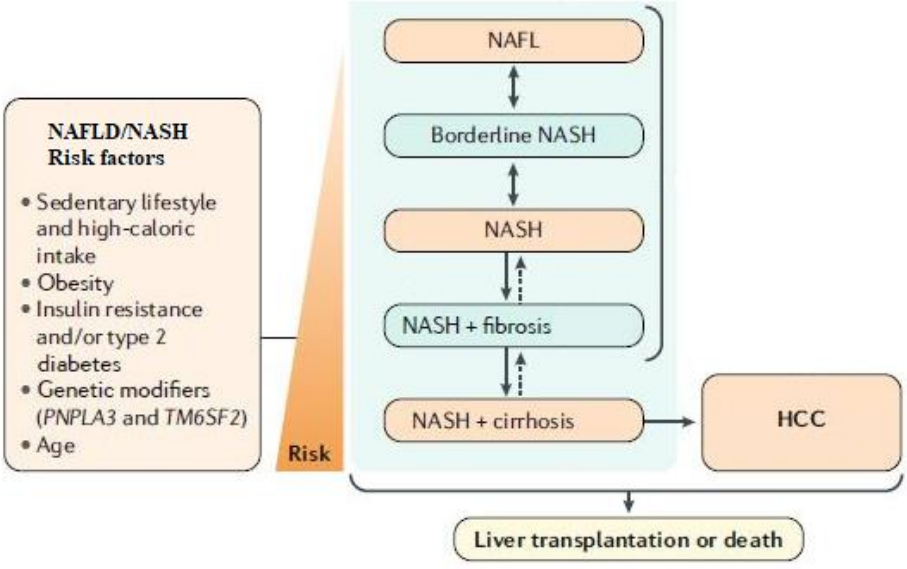

Figure 2. Risk factors and pathophysiology of NAFLD/NASH and HCC. Sedentary lifestyle and high-caloric intake are among the most prominent risk factors for NAFLD/NASH development. Steatosis and NASH are dynamic conditions that are most likely reversible in the context of treatment response or lifestyle changes. NASH can trigger liver cancer through the development of fibrosis and cirrhosis. Development of fibrosis in NASH is more frequent than the reversal of fibrosis to NASH (Adapted from Anstee, Reeves, Kotsiliti et al, *Nat Rev Gastroenterol Hepatol*, 2019[83]).

4. B.4. Histopathology of NASH

In 2003 the NASH Clinical Research Network defined that the diagnosis of NASH is established by the presence of fat, inflammation and ballooning degeneration with either pericellular fibrosis or Mallory bodies [84] **(fig. 3)**. In order to distinguish NASH between "simple" steatosis and steatosis with inflammation and to accurately assess the degree of steatosis, the necroinflammatory lesions and fibrosis of NASH, it is necessary for the different histological specimens to be properly evaluated. It is agreed that H&E and Masson's trichrome stains are sufficient tools to perform the evaluation. The histological features were grouped into five broad categories: steatosis, inflammation, hepatocellular injury, fibrosis, and miscellaneous features. The proposed NAFLD Activity Score (NAS) includes features of active injury and is the defined sum of the scores for steatosis (0-3), lobular inflammation (0-3), and ballooning (0-2); hence ranging from 0 to 8. Fibrosis is not included as a component of the activity score. Cases with NAS of 0 to 2 were largely considered not diagnostic of steatohepatitis; on the other hand, most cases with scores of ≥5 were diagnosed as steatohepatitis. Cases with activity scores of 3 and 4 were divided almost evenly between the 3 diagnostic categories [85].

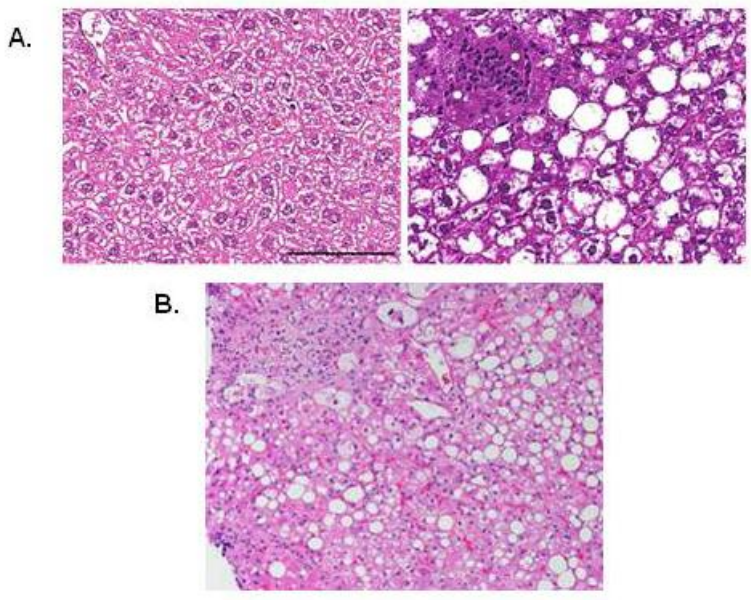

Figure 3. **A.** Histology of our mouse NASH model. Left: Liver section, hematoxylin & eosin staining from C57BL/6 mouse, male, under chow diet (ND) for 6 months. Right: Liver section, hematoxylin & eosin staining from C57BL/6 mouse, male, under choline deficient - high fat diet (CD-HFD) for 6 months. On the right the features of NASH are represented: hepatic inflammation, steatosis, ballooning hepatocytes. Scale bar: 100 µm. **B.** Liver biopsy of human NASH displaying steatosis, ballooning and lobular inflammation. (Fig. 2B. adapted from Brown & Kleiner, *Metabolism*, 2016[86])

4. B.5. Immunology of NASH and NASH-driven HCC

Accumulating human data have identified the prevalence of obesity-induced HCC with recent publications to pinpoint the need for a better understanding of NAFLD-induced HCC progression [87]. In addition, murine studies have demonstrated the role of local intra-hepatic chronic inflammatory responses in hepatocarcinogenesis under the context of NASH [49,88] **(fig. 4)**.

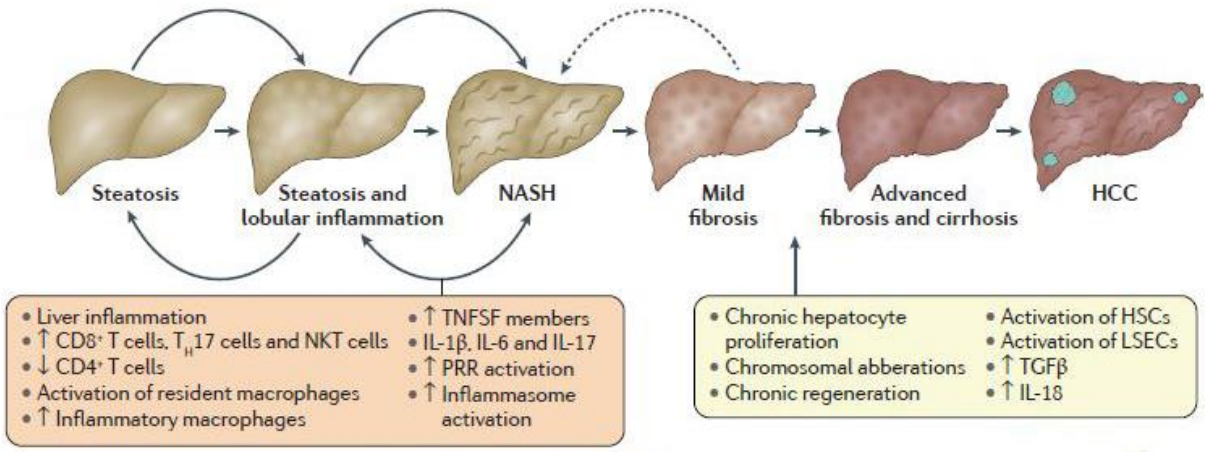

Figure 4. Immunology of NASH and HCC. The augmentation of intrahepatic lymphocyte populations during liver inflammation in NASH, such as CD8+ T cells, T helper 17 (TH17) cells, natural killer T (NKT) cells and infiltrating inflammatory macrophages, along with inflammatory cytokines, can lead to chronic necroinflammation, facilitating nonalcoholic fatty liver (NAFL)-to-NASH transition. Depending on treatment responses and lifestyle changes, these disease states are to some degree reversible. Chronic hepatocyte cell death and compensatory proliferation during NASH with mild to advanced fibrosis, together with increased levels of TNF superfamily (TNFSF) members, transforming growth factor β (TGFβ) and IL-18, contribute to increased hepatocellular carcinoma (HCC) risk. These factors, together with activation of hepatic stellate cells (HSCs), liver sinusoidal endothelial cells (LSECs) and chronic hepatic proliferation in a chronic regenerative environment, accompanied by chromosomal aberrations, all contribute to HCC development. ER , endoplasmic reticulum; PRR , pattern recognition receptors. (Adapted from Anstee, Reeves, Kotsiliti et al, *Nat Rev Gastroenterol Hepatol*, 2019[83])

T cells, natural killer T (NKT) & NK cells

Our lab has shown that under long-term choline-deficient high fat diet (CD-HFD) mice developed NASH-induced HCC through the activation of intrahepatic $CD8^+$ T cells and natural killer T (NKT) cells while activation of hepatocellular lymphotoxin-β

receptor (LTβR) and canonical NK-κB signalling facilitated NASH-to-HCC transition [88]. It has also been reported $CD4^+$ T lymphocytes to inhibit HCC initiation and mediate tumor regression [89,90]. Towards the same direction, Ma et al, using a series of different murine NAFLD and HCC models, have reported that NAFLD induced a selective loss of intrahepatic $CD4^+$ T lymphocytes and that depletion of $CD4^+$ cells accelerated tumor development in liver-specific avian myelocytomatosis viral oncogene homolog (*MYC*) oncogene transgenic methionine choline-deficient diet (MCD) fed mice [91].

Studies in HCC have demonstrated the relevance of different cell types, cytokines and chemokines for patient outcome. For example tumor infiltrating $CD4^+$ regulatory T-cells correlate with poor outcome in patients who undergo surgical resection [92,93]. Furthermore, it has been shown that in HCC patients, NK cell function inhibition occurred in a myeloid-derived suppressor cell (MDSC)-mediated manner and was mainly natural killer cell p30-related protein (NKp30) dependent [94].

Kupffer cells (KCs)

Kupffer cells (KCs) are the resident MΦs of the liver and their role in NAFLD initiation and progression has been shown in animal as in human studies [95]. For example, Reid et al using MCD showed that KCs are lost in the early stages of NASH onset followed by infiltration of $Ly6C^+$ monocyte-derived MΦs [96]. KCs express TLR4 and the binding of the receptor to LPS, results to the activation of NF-κB, mitogen-activated protein kinase (MAPK), extracellular signal–regulated kinase 1 (ERK1), p38 MAPK, JNK, and interferon regulatory factor 3 (IRF3) [97].The production of proinflammatory cytokines that follows, contribute to hepatic damage, leukocyte infiltration and activation of HSCs through the secretion of profibrotic cytokines, like transforming growth factor-β (TGF-β) and platelet-derived growth factor (PDGF) [97].

B cells

Further studies to clarify the role of B-cell responses in NASH as well as NASH to HCC transition are warranted. It has been reported that in about 40% of adults with NAFLD/NASH and 60% of children with NASH, there were high titers of immunoglobulin G (IgG) against malondialdehyde (MDA)-derived adducts, antigens derived from oxidative stress [98,99]. Furthermore, B cells have been shown to drive

CD4 T-cell activation and cytokine production in the adipose tissue during obesity [100] and that they play an important antibody (Ab)-independent role in the development of liver fibrosis in NAFLD [101]. Extending these observations, Shalapour et al. have recently shown that chronic inflammation and fibrosis in humans and mice with NAFLD is accompanied by accumulation of liver-resident immunoglobulin A-producing (IgA) programmed death ligand 1 (PDL1) positive cells, which suppress an efficient immune response in the context of NASH-induced liver cancer [102]. Towards the direction of IgA B cells and the gut-liver axis, in 2016 a study by Moro-Sibilot et al has shown that the liver harbors an important pool of IgA B cells that can drive antigen-specific responses after oral immunization with T-cell independent (TI) or T-cell dependent (TD) antigens. They have also demonstrated that it is highly unlikely that IgA class switch recombination occurs in the liver but IgA B cells originate from the Peyer's patches of the small intestine can migrate through the gut-liver axis to the liver in both humans and mice [103].

Sterile inflammation

Sterile inflammation, which occurs in the absence of pathogens, is an important mechanism of liver injury in NASH [104]. Damage-associated molecular patters (DAMPs) are molecules, such as nuclear and mitochondrial DNA, uric acid and purine nucleotides, that can activate inflammation [104]. Inflammasome is the necessary cytosolic machinery required for the conversion of DAMP signals into proinflammatory cytokines such as pro-IL1β and pro-IL18 with the help of Toll-like receptors (TLRs) amongst others [105]. The inflammasome-mediated immune response can trigger inflammatory processes by activating pro-IL1β and pro-IL18 in a caspase-1 depended manner that leads to liver damage [104]. In addition, pathogen-associated molecular patterns (PAMPs), which include bacterial products like the bacterial lipopolysaccharide (LPS), play an important role in NAFLD/NASH liver injury [106]. Conceptually pathogen-driven inflammation and sterile inflammation are distinct but functionally they overlap in several areas[104]. DAMPs and PAMPs bind to pattern recognition receptors (PRRs), including TLRs, triggering a local inflammatory response mediated by cytokines such as TNF-α and IL-6, having an impact on insulin resistance and lipid metabolism [107,108]. Hepatic cells that express TLRs include KCs, hepatic stellate cells (HSCs), biliary epithelial cells and sinusiodial endothelial cells with the most studied in NASH to be TLR2, TLR4 and TLR9 [106].

4. B.6. Liver fibrosis in NASH and NASH-driven HCC

Liver fibrosis is a process involving a complex interaction between fibrogenic and inflammatory pathways. It results from chronic liver injury and it is considered an early step in liver cirrhosis progression [109]. The liver tissue repair process involves a regenerative phase, where injured cells are replaced by cells of the same type leaving no evidence of damage, and by a phase of fibrosis where connective tissue replaces normal parenchymal tissue [110]. Continuous accumulation of extracellular matrix (ECM) in the liver, rich in collagen I and III, leads to scar deposition and eventually in liver fibrosis. When left untreated, it can develop in cirrhosis and subsequent clinical complications including increased risk of HCC [109].

Cirrhosis is defined as an advanced stage of fibrosis and is characterized by the formation of regenerative nodules of liver parenchyma, separated by and encapsulated in fibrotic septa and associated with major angioarchitectural changes [111]. In general, the fibrogenic mechanisms in chronic liver disease can be summarized in chronic activation of wound-healing reaction, oxidative stress-related molecular responses, and the generation of reactive cholangiocytes and peribiliary fibrosis [112].

In the event of liver injury, an antifibrinolytic-coagulation cascade occurs that leads to secretion of cytokines and chemokines resulting in the recruitment of neutrophils, macrophages and of, subsequently, T cells. When T cells become activated they secrete profibrotic cytokines, such as IL-3 and TGF-β, which activate further the macrophages and fibroblasts. Activated fibroblasts transform into α-SMA-expressing myofibroblasts as they migrate into the wounded tissue. When repeated injury occurs, chronic inflammation and repair cause an excessive accumulation of ECM components (such as hyalouronic acid and fibronectin) which contribute to the formation of a permanent fibrotic scar [110]. The fibrogenic cells of the liver are the hepatic stellate cells (HSCs). Upon activation the HSCs transform into myofibroblasts [111].

NASH presents a balloon-like hepatocellular injury with or without hepatic fibrosis [113]. The inflammatory signals in NASH result in the activation and proliferation of HSCs and consequently their differentiation in myofibroblasts. This leads to further driving ECM synthesis and ultimately liver fibrosis [109]. In NASH, as well as in alcoholic

steatohepatitis, fibrosis has a distinctive pattern: intercellular fibrosis and deposition of fibrillar matrix around the sinusoids (capillarization) [114]. In the NAFLD/NASH murine models available, fibrosis is most evident in the tissue margins but it also penetrates into the center of the tissue, affecting nearly all portal triads and in many cases is present in a “bridging” pattern throughout the hepatic lobule [115].

Polyclonal increase in serum immunoglobulin levels is frequently seen in patients with liver cirrhosis [116]. Additionally elevated serum immunoglobulins are observed in specific liver diseases such as autoimmune hepatitis (raised IgG), primary biliary cirrhosis (raised IgM) and alcoholic liver disease (ALD) (raised IgA) [117,118]. In ALD raised serum IgA levels are associated with more advanced fibrosis while deposistion of IgA in the liver has also been described in ALD [119,120]. Studies have also shown that serum IgA levels are increased in subjects with the metabolic syndrome and T2D [121,122]. Along the same lines McPherson et al have shown that serum IgA levels were elevated in patients with NAFLD and that this marker could be potentially used as an independent predictor of advanced fibrosis [123].

4. B.7. Therapeutic approaches for NAFL/NASH

Patients with NAFLD often remain asymptomatic, however they may sometimes present with vague right upper quadrant pain, hepatomegaly, and normal or high alanine transaminase (ALT) and usually have risk factors for metabolic syndrome [67]. There is no optimal ALT level to predict the extent of NASH and advanced fibrosis [124] and laboratory testing and radiological imaging cannot differentiate NASH from simple steatosis. Most commonly used technique is the abdominal ultrasound that is nevertheless lacking diagnostic sensitivity [125]. Till now the most reliable method for NASH diagnosis is invasive through liver biopsy and despite growing understanding of the global epidemic of NAFLD, there is no definite pharmacotherapy available [67] **(table 1)**. The probiotics and the bile acids receptors will be discussed in a separated section below.

Table 1. Treatment options for NAFL/NASH (*adapted from Hossain et al, 2016 [67]*)

Treatment	Medication/intervention	Comment
Lifestyle Modification	Weight loss	5-10% weight loss can lead to biochemical and histological improvement
	Hypocaloric diet alone	Better response when combined

		with exercise
	Exercise alone	
	Diet & Exercise	
	Dietary composition	Addition of PUFA and decreased saturated and transfatty acids
	Bariatric surgery	
Insulin sensitivity	Thiazolidinediones	Improvement in inslulin resistance, steatosis and inflammation
	Statins	Decrease in transaminases
Antilipidemic	Niacin	
	n-3 polyunsaturated fatty acids	May help reverse NAFLD
Antioxidant	Vitamin E	Histological improvement in nondiabetic NASH
Anti-inflammatory	Pentoxifylline	
Cytoprotective & antiapoptotic agents	Ursodeoxycholic acid	
Herbal	Milk thistle	Better results when combined with Vitamine E (among other agents)

4. C. The gut microbiome and liver disease

4. C.1. The gut-liver-axis

The concept that the nutrients travel from the gut to the liver through the portal vein is not new; it has been described two millennia ago by Galen (129 – c. 216 CE) in ancient Greece. Nowadays it is well known that the liver receives ~70% of its blood supply from the portal vein and that makes the liver the first and principal organ, apart from the intestine, that is exposed to gut-derived products (i.e. ingested nutrients, products of bacterial metabolism). Moreover the liver by producing bile acids that are later released to the small intestine, it modulates intestinal functions [126]. It has been already mentioned above the importance of DAMPS and PAMPS in NAFLD/NASH development. Increased permeability due to disruptions of the intestinal barrier influences the quantity and the quality of DAMPS and PAMPS that reach the liver. Consequently, the gut-vascular barrier determines what exactly circulates the portal vein [127]. Traces of bacterial mRNA and LPS are detectable in the liver and the peripheral blood even under physiological conditions [128,129; 130]. Furthermore, dietary factors influence the absorption of bacterial products from the intestine to the portal and systemic circulation. For example, it has been shown that high fat diet (HFD) increases plasma LPS concentrations in mice, leading to

metabolic endotoxemia [131]. In addition, *in vitro* studies have demonstrated that fatty acids can promote transepithelial LPS absorption [132].

4. C.2. The gut microbiome in obesity and NASH

The microbiota has been recently shown to play a key role in inducing obesity, systemic inflammation and metabolic disease, highlighting new therapeutic avenues and mechanistic underpinnings. The human intestinal lumen is occupied by 10^{13}-10^{14} microorganisms belonging to more than a thousand different bacterial species that encompass the microbiota [133,134]. The majority of these microbes reside in the colon, where they are present in a concentration of 10^{9}–10^{12} colony forming units (CFU) / mL. The microbiome maintains the integrity of the intestinal epithelial barrier and it is essential for metabolizing indigestible polysaccharides and in the absorption of short-chain fatty acids produced by bacterial fermentation. Moreover it plays a key role in the regulation of intestinal transit, thereby affecting the amount of energy absorbed from the diet; the microbiome, therefore, plays an important role in weight gain and metabolism [135].

The most important microbial factor that differentiates between obese and healthy individuals has been the shift in the proportion of bacterial flora belonging to the *Firmicutes* and *Bacteroidetes* phyla, which together comprise about 90 % of the microbiota of the adult gut. The *Firmicutes* phylum comprises gram positive organisms from greater than 200 different genera including *Catenibacterium*, *Clostridium*, *Eubacterium*, *Dorea*, *Faecalibacterium*, *Lactobacillus*, *Roseburia*, *Ruminococcus*, and *Veillonella* while the *Bacteroidetes* phylum consists of gram negative bacteria from approximately 20 genera including *Bacteroides*, *Odoribacter*, *Prevotella*, and *Tannerella* [135]. Studies in *ob/ob* mice have shown that there is significant reduction in the abundance of *Bacteroidetes* and a similar increase in the *Firmicutes* phyla in obese mice, resulting in increased fermentation of dietary polysaccharides and lesser energy remaining in feces [136]. These murine findings have been mirrored in human studies. It has been reported that obese participants on a calorie-restricted diet had an increase in the proportion of *Bacteroidetes* over the period of 12 months, which correlated with weight loss [137]. Reduced levels of *Bacteroidetes* and microbial diversity have been demonstrated in monozygotic and dizygotic obese twins compared to their lean twins with the metagenomes of the obese group being higher in energy harvesting genes related to lipid and

carbohydrate metabolism [138]. On the other hand, there are studies regarding the *Bacteroidetes* that show none or positive association with weight gain and obesity [139-141].

There is a growing number of studies suggesting that dysbiosis [142] contributes to the development of chronic liver diseases such as NAFLD [143], NASH [144,145] and alcoholic liver diseases [146]. For example, Okubo et al [147] have shown a decrease in body weight and NASH development suppression in mice lacking resistin-like molecule β (RELMβ) fed with MCD. They attributed the reduction in NASH development to the reported increased proportion of *Lactobacillus* bacteria by acting protectively against the gut permeability induced by MCD diet [147]. RELMβ is a molecule that contributes to local immune function in the gut and has been reported as a potential regulator of gut microbiota [148]. In the same direction, a few years later the same group demonstrated that *Bifidobacterium* and *Lactobacillus* were reduced under MCD diet leading to NASH development [149].

In a human metabolic study where 15 healthy females were subjected to a choline depletion diet, shifts were observed in the microbial community profiles. More specifically, *Gammaproteobacteria* class was decreased with restoration of choline diet [150]. Along the same lines, abundance of *Gammaproteobacteria and Prevotella* was observed in the fecal samples of obese children with NAFLD [151]. Choline, an essential nutrient that can be acquired from the diet and via *de novo* synthesis, is involved in physiological processes such as normal metabolism and neurological development in the fetus and is also required for the correct structures of all membranes [152]

Modulation of the microbiome: probiotics and antibiotics

The correct use of the term probiotics has been a subject of interest for Food and Agriculture Organization of the United Nations (FAO) and the World Health Organization (WHO), which have agreed on the following definition: “live microorganisms that, when administered in adequate amounts, confer a health benefit on the host”. This definition is inclusive of a broad range of microbes and applications and it differentiates live microbes used as processing aids or sources of useful compounds from those that are administered primarily for their health benefits [153]. Probiotics can affect obesity **(table 2)** not only through the modulation of the

respective gut bacterial populations but also through the bile acids. Probiotics may lead to a decrease in adiposity through the deconjugation of bile acids [154].

Table 2. Probiotics and obesity

Probiotics	Comment
Lactobacillus acidophilus, L. fermentum, L. ingluviei, L. reuteri	Likely to cause weight gain in humans and animals[155,156]
Lactobacillus gasseri, L. plantarum	Seem to be protective against obesity[152]
***Bifidobacterium* & *Enterococcus* spp**	Induce weight gain[154]

The use of antibiotics is another major intervention which can significantly impact the development of obesity by altering the gut microbiota [154]. In humans, *Firmicutes* and *Bacteroidetes* may impact insulin resistance by mediating glucagon-like peptide-1 (GLP-1) secretion in obesity [157]. In murine studies, antibiotic induced depletion of *Firmicutes* and *Bacteroidetes* resulted in increased GLP-1 secretion, which ultimately resulted in improved systemic glucose intolerance, hyperinsulinemia, and insulin resistance independent of obesity as compared with untreated controls when exposed to diet-induced obesity. In addition, depletion of *Firmicutes* and *Bacteroidetes* resulted in increases in metabolically beneficial gut-derived metabolites [158]. Cho et al have demonstrated that upon administration of low dose penicillin, chlortetracycline, or vancomycin to young mice at weaning, adiposity in young mice was increased. They have also reported changes in the taxonomy of the microbiome, changes in copies of key genes involved in the metabolism of carbohydrates to short-chain fatty acids, increases in colonic short-chain fatty acid levels, and alterations in the regulation of hepatic metabolism of lipids and cholesterol [159]. In a follow up study, the same group has shown that low dose penicillin in weaning mice caused changes in the ileal expression of genes involved in immunity and it enhanced obesity inducing changes in genes involved in hepatic metabolism and visceral adipocity. The above effects were transferrable when germ-free mice were transplanted with microbiota from the treated groups, suggesting that the changes are due to the altered microbiome and not the antibiotics [160].

4. D. B cells and IgA synthesis

4. D.1a. B-cell development

B cells develop in the bone marrow (BM) from hematopoietic precursor cells and are an essential part of the humoral immune system while defects in their development, section and function lead to autoimmunity, malignancy, immunodeficiencies and allergy [161]. Antibodies are produced by plasmablasts (PBs) and plasma cells (PCs), populations of terminally differentiated B cells. PBs are dividing antibody-secreting cells (ASCs) with migratory potential that can further mature into PCs, the final stage of B cell differentiation. The term ASCs refers to both proliferating PBs and non-proliferating PCs and they are associated with alterations in their morphology, gene expression profile and lifespan. Mature B cells are divided into follicular B cells (B2), marginal zone (MZ) B cells and B1 B cells. B2 B cells are located in the lymphoid follicles of the spleen and lymph nodes whereas MZ B cells are placed about the marginal sinus of the spleen. B1 B cells are located mostly in the peritoneal and pleural cavities and at mucosal sites where they encounter environmental pathogens [162,163] **(table 3)**.

Table 3. Selective mouse positive markers for the different development B cell subsets (*adapted from www.bdbiosciences.com*)

B cell developmental stage	Mouse positive markers
Pre-Pro-B cells	CD43, CD93, CXCR4, B220, CD135, IL7R
Pro-B cells	CD19, CD43, CD24, B220, IL7R
Pre-B cells	CD19, CD25^{var}, CD24, B220, BP1, IL7R
Immature B cells	CD19, CD24, CD93, B220
Transitional B cells	CD19, CD24, CD93, CD21^{var}, CD23^{var}, B220
Marginal Zone B cells	CD1d, CD9, CD21^{high}, CD22^{var}, CD35^{high}, B220
Regulatory B cells	CD1d^{high}, CD5, CD19, CD24, TIM
Follicular B cells	CD19, CD22, CD23, CD38, B220
Activated B cells	CD27, CD69, CD80/CD86, B220, CD135, MHCII^{high}
Germinal center B cells	CD19, CD37, CD20, GL7
Plasmablasts	CD19, CD138, CXCR4, MHCII
Plasma cells long lived	CD138, CXCR4^{high}
Plasma cells short lived	CD19^{low}, CD138, CD93, CXCR4^{high}
Memory B cells	B220, CD38^{var}, CD62L^{var}, CD802/CD86^{var}, CD95^{low}

V(D)J recombination

Antibodies are members of the immunoglobulin superfamily and they are made up of two heavy (H) and two light (L) chains and the L chain can consist of either a κ or a λ chain. All H chains are expressed from the Igh locus whereas L chains are expressed from the Igκ or Igλ locus [164]. Each component chain contains one NH_2-terminal variable (V) domain and one or more COOH-terminal constant (C). The L chains contain only one C domain, whereas the H chains contain three or four such domains [165]. The DNA segments that rearrange to create the H and L chains include variable (V) and joining (J) elements and in addition the H chains include a third, diversity (Dh), gene segment [166]. The Igh locus consists of Vh, Dh and and Ch segments arranged in adjacent regions [167]. In developing B cells, Vh. Dh and Jh segments recombine to encode the antibody H chain [166]. Each segment is flanked by a short DNA sequence called the recombination signal sequence (RSS). RSS is recognized by the recombination activation gene (*RAG*) 1 and 2. RAG1 and RAG2, along with additional proteins, form the RAG complex which creates a loop between two RSSs bringing them into proximity. The RAG complex then induces breaks and promotes ligations of appropriate coding segments via the nonhomologous end-joining machinery [168].

The κ L chain locus contains V and J segments as well. L chains do not use D segments. Here there is the possibility for secondary rearrangements between the Vκ and Jκ segments contrary to V(D)J recombination of the H chains where the final result is irreversible [169]. In mice λ chain locus is quite small, opposite to κ L chain and Igh locus. The major rearranged combinations are expressed in serum antibodies which are though 95% kappa [170].

The different developmental stages of B cells are defined by the recombination steps. Before V(D)J recombination the B cells are called pre-pro-B cells and the Igh locus recombination between Dh and Jh can occur at this stage. V(D)J recombination takes place in the pro-B cell stage and the successful production of an H chain is necessary for the transition from the pro-B cell to the pre-B cell stage. Pre-B cells express the pre-B cell receptor that suppresses the activity of the RAG complex therefore preventing the continuation of V(D)J recombination in the Igh locus. Large pre-B cells with functional H chains divide several times to increase in

numbers and then differentiate into small pre-B cells. The small pre-B cells express again the *RAG* genes to allow for Ig L chain rearrangement. Under successful recombination the small pre-B cells will express a B cell receptor (BCR). Before the cells are released from the BM they undergo negative selection. Self-antigens are presented by antigen presenting cells (APCs) and the B-cells that express receptors with high affinity towards self-antigens will undergo apoptosis or further L chain recombination. The B cells that survive the negative selection migrate to the periphery as naïve cells [168].

Class switch recombination (CSR) and somatic hypermutation (SHM)

The product elements of V(D)J recombination are fused to a constant (C) region through RNA splicing. There are several IgH C regions each of which corresponds to different Ig isotype. In the mouse there are eight different IgH C regions: Cμ, Cδ, Cγ3, Cγ1, Cγ2a, Cγ2b, Cε and Cα. The IgH C_H region defines the antibody class also referred as isotype. Therefore antibodies are divided into five isotypes: IgM (Cμ), IgG (Cγ), IgE (Cε), IgD (Cδ). IgM is produced prior to class switch recombination (CSR) and is important for the early stage of the immune response. Upon CSR and somatic hypermutation (SHM) the B cells differentiate into PCs and produce high-affinity IgG, IgA, IgE and IgD. IgG is the major serum isotype and consists of the IgG1, IgG2, IgG3 and IgG4 isotypes [171].

Both events are critical for generating antigen-induced antibody memory and both are initiated by the enzyme activation-induced cytidine (AID). During SHM, AID specifically deaminates cytidines in the V(D)J exons of H and L Ig locus. These deaminations lead into mutations and/or small deletions/insertions. This way, SHM diversifies the repertoires of the BCR antigen binding sites; B cells expressing BCRs with higher antigen affinity are positively selected in the light zone of GCs to effect affinity maturations of the immune response [168]. CSR can take place both inside and outside GCs [172]. During CSR, Sμ (donor S region that lies just upstream of each set of C_H exons) is fused to one of the other downstream acceptor S regions. As a result the two sequences between the two fused S regions are deleted from the IgH locus as an extrachromosomal circle. This way a downstream C_H replaces Cμ leading to an expression of a new C_H, such as γ, α or ε and correspondingly, a new class of BCR/antibody (IgG, IgA or IgE). CSR does not affect antigen-binding specificity [168].

4. D.1b. B cell Function

Antigen encounter and antigen presentation

Naïve B cells travel from the BM to secondary lymphoid organs (SLOs) to sample antigens from the blood (spleen) and from the tissues (lymph nodes). A number of naïve B cells moves also to mucosa-associated lymphoid tissues (MALT). APCs, such as DCs and MΦs, convey the antigens to the B cells but special types of antigens, especially TI Ags, are capable of activating B cells directly [173].

The BCR is composed of a membrane-bound immunoglobulin (mIg) for antigen binding and a transmembrane Igα/Igβ heterodimer for signaling [174]. Ultimately, the BCR bound with antigen and other co-receptors form a complex that encounters the intracellular tyrosine kinase Lyn. Lyn phosphorylates the cytoplasmic immunoreceptor tyrosine activation motifs (ITAMs) on the Igα/Igβ heterodimer that provides a docking site for the tyrosine kinase Syk to initiate intracellular signaling cascades that allow the B cell to internalize antigen [175].

B cells internalize antigens mainly through clathrin-dependent, BCR-mediated endocytosis. After vesicle formation, clathrin disassociates and the vesicle evolves into an endosome. The final stage is delivery of vesicles carrying the antigen-bound BCR to MHCII peptide-loading compartments. Internalization of BCR inhibits signaling, as localization in endosomal compartments reduces surface BCR and abrogates the activity of signaling proteins, such as Lyn and Syk. Endocytosed BCR/antigen complexes intersect with newly synthesized MHCII en route to the cell surface [173]. During this process, proteolytic events take place in B cells that involve epitope generation for MHCII presentation [176,177]. Finally, the new loaded MHCII/peptide complexes reach the cell surface for antigen presentation [173].

Interestingly, antigen-presenting machinery is present in pro- and pre-B stages with the most common MHCII pathway components to be present in the absence of mature BCR; most likely they are involved in B cell maintenance and survival [173]. In contrast, MHCII-deficient mice show a mature B cell population with impaired number in the overall B cells and their ability to antigen present [178,179]. It has been proposed that the presence of MHCII antigen presentation machinery in pre-, pro- and immature BM B cells plays a role in the induction of the peripheral $CD4^+$ T cell tolerance through presentation of peptides from self-antigens [179]. In addition, lack of

MHCII expression in memory B cells impairs their ability to differentiate into PC upon antigen restimulation [180].

Antibody secretion

Antibodies contribute to immunity mainly through three different mechanisms: 1) They can bind to a pathogen/antigen, such as viruses and bacteria, and through neutralization they prevent their entrance in the cells, 2) antibodies can coat the surface of an antigen, a process called opsonization, and they can enhance its phagocytosis and 3) by binding to the surface of an antigen they can activate the complement system [181].

All the subtypes of mature murine B cells have the ability to differentiate into PCs. B-cell activation and differentiation can occur either through TI or TD antigen (Ag) responses. TD Ags contain protein components whereas TI Ags include bacterial components and polysaccharides. In general, TI Ags do not evoke long-lived Ab responses due to the lack of germinal centers (GCs) and memory formation[163]. TD Ags on the other hand, can establish long-lasting GC responses with the generation of memory B cells and long-lived plasma cells [182].

The humoral defense system includes: 1) the production of natural Abs that respond immediately on Ags 2) innate-like MZ and B1 B cells low-affinity but rapid response and 3) the adaptive, late-phase GC-derived response of higher affinity [163]. During the primary innate immune response, APCs such as dendritic cells (DCs) and MΦs recognize and present processed Ags to B cells. The Ag-stimulated B cells undergo CSR and the B cells differentiate into short-lived PBs and become ASCs. SHM and clonal expansion follow that lead to the generation of higher affinity antibodies [162,171].

4. D.2. The mucosal IgA synthesis

Mucosal membranes provide a dynamic interface that facilitates the absorption of beneficial substances, while blocking the penetration of noxious agents and microbes. In the mutualistic gut lumen environment, the microbial signals generate non-inflammatory homeostatic balance by stimulating the intestinal mucosa. This balance mostly involves the transepithelial release of IgA into mucosal secretions. IgA is mostly produced by B cells located in gut-associated lymphoid follicles and constitutes the most abundant antibody class in the intestine [168]. The number of IgA-producing plasma cells exceeds the total number of plasma cells in the rest of the

body combined, including bone marrow, lymph nodes and spleen. Human intestinal IgA is mostly dimeric (secretory IgA, SIgA), while most IgA in serum is monomeric, and comprises both the IgA1 and IgA2 subclass. Most plasma cells in the small intestine secrete IgA1; nevertheless the IgA2 proportion increases from the duodenum through the terminal ileum and the two subclasses are present in approximately equal numbers in the colon**.** Mature B cells develop into IgA plasma cells by replacing the Cμ gene with the Cα gene in the human Ig heavy chain locus through CSR [183].

The precursors of lamina propria IgA PCs are generated in discrete zones of organized lymphoid inductive sites, such as the gut-associated lymphoid tissue (GALT, part of MALT). GALT is associated with an epithelial structure that facilitates antigen entry. Antigens may be sampled by epithelial cells termed microfold (M) cells that comprise part of the specialized follicle-associated epithelium (FAE). GCs of the small intestine, that are part of GALT, contain a diverse population of B cells surrounded by follicle DCs, follicular T_H and MΦs that support GC B cell clonal expansion and selection. $CD20^+$ B cells are numerous in GALT structures but they are scarce in the lamina propria where PCs and PBs have an almost exclusive distribution with the IgA to be the dominant isotype [184].

Mucosal IgA is secreted across the epithelium by binding to the polymeric immunoglobulin receptor, after which it binds to microbes, various components of the diet and antigens in the lumen of the intestine. These interactions protect the immune system from potentially harmful stimulation by the contents of the lumen and in addition regulate the composition of the microbiota. IgA provides a physical barrier and can control the expression of genes by microbes in the intestine. As a consequence, deficiencies in IgA synthesis can elicit pro-inflammatory signals in the host [185]. In animal models, isolated IgA deficiency leads to compensatory increases of mucosal and serum levels of IgG and IgM (for example the $AID^{-/-}$ mice that abolish both CSR and SHM) [186]. IgA-producing gut PCs can be generated by both T-cell-dependent and T-cell-independent mechanisms that involve the cooperation of epithelial cells, DCs, and innate lymphoid cells (ILCs) **(fig. 5)** [185]. Naive B cell precursors expressing IgM and IgD are induced to switch to the IgA isotype through T-cell-dependent or T-cell-independent pathways of activation. In both cases, BCR stimulation is necessary to induce AID activation. Murine small intestinal IgA PCs

have an average half-life of 5 days and a maximum lifespan of 7-8 weeks. The IgA PC population is heterogeneous and contains both short-lived major histocompatibility complex class II^{+} cells (MHCII^{+}) and long-lived MHCII^{-} cells [187].

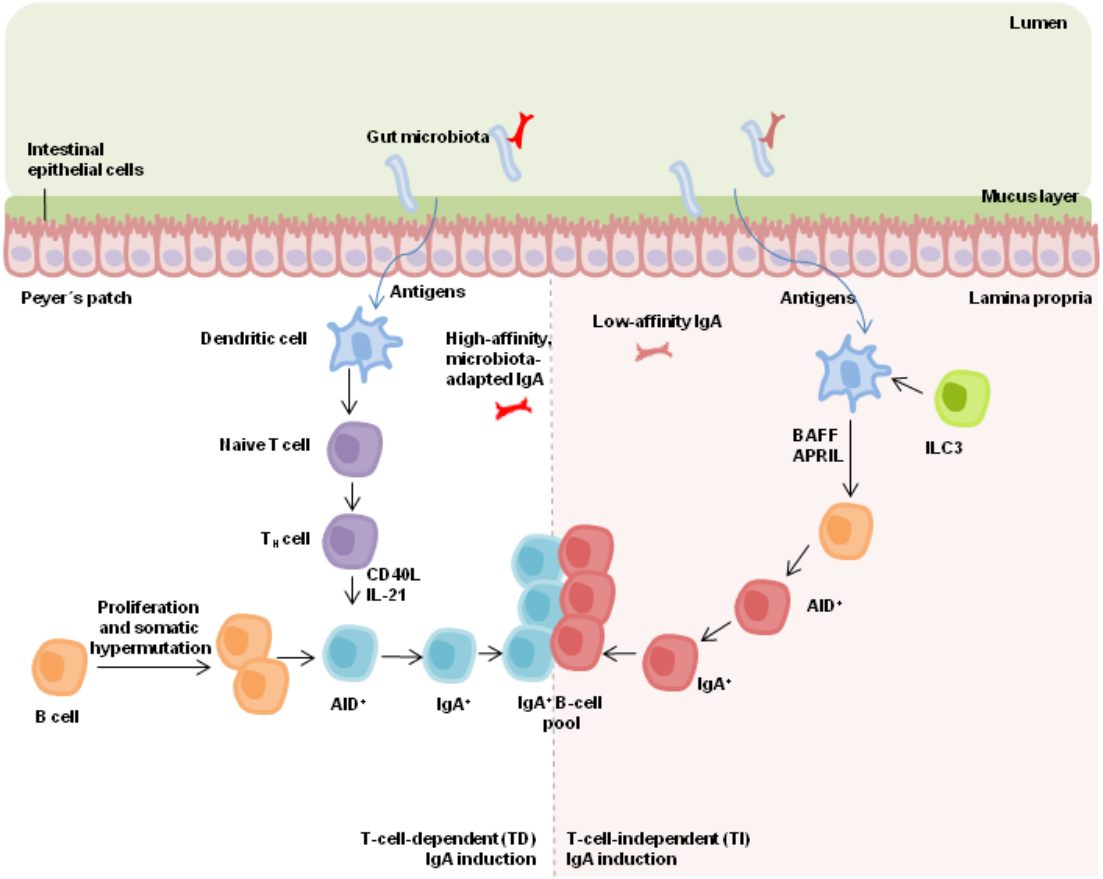

Figure 5. TD IgA CSR (left) takes place mostly in Peyer's patches. DCs induce the differentiation of CD4-expressing T cells into T_H cells. CD40 ligand (CD40L) and IL-21 from T_H cells induce the expression of AID in B cells and promote IgA cCSR. TI IgA CSR (right) occurs predominantly in the lamina propria and isolated lymphoid follicles (ILFs), where B-cell activating factor (BAFF) and its homologue APRIL, which are derived from DCs, promote the induction of AID expression in B cells. ILC3s also contribute to those pathways, through the expression of LTα and LTβ, which activate DCs. The gut microbiota affects IgA CSR in both pathways. The TI pathway produces IgA with low affinity but directed towards the microbiota. The IgA-expressing B-cell clones that this pathway induces persist for a long time and can re-enter a GC, where they undergo further somatic hypermutation to produce high-affinity IgA that is adapted to the changing composition of the microbiota (adapted from Honda & Littman, *Nature*, 2016 [185]).

IgA is induced mainly in the secondary lymphoid structures of the intestine, known as Peyer patches; nevertheless IgA's induction can be Peyer-patches- independent and can occur in other sites that can also sustain CSR [186]. T-cell-dependent responses in GCs lead to high-affinity binding of IgA to antigen whereas T-cell-independent

responses can occur in the lamina propria; the latter interactions lead usually to the production of low-affinity binding of IgA to antigens [185,186]. The above are consistent with observations that even though CD40-deficient mice lack GCs in the Peyer patches, IgA levels are normal. The CD40 pathway is not the only one involved in the expression of AID and its functions on CSR and SHM: the dendritic and monuclear cell soluble ligands a proliferation-inducing ligand (APRIL) and B cell-activating factor (BAFF) are important for T-cell-independent extrafollicular AID induction [186]. It should be noted that IgA production through T-cell-independent CSR it accounts for a quarter of total IgA that is produced in presence of T cells [188].

4. 3. Aim of the study

The aim of this study was to illuminate the role of B cells and the microbiota in NASH development by using different dietary and genetic mouse models, and antibiotic and antibody-based therapeutic strategies.

There is an increasing interest in the role of immune cells in NASH development and the subsequent HCC; an interest that is mostly focused in the discovery of new and more effective therapies for the human situation. One of the hallmarks of our NASH dietary model is the activation of hepatic T cells and we hypothesized that that B cells are important for their activation either in the liver in the periphery, like in the small intestine. In order to address the hypothesis we characterized different B-cell and immunoglobulin knock out mouse models with a focus in the role of antibodies in NASH pathology. In addition we characterized antibody-based therapies to evaluate our genetic models and to further highlight potential mechanistic underpinnings.

The role of microbiome in obesity and the metabolic syndrome is a research area that continuously and feverishly attracts the attention of the scientific and medical community. Drug research based on microbiome modulation is of great interest and therefore we hypothesized that microbiome plays a role in NASH development. To address this hypothesis we characterized wild type conventional mice in a dietary model treated with wide spectrum antibiotics, in a prophylactic and therapeutic manner, and germ free mice on a long-term diet model.

5. Materials and methods

5.1 Mice, diets and treatments

4-6 weeks old male C57BL/6J mice were purchased from Charles River. All strains of genetically-altered mice were on a C57BL/6J background. Control mice were matched by genetic background and age. Mice were housed at the German Cancer Research Center (DKFZ), Heidelberg. Animals were maintained under specific pathogen-free conditions and experiments were performed in accordance according to German Law (G11/16, G7/17).

4 weeks old male C57Bl/6N mice were provided by Prof. Dr. Dirk Haller and the diet experiments took place in his germ free facility at the Technical University of Munich (TUM) (School of Life Sciences Weihenstephan) according to the German Law (Regierung von Oberbayern, approval no. 55.2-1-54-2532-72-2015).

4-6 weeks old male mice were fed a normal chow diet (ND), a choline deficient high-fat diet (CD-HFD) (Research Diets; D05010402) and a western diet with trans-fat (Research Diets; D09100301 - 40 kcal % fat (Primex shortening), 20 kcal % fructose, 2% cholesterol).

For the antibody- and antibiotic-treated studies, male mice were fed CD-HFD and western diet for the indicated timeframes. The mice were treated intraperitoneally (i.p) with CD20 depleted antibody (Genentech, clone 5D2 and Biogen, clone 2B8 - Rituximab) and antibody that blocks CD40-CD40L interaction (clone MR1, a gift from Prof. Dr. Burkhard Becher). αCD20 antibody clone 5D2 was given in a dosage of 200μg in PBS for three times (once every two weeks, in total 6 weeks of treatment) whereas Rituximab was given 150μg in PBS twice a week for 8 weeks and MR1, 300μg in PBS once per week for 8 weeks. Animals were sacrificed at the endpoint of 6 months on diet; serum and organs were harvested for biochemical, molecular analysis and for immunohistochemistry (IHC) and flow cytometry (FACS) analysis.

Wide spectrum antibiotic cocktail (Ciprofloxacin, 20mg/100ml, Sigma-Aldrich; Ampicillin, 100mg/100ml, Sigma-Aldrich; Metronidazole, 100mg/ml, Sigma-Aldrich; Vancomycin, 50mg/100ml, Alfa Aesar) was administrated through drinking water either prophylactically (during 6 months on diet) either therapeutically (for 8 weeks, between 4 and 6 months on diet). Animals were sacrificed at the endpoint of 6

months on diet; serum and organs were harvested for biochemical, molecular analysis and for immunohistochemistry (IHC) and flow cytometry (FACS) analysis.

5.2 Measurements of serum parameters

Serum was isolated from the heart blood after sacrifice, and parameters were measured on a Cobas Reader in collaboration with the Institute for Clinical Chemistry and Pathobiochemistry, TUM, Munich.

5.3 Measurements of hepatic triglycerides

Liver triglycerides were measured by crushing 20 - 50 mg of tissue in liquid with a pestle and adding 250µl 0.9% NaCl. After incubation on heat block for 10min, RT, 450rpm, 250µl ethanolic 0.5KOH was added, samples were vortexed and incubated for 30min, 71°C, 450rpm. 500µl 0.15M MgSO4 was added, and samples were vortexed. After centrifugation for 10min, RT, 13,000g supernatants were collected and analyzed by using optical densitometry O.D. 505 with 1:4 diluted liver samples by GPO-PAP from Roche Diagnostics.

The hepatic triglyceride assay was performed by Dominik Pfister.

5.4 Intraperitoneal glucose tolerance test

After overnight fasting, mice were i.p. injected with 5µl/gr body weight of a 20% glucose solution (NaCl, 0.9%). Blood glucose was measured using “Accu-chek Performa Glucometer” at the indicated time intervals, by puncturing the lateral tail vein.

5.5 Isolation and staining of lymphocytes (from liver, spleen & blood) for flow cytometry (FACS)

Mice were sacrificed and livers were dissected. Livers were incubated for up to 35min in 37°C with digestion buffer (Collagen IV 1:10 (60 U f.c.) and DNase I 1:100 (25 µg/ml f.c.)) and subsequently passed through a 100µm filter. Livers were Washed with RPMI1640 medium and subsequently centrifuged for 7min/300g/4°C. Lymphocyte enrichment was achieved by a 2-step Percoll gradient (20ml 25% Percoll/HBSS underlay with 20ml 50% Percoll/HBSS) and centrifugation for 15min/1800g/4°C (Acc:1 Dcc:0). Leukocytes were collected, washed with HBSS, centrifuged for 10min/700g/4°C, counted and transferred to a 15ml Falcon for a final washing step with FACS buffer (PBS supplemented with v/v 0.4% 0.5M EDTA pH= 8 and w/v 0.5% albumin fraction V (#90604-29-8)).

Isolation of splenic lymphocytes was done by passing spleens through a 100µm mesh and subsequent washing. Afterwards, an erythrocyte lysis using ACK-buffer 1x 2ml for 5 min RT and then a wash was performed.

Isolation of blood-derived lymphocytes was done by collection of blood in FACS buffer and performing erythrocyte lysis two times using ACK-buffer 1x 2ml for 5 min RT and then washing.

For T-cell restimulation, cells were incubated for 2h, 37°C, 5% CO_2 in RPMI 1640 supplemented with v/v 2% fetal calf serum using 1:500 Biolegend´s Cell Activation Cocktail (with Brefeldin A) (#423304) and 1:1000 Monensin Solution (1,000X) (#420701).

Staining was performed using Live/Dead discrimination by using DAPI or ZombieDyeNIR according to the manufacturer´s instructions. After washing (~400g, 5min, 4°C), cells were stained in 25µl of titrated antibody (table 4) master mix for 20min at 4°C and washed again. Samples for flow cytometric activated cell sorting (FACS) were then sorted. Samples for flow cytometry were fixed using eBioscience IC fixation (#00-8222-49) or Foxp3 Fix/Perm kit (#00-5523-00) according to the manufacturer´s instruction. Intracellular staining was performed in eBioscience Perm buffer (#00-8333-56).

Cells were analyzed using BD FACSFortessa, Sony spectral analyzer SP6800 and data were analyzed using FlowJo. For sorting, a FACS Aria II and a FACSAria FUSION in collaboration with the DKFZ FACS core facility were used.

5.6 Isolation and staining of lymphocytes from the lamina propria of the small intestine for flow cytometry (FACS)

Small intestines were transferred onto an ice basin station. Peyer's patches were removed and the intestines were flushed with PBS and lumen material was removed. The tissue was cut into small pieces (about 5mm each) and transferred in 20ml HBSS 2% FCS solution. The tissue pieces were put through a large piece of nitex mesh to rinse out mucus, and then picked out by using forceps, transferred in 10ml HBSS 2mM EDTA, were shaken manually and vigorously for about 10 seconds. The tissue was incubated for 20 min in the shaker at the highest speed (240rpm) at 37°C. Supernatant was discarded by filtering pieces through nitex mesh. The pieces were

rinsed with HBSS, transferred in 10ml HBSS 2mM EDTA, were shaken manually and vigorously for about 10 seconds and incubated for 20 min in the shaker at the highest speed (240rpm) at 37°C. Supernatant was discarded, the intestine pieces were rinsed with HBSS and filtered through a nitex mesh.

The tissue was digested in 15 ml IMDM (Gibco) +10% FCS containing 1mg/ml collagenase VIII (Sigma-Aldrich), was shaken manually for 15 seconds then incubated in shaker at the highest speed (240 rpm) at 37°C for about 15 minutes. The digested tissue was filtered through 100µm, then through 40µm filter, and was centrifuged at 400g for 10 minutes. The pellet was resuspended in RPMI1640 medium. Staining and cell analysis were performed as described above, in section 5.5.

Table 4: Flow cytometry antibodies

Fluorochrome	Name	Clone	Company
Alexa700	CD4	RM4-5	Biolegend
Alexa700	CD45	30-F11	Biolegend
APC	CD3	17A2	Biolegend
APC	CD44	IM7	Biolegend
APC	CD20	SA275A11	Biolegend
FITC	CD19	6D5	Biolegend
FITC	CD45	I3/2.3	Biolegend
FITC	IgA	C10-3	Biolegend
PE	CD69	H1.2F3	Biolegend
PE	IgM	RMM-1	Biolegend
PE/Cy7	CD3	17A2	Biolegend
PE/Cy7	CD19	6D5	Biolegend
PE/Dazzle	CD62L	MEL-14	Biolegend
PE/Dazzle	IgD	11-26c.2a	Biolegend
PerCP/Cy5.5	CD8a	53-6.7	Biolegend
PerCP/Cy5.5	I-A/I-E (MHCII)	M5/114.15.2	Biolegend
	CD16/32	93	Biolegend

5.7 Histology, immunohistochemistry, scanning and analysis

Tissues were fixed in 4% paraformaldehyde and paraffin-embedded at the Technical University of Munich (TUM) or at the DKFZ, Department of Chronic Inflammation and Cancer (Heidelberg). Briefly, 2µm sections from FFPE and cryo-preserved tissues were prepared and stained with Hematoxylin/Eosin or IHC antibodies (table 5) on a

Bond MAX (Leica). For Sudan Red staining, cryo sections (5µm) were cut and stained with Sudan Red (0.25% Sudan IV in ethanolic solution). Slides were scanned with SCN400 slide scanner (Leica) and analyzed either using ImageJ for area based staining.

The tissue preparation, staining and scanning were done by the technical assistants, Danijela Heide, Jenny Hetzer and Anne Jacob.

Table 5. IHC antibodies

Target	Dilution	Company
MHCII	1:500	Novus Biologicals
CD3	1:250	Zytomed
F4/80	1:120	Linaris
Collagen IV	1:50	Cedarlane
Ki-67	1:200	Thermo Scientific
B220	1:3000	BD Biosciences
IgA	1:200	DAKO
IgM	1:250	DAKO
IgG	1:200	DAKO

5.8 Isolation of RNA and quantitative real-time PCR

Total RNA from whole liver homogenates was isolated from frozen liver tissues according to the manufacturer's protocol using RNeasyMini Kit (Qiagen). The quantity and quality of the RNA was analyzed by Nanodrop analyzer (Thermo Scientific). For cDNA production 1 µg of RNA was used by using Quantitect Reverse Transcription Kit (Qiagen) according to the manufacturer's protocol. qRT-PCR was performed in duplicates in a in 384-well plate using Fast Start SYBR Green Master Rox (Roche) with custom made primers purchased from Eurofins with a 7900 HT qRT-PCR system (Applied Biosystems, Life Technologies Darmstadt, Germany). The primer sequences of the genes of interest were listed in table 6.

Table 6. Primer sequences

Gene	Forward primer	Reverse primer
Acad10	TGG CTG TGG GCT GGG AG	AAA TAG GAG CTG ACG GGC AC
Acat2	GAC CCC GTG GTC ATC GTC	CCA CAA CCT GCC GTC AAG A
Acat3	TGGCCACTTTGACAAGGAGAT	CTGTTGCATTAGCAGTTGTGA
Acot2	CTC GTC TTT CGC TGT CCT GA	CTC AGC GTC GCA TTT GTC CG
Acox3	GGG TGA TGG TCG GTG ACA TT	CGG ACA TCC TTA AAG GGG CT
Acsl1	ATC TGG TGG AAC GAG GCA AG	TCC TTT GGG GTT GCC TGT AG
Acsm2	GCC AGA CAG AAA CGG GAC TT	ACA TGC CGA TAG GCC AGA TG
Cpt1	CAG CTG CTG ACC TCT GAC C	AAA GTC ATT CCA GAC ACG CCA
Lipe	CTT CCA GTT ACC TGC CA	AAT CGG CCA CCG GTA AAG AG
Mvd	GAG GGA GAC CTC TCC GAA GT	GTC TGC ARG CCC ACT GTA CT
HL	CTA TGG CTG GAG GAA TCT G	TGG CAT CAT CAG GAG AAA G
Sqle	GCA ATC TAC GCC ACG TAT TTC T	GGG CCC GTG GTT TTG T
Lpl	TGG ATG AGC GAC TCC TAC TTC A	CGG ATC CTC TCG ATG ACG AA
EL	CTA TCC CAA TGG CGG TGA CTT C	CGT GCT CGC ATT TCA CCA TC
PPARd	GAA CAG CCA CAG GAG GAG AC	GAG GAA GGG GAG GAA TTC TG
GPAT	GCT GCA ACT GAG ACG AAC CT	AAG CCC CCA AGC TTG TGA AT
ABCA1	GTT TTG GAG ATG GTT ATA CAA TAG TTG T	TTC CCG GAA ACG CAA GTC
Acsbg1	ACTCGCAAACCAGCTCC	AGTACAGAAAGGTTCCAGGCG

5.9 Elisa assays

Serum, intestinal lumen and tissue samples were collected. ELISA plates (Nunc) were coated the night before with 100µl of the coated antibody (coating buffer: 0.1M $NaHCO_3$) and incubated at 4°C overnight. The next morning the plates were washed 4 times immersing in washing buffer (0.05% Tween 20 in PBS). 100µl/well were added of blocking buffer (2% w/v in PBS). The plate was incubated at room temperature (RT) for 1-2 hours and then the plate was washed 4 times. The diluents (0.5% BSA in PBS) were added in the wells, then the samples and the standard solutions that were serially diluted. The plate was incubated 90 min at RT and then washed 4 times. 100µl of secondary antibody was added and the plate was incubated for 30-60 min. at RT. After the incubation the plate was washed 4 times and 100µl of substrate buffer (0.1M $NaH_2PO_4.H_20$) and after 30-60 min. the colour reaction reached the optimal. The plate was read at OD450mm in a 96 well plate reader.

The dilution of all coating antibodies was 1:1000. The standards were diluted as follows: 6µl standard added to 94µl diluents, for IgA 12µl were added to 88µl diluents. Final concentration was 2µg/ml of antibody. The dilution of all secondary antibodies was 1:1000.

The ELISA assay was performed by Dr. Hai Li in Bern, Switzerland (lab of Prof. Dr. Andrew Macpherson). The respective antibodies were listed in table 7.

Table 7. ELISA antibodies

Immunoglobuln isotype	Coating antibody	Standard	Secondary antibody
IgM	Goat anti-mouse IgM (1020-01 Southern)	Purified mouse myeloma IgM (02-6800 Zymed)	Anti-mouse IgM µ chain specific; peroxidise conjugated (A8786 Sigma)
IgG_{2b}	Goat anti-mouse IgG_{2b} (1090-01 Southern)	Purified mouse myeloma IgG_{2b} (02-6300 Zymed)	Anti-mouse IgG γ chain specific; peroxidise conjugated (A3673 Sigma)
IgA	Goat anti-mouse IgA (1040-01 Southern)	Purified mouse IgA (553476 PharMingen)	Anti-mouse IgA α chain specific; peroxidise conjugated (A4789 Sigma)

5.10 16s microbiome sequencing

Fresh mouse faecal samples were collected and were snap-frozen in liquid nitrogen. The 16s sequencing was performed by Catherine Mooser in Bern, Switzerland (lab of Prof. Dr. Andrew Macpherson), using the QIME pipeline version 1.8.0.

5.11 Non-Alcoholic Fatty Liver Disease (NAFLD) activity score (NAS)

For the grading of NAFLD-NASH, NAS was used accordingly[189]. Mouse liver sections stained with Hematoxylin/Eosin were evaluated and the score was calculated as the sum of the scores for steatosis (0-3), lobular inflammation (0-3), and ballooning (0-2), and ranges from 0 to 8 as described in table 8.

Table 8. Components of nonalcoholic fatty liver disease activity score

Item	Definition	Score
	<5%	0
Steatosis	5% - 33%	1
	>33%-66%	2
	>66%	3
	No foci	0
Lobular inflammation	<2 foci per 200x field	1
	2-4 foci per 200x field	2
	>4 foci per 200x field	3
	None	0
Ballooning	Few ballooning hepatocytes	1
	Many ballooning hepatocytes	2

5.12 Statistical analysis

Mouse data are presented as the mean±SEM. Statistical analysis was performed using GraphPad Prism software version 7.03 (GraphPad Software). All data were analyzed by unpaired, parametric t test and when comparing multiple groups by ordinary one-way ANOVA with Turkey's multiple comparison test. Statistics for HCC incidence were calculated using Fisher's exact test. Statistical significance is indicated as follows:*$p < 0.05$, **$p < 0.01$, ***$p < 0.001$ and ****$p < 0.0001$.

6. Results

6.1. B cells are required for NASH and NASH-driven HCC development

We first wanted to investigate the effects on NASH, as it was previously described in C57BL/6J (WT) mice [88], and subsequent HCC development of long-term CD-HFD feeding on body weight, glucose metabolism and liver integrity, in $JH^{-/-}$ mice lacking mature B cells [190].

6.1.1. Long term CD-HFD leads to metabolic syndrome, liver fibrosis and NASH in WT mice but not in JH-/-

As previously described, WT CD-HFD mice showed a constant rise in body weight **(fig. 6A)** compared with ND mice. Interestingly $JH^{-/-}$ CD-HFD mice started to gain significantly more weight (than ND mice) around nine months of age, reaching the same levels of body weight as their WT CD-HFD counterparts at the age of twelve months. Absence of liver steatosis as determined by Hematoxylin and Eosin (H/E) staining of liver sections and NAFLD activity score (NAS) **(fig. 6B, C)**. Strikingly, liver damage, normally seen in WT CD-HFD, was abrogated in $JH^{-/-}$ CD-HFD, as serum analysis revealed reduction in alanine transaminase (ALT) levels in $JH^{-/-}$ CD-HFD**(fig. 6D)**. $JH^{-/-}$ CD-HFD serum cholesterol and hepatic triglycerides levels were also decreased **(fig. 6E, F)**; consistently Sudan red staining of liver sections showed a strong decrease of large lipid droplets **(fig. 6G)**. Moreover, Sirius red staining of $JH^{-/-}$ CD-HFD livers revealed absent perisinusoidal fibrosis, in contrast to WT CD-HFD livers **(fig. 6H)**. WT CD-HFD mice developed fibrosis with an incidence of 28.57% for mild and severe and 42.85% for moderate **(fig. 6I).** Metabolic analysis with an intraperitoneal glucose tolerance test (IPGTT) revealed a normal glucose response in $JH^{-/-}$ in contrast to WT CD-HFD **(fig. 6J)**. Transcriptional analysis demonstrated that the deregulation of several genes involved in lipid metabolism observed in WT CD-HFD is prevented in $JH^{-/-}$ CD-HFD mice **(fig. 6K)**.

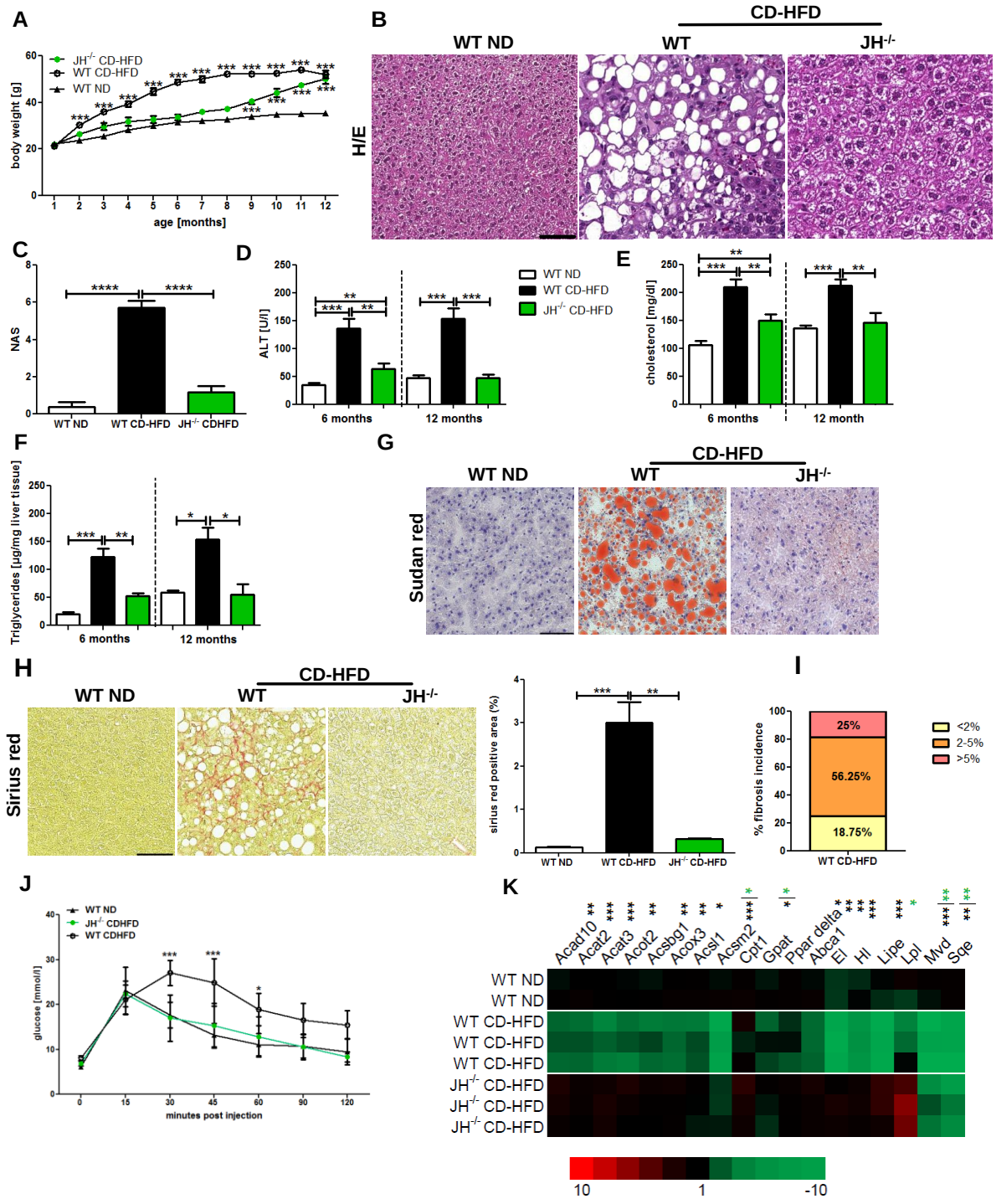

Figure 6. B cells are playing a role in NASH development

(A) Weight development in male WT ND, CD-HFD and JH$^{-/-}$ CD-HFD mice (n=20). **(B)** Representative H&E staining of 12-month-old, WT ND, WT CD-HFD mice illustrating NASH, and JH$^{-/-}$ CD-HFD showing absence of NASH. **(C)** NAFLD score (NAS) for the three respective groups. **(D)** Quantification of serum ALT in male 6- and 12-month-old WT and JH$^{-/-}$ mice (n=10 each). **(E)** Quantification of serum cholesterol in male 6- and 12-month-old WT and JH$^{-/-}$ mice (n=10 each). **(F)** Quantification of hepatic triglycerides in male 6- and 12-month-old WT and JH$^{-/-}$ mice (n=6 each). **(G)** Representative Sudan red staining illustrating fat accumulation in livers of WT ND, WT CD-HFD and JH$^{-/-}$ CD-HFD mice. To the right, quantification of total Sudan red^{+} area (n=6 each).

(H) Representative Sirius red staining illustrating the status of perisinusoidal fibrosis in livers of WT ND, WT CD-HFD and JH$^{-/-}$ CD-HFD mice. To the right, quantification of total Sirius red^{+} area (n=6 each). **(I)** Incidence of fibrosis as it was quantified through total Sirius red^{+} area in WT ND and CD-HFD livers (n=10 each). **(J)** Glucose tolerance test performed with 9-month-old male mice (n=6 each). **(K)** Real-time PCR analysis for lipid metabolism genes on mRNA isolated from WT ND and CD-HFD and JH$^{-/-}$ CD-HFD livers.
The scale bar represents 100 µm. All data are presented as mean ± SEM.

6.1.2 Differential fat deposition in JH$^{-/-}$ CD-HFD mice

JH$^{-/-}$ CD-HFD liver-to-body weight ratio was reduced **(fig. 7A)** in agreement with the whole-body echo magnetic resonance (MRI) analysis that showed an increase in JH$^{-/-}$ fat mass. The subcutaneous (inguinal) white adipose tissue was significantly reduced but not the perigonadal white adipose tissue **(fig. 7B, C).**

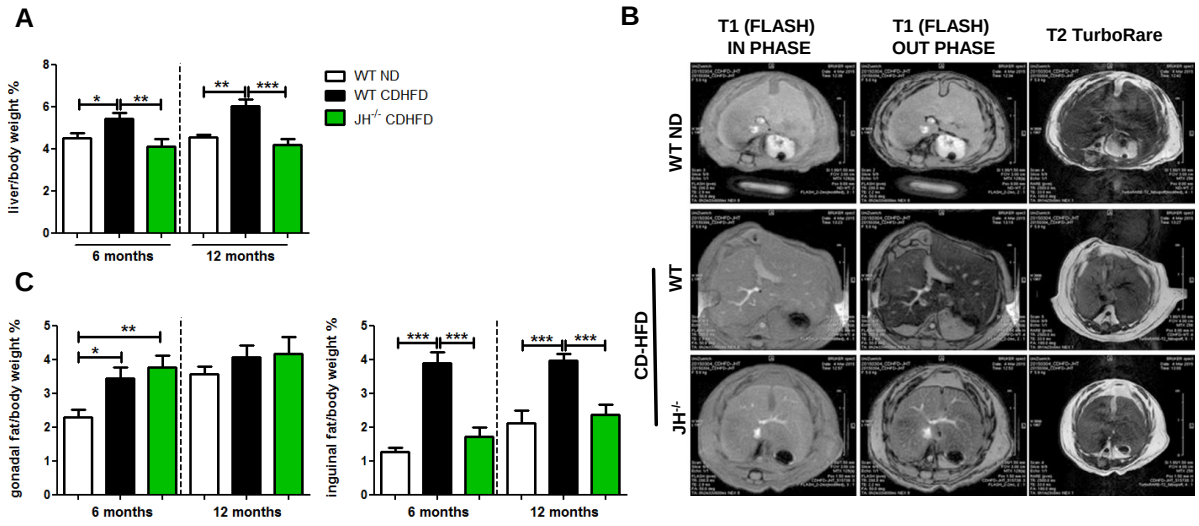

Figure 7. In JH$^{-/-}$CD-HFD mice the fat deposition is affected
(A) Quantitative analysis of liver-to-body weight ratio of WT ND, CD-HFD and JH$^{-/-}$ CD-HFD livers in 6- and 12-month-old mice (n=10 each). **(B)** MRI analyses on livers of 12-month-old WT ND, CD-HFD and JH$^{-/-}$ CD-HFD mice. T1 (fast low-angle shot [FLASH]) OUT phase: dark color indicative of steatosis. T2. TurboRare visualizes increase in subcutaneous and abdominal fat and hepatic lipid accumulation (bright regions) in CD-HFD mice. **(C)** Quantitative analysis of perigonadal white adipose tissue and inguinal white adipose tissue-to-body weight ratio of 6- and 12-month-old WT ND, CD-HFD and JH$^{-/-}$ CD-HFD mice (n=10 each).
All data are presented as mean ± SEM.

6.1.3 Hepatic infiltration and activation of immune cells in C57BL/6 but not in JH$^{-/-}$ CD-HFD mice

Flow cytometry analysis (FACS) showed an absence of CD19^{+} B cells in the liver and significantly fewer hepatic CD3^{+} T cells in JH$^{-/-}$ CD-HFD mice **(fig. 8A)**. Moreover, FACS showed a significant reduction of activated hepatic CD4^{+} T cells in JH$^{-/-}$ CD-HFD mice compared to WT CD-HFD **(fig. 8B)**. Accordingly, IHC showed a reduction of CD3^{+} T cells and CD3^{+} foci **(fig. 8C, D)**. Further IHC analysis revealed

no B220^{+} positivity in the JH$^{-/-}$ CD-HFD livers **(fig. 8E, F, upper row)**, and decrease in F4/80^{+} and MHCII^{+} cells compared to WT CD-HFD **(fig. 8E, F, middle and lower row).**

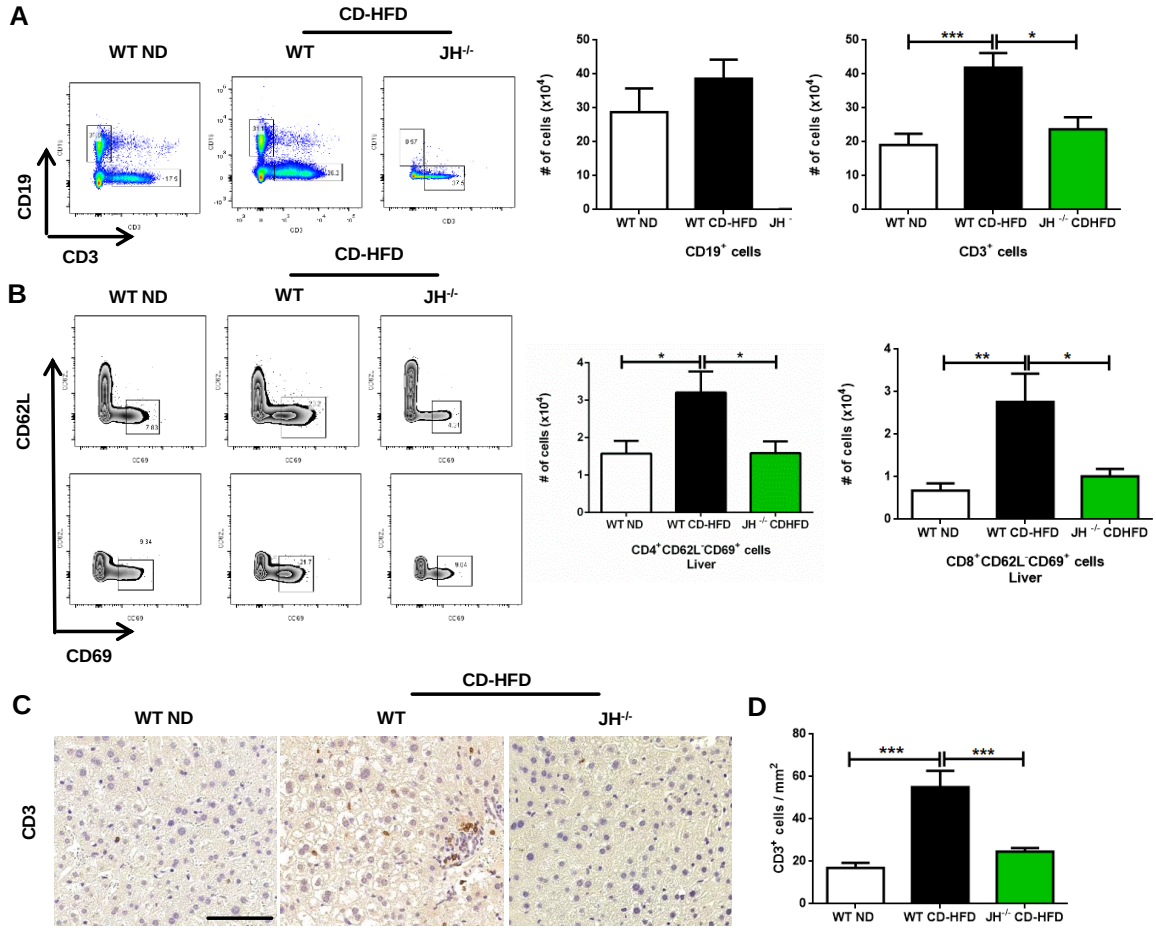

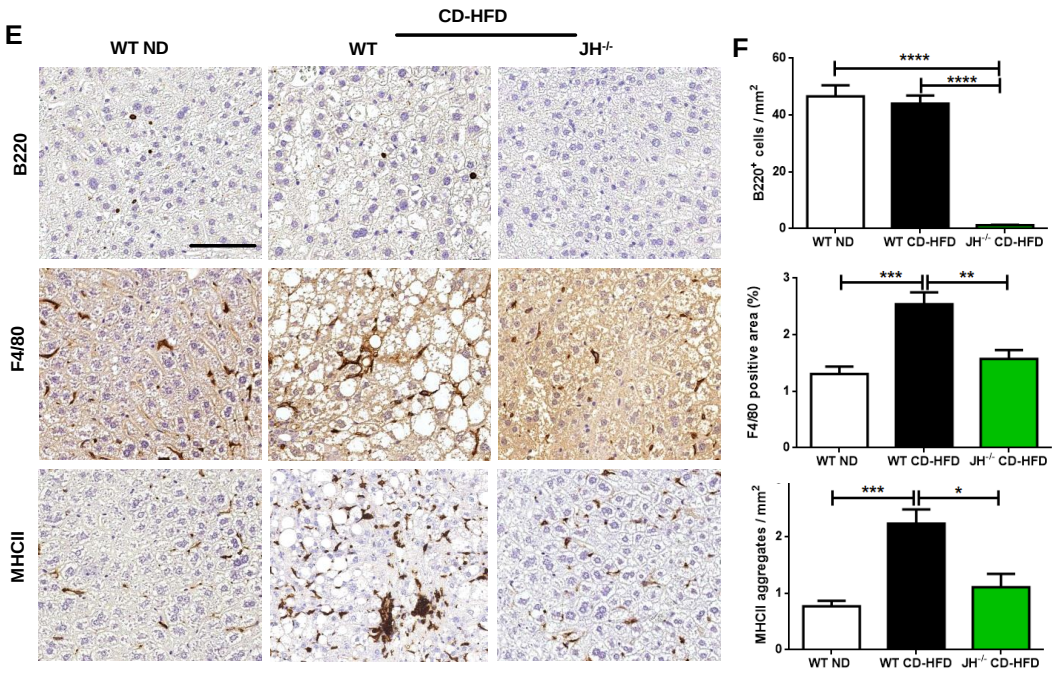

Figure 8. In the absence of B cells, CD-HFD does not induce infiltration and activation of hepatic lymphocytes

(A,B) Representative zebra plots and quantifications of flow cytometric analyses comparing 6-month-old WT ND, CD-HFD and $JH^{-/-}$ CD-HFD mice (n≥6); **(A)** $CD19^{+}CD3^{-}$ B cells, $CD19^{-}CD3^{+}$ T cells and **(B)**, $CD69^{+}CD4+CD62L^{-}$ T cells. **(C, D)** Representative histology and IHC on liver sections of 6-month-old WT ND, CD-HFD and $JH^{-/-}$ CD-HFD; **(C)** CD3 and quantification of $CD3^{+}$ T cells per mm^2 (n=6) **(D)**. **(E, F)** Representative histology and IHC on liver sections of 6-month-old WT ND, CD-HFD and $JH^{-/-}$ CD-HFD; **(E)** B220, F4/80 and MHCII and quantification of the respective cells per mm^2 (n=6) **(F).**

The scale bar represents 100 µm. All data are presented as mean ± SEM.

6.1.4 WT CD-HFD mice develop HCC but not $JH^{-/-}$

Of 61 $JH^{-/-}$ CD-HFD mice that were sacrificed at 12 months, none displayed tumors macro- or microscopically, contrary to WT CD-HFD mice which developed tumors at an incidence of ~25% as previously reported **(fig. 9A, B)**.

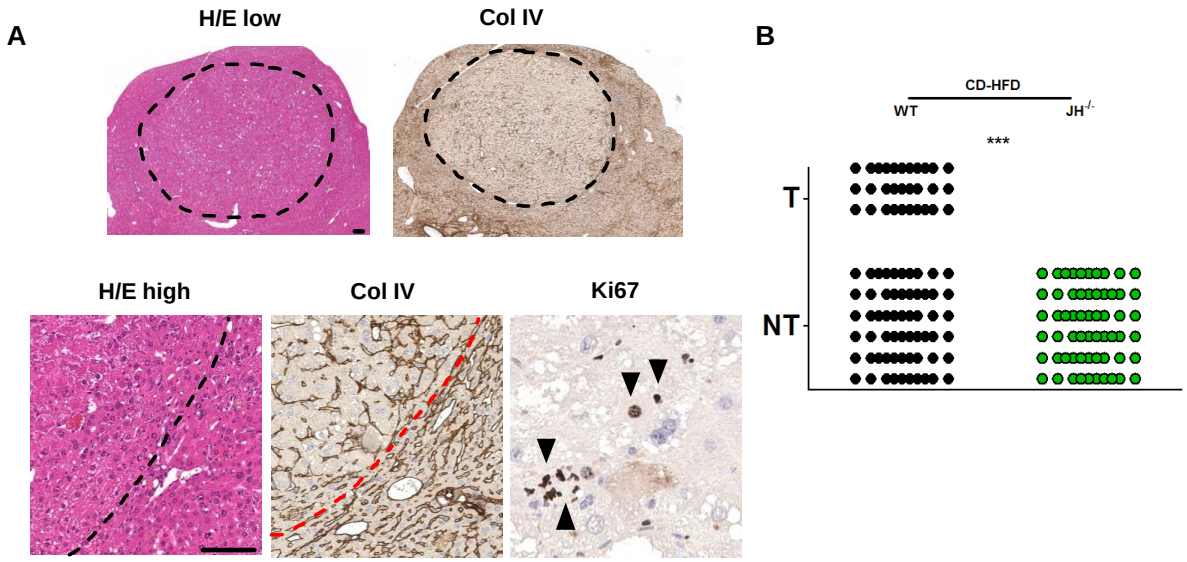

Figure 9. Absence of B cells leads to absence of NASH-driven HCC development in long-term JH$^{-/-}$ CD-HFD mice

(A) H/E and IHC of liver derived from 12-month-old WT CD-HFD mice with HCC. Dashed lines depict HCC border. The scale bars represent H/E: 100 µm (low) and 100 µm (high); collagen IV: 100 µm; Ki67: 100 µm (depicted by arrowheads). **(B)** Graph summarizing C57BL/6 mice without tumor (NT) and with tumor (T) on WT and JH$^{-/-}$ CD-HFD. Symbols depict individual mice.

6.1.5 Therapeutic αCD20 treatment abrogates NASH and fibrosis in C57BL/6 CD-HFD mice but not glucose intolerance

In order to further evaluate the importance of B cells in NASH development, we treated WT mice fed with CD-HFD intraperitoneally (i.p.) (**fig. 10A)** for four months with an antibody that depletes CD20^{+} cells (GenTech, clone 5D2). The treatment lasted for 6 weeks while the mice were continuously under CDHFD **(fig. 10B, C)**. From our studies we have seen that NASH starts to escalate already by month three under diet and by month four we can observe the presence of NASH (**fig. 10D, E)**. The WT CD-HFD αCD20 treated livers showed NASH abrogation as determined by H/E staining **(fig. 10F, G)**. Accordingly, ALT **(fig. 10H)** levels were reduced compared to mock (treated ip with IgG) and untreated WT CD-HFD mice. Serum cholesterol remained at high levels **(fig. 10I)**, whereas hepatic triglycerides were decreased **(fig. 10J)**. Consistently, Sudan red staining in liver sections showed a strong decrease of large lipid droplets **(fig. 10K, upper row)**. Sirius red staining of WT CD-HFD αCD20 treated livers demonstrated an absence of perisinusoidal fibrosis compared to WT CD-HFD mock and untreated livers **(fig. 10K, lower row)**. In contrast, IPGTT test showed an impaired glucose response in WT CD-HFD αCD20 mice, similar to mock and untreated WT CD-HFD **(fig. 10L)**.

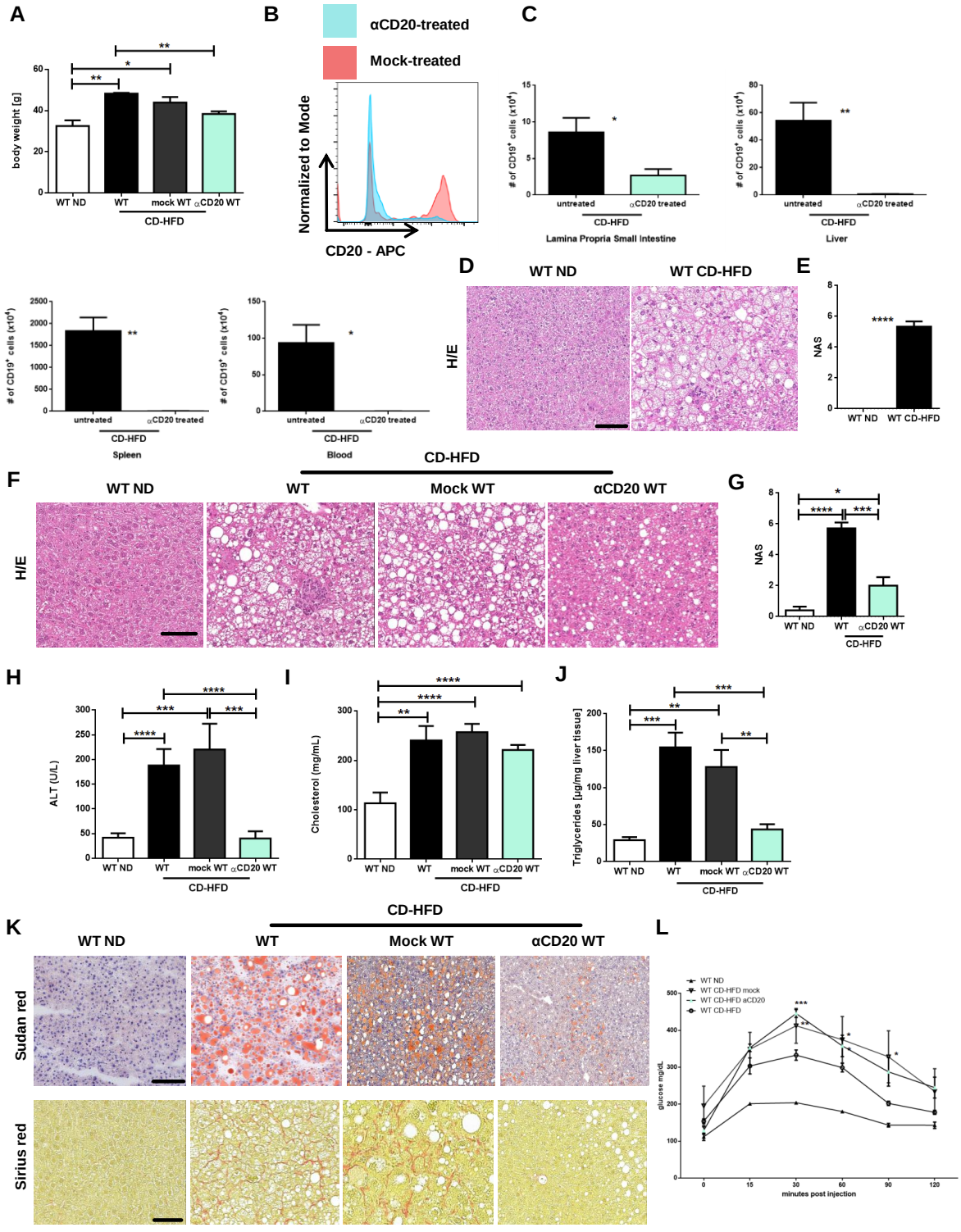

Figure 10. NASH development depends on the presence of B cells

(A) Body weight in male WT ND, CD-HFD, CD-HFD mock (i.p. injection of IgG) and WT αCD20 CD-HFD mice (n=6 each). **(B-C)** Flow cytometric analyses and quantification of the efficacy of $CD20^{+}$ depletion in lamina propria of the small intestine, liver, spleen and blood. $CD19^{+}$ B cells (n=3 each). **(D)** Representative H&E staining of 4-month-old WT ND and CD-HFD mice illustrating NASH. **(E)** NAFLD score (NAS) for the livers derived from 4-month-old WT ND and CD-HFD mice (n=3 each). **(F)** Representative H&E staining of 6-month-old WT ND, CD-HFD, CD-HFD mick, αCD20 CD-HFD livers illustrating absence of NASH for the WT αCD20 CD-HFD.

(G) NAFLD score (NAS) for the livers derived from 6-month-old WT ND, CD-HFD and αCD20 CD-HFD mice (n=6 each). **(H)** Quantification of serum ALT in the 6-month-old respective groups (n=6 each). **(I)** Quantification of serum cholesterol in the 6-month-old respective groups (n=6 each). **(J)** Quantification of hepatic triglycerides in the 6-month-old respective groups (n=6 each). **(K)** Upper row: Representative Sudan red staining illustrating fat accumulation in livers of the four groups. To the right, quantification of total Sudan red^{+} area. Lower row: Sirius red staining illustrating the status of perisinusoidal fibrosis in livers of the respective groups (n=6 each). **(L)** Glucose tolerance test performed with 6-month-old male mice (n=6 each).
The scale bar represents 100 µm. All data are presented as mean ± SEM.

6.1.6 Fat deposition in WT αCD20 CD-HFD mice

In αCD20 treated CD-HFD mice, liver-to-body weight ratio was reduced **(fig. 11A)**. Similar to the JH$^{-/-}$ CD-HFD mice, the inguinal white adipose tissue was significantly reduced but not the perigonadal white adipose tissue **(fig. 11B).**

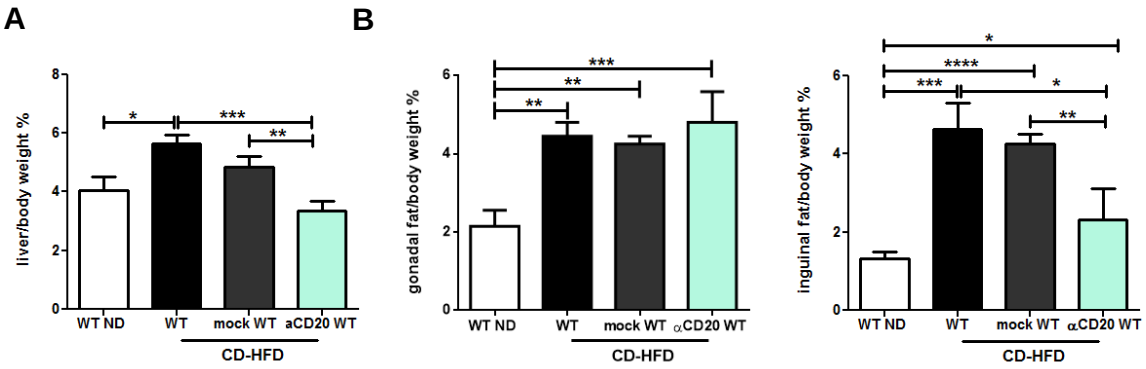

Figure 11. In αCD20 treated mice the fat deposition is affected
(A) Quantitative analysis of liver-to-body weight ratio of WT ND, CD-HFD, CD-HFD mock and αCD20 CD-HFD livers in 6-month-old mice (n=6 each). **(B)** Quantitative analysis of perigonadal white adipose tissue and inguinal white adipose tissue-to-body weight ratio of the respective 6-month-old mice (n=6 each).
All data are presented as mean ± SEM.

6.1.7 Hepatic infiltration and activation of immune cells is abolished in C57BL/6 CD-HFD mice by αCD20 therapeutic treatment

FACS analysis showed a strong reduction of activated hepatic CD4^{+} T cells in treated mice compared to WT CD-HFD **(fig. 12A)**. Accordingly, IHC showed a reduction of CD3^{+} T cells and CD3^{+} foci as it was shown by CD3^{+} staining in liver sections **(fig. 12B, C)**. Further IHC analysis revealed strong reduction (depletion) of B220^{+} cells and decrease of F4/80^{+} and MHCII^{+} cells in WT CD-HFD αCD20 treated livers **(fig. 12D, E).**

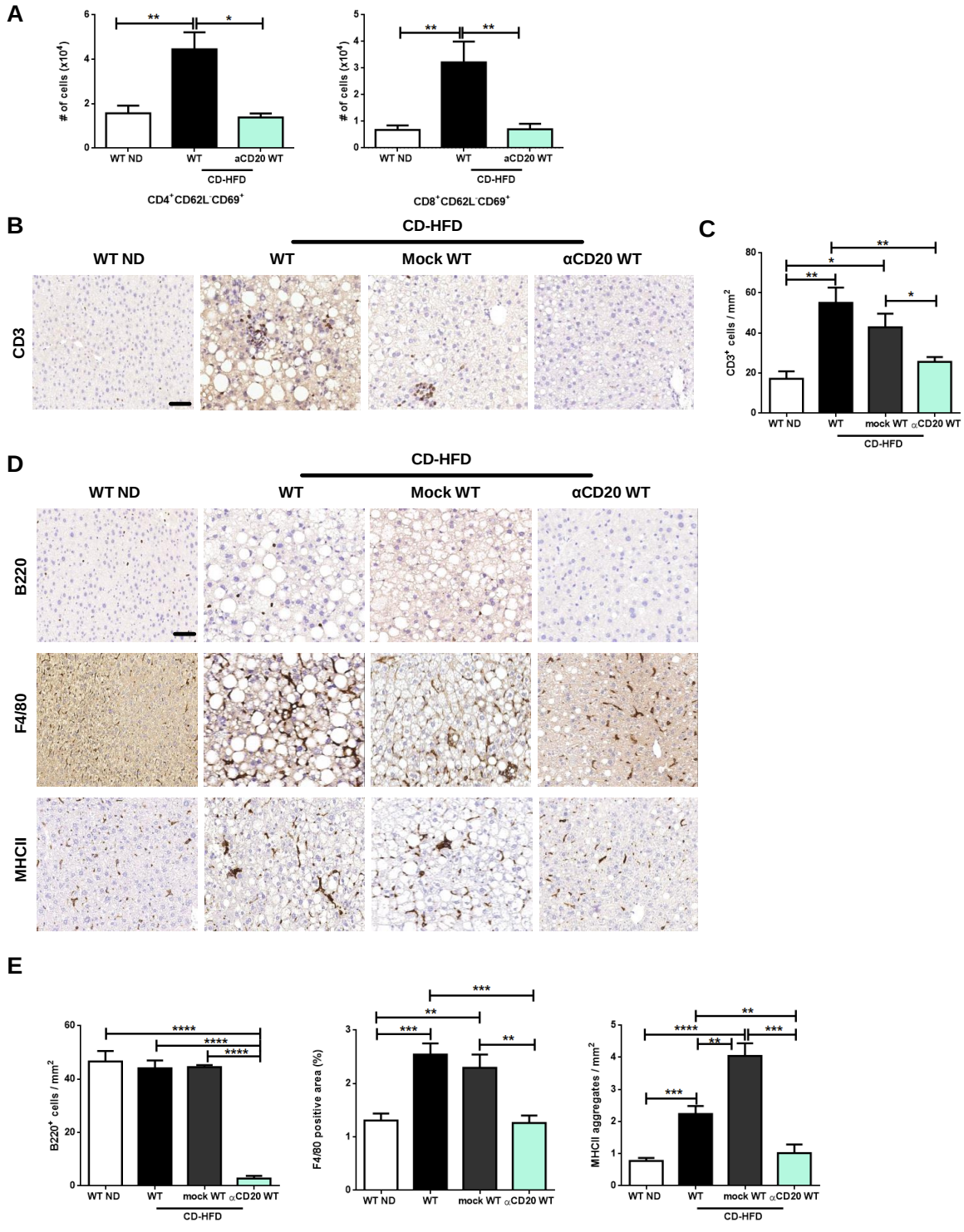

Figure 12. Therapeutic depletion of B cells leads to abrogation of infiltration and activation of lymphocytes in CD-HFD livers

(A) Quantification of flow cytometric analysis comparing 6-month-old WT ND, CD-HFD, CD-HFD mock and αCD20 CD-HFD mice (n≥3); $CD69^{+}CD4{+}CD62L^{-}$ T cells. **(B - D)** Representative histology and IHC of liver sections from the respective groups; **(C)** CD3 and quantification of $CD3^{+}$ T cells per mm^2 (n=6), **(D)** B220, F4/80 and MHCII, **(E)** Quantification of $B220^{+}$, $F4/80^{+}$ and $MHCII^{+}$ cells per mm^2 (n=6). The scale bar represents 100 µm. All data are presented as mean ± SEM.

6.2. Intestinal B cell response in the lamina propria of the small intestine is sufficient to induce NASH

Next we wanted to corroborate the $JH^{-/-}$ CD-HFD data using μMT, another B –cell deficient mouse line. These mice are lacking mature B-cells apart from IgA^+ B cells in the gut[191].

6.2.1 μMT mice express $CD20^+$ IgA^+ B cells in the lamina propria of the small intestine

It has been shown by Macpherson et al[191] that IgA^+ B cells can be also found in the μMT spleen in low numbers. We observed $B220^+$ cells by IHC staining but not with IHC IgA^+ staining or FACS **(fig. 13A, C)**. μMT liver sections were negative for $B220^+$ by IHC and $CD19^+$ by FACS and IgA^+ by IHC **(fig. 13B, C)**. Similar to what has been reported, we observed the presence of IgA^+ B cells in the lamina propria of the μMT small intestine (LP SI) by IHC and FACS **(fig. 13D, E)**. In addition, we were able to identify that the specific B cell population that populates the LP SI is $CD20^+$ IgA^+ **(fig. 13F, G)**.

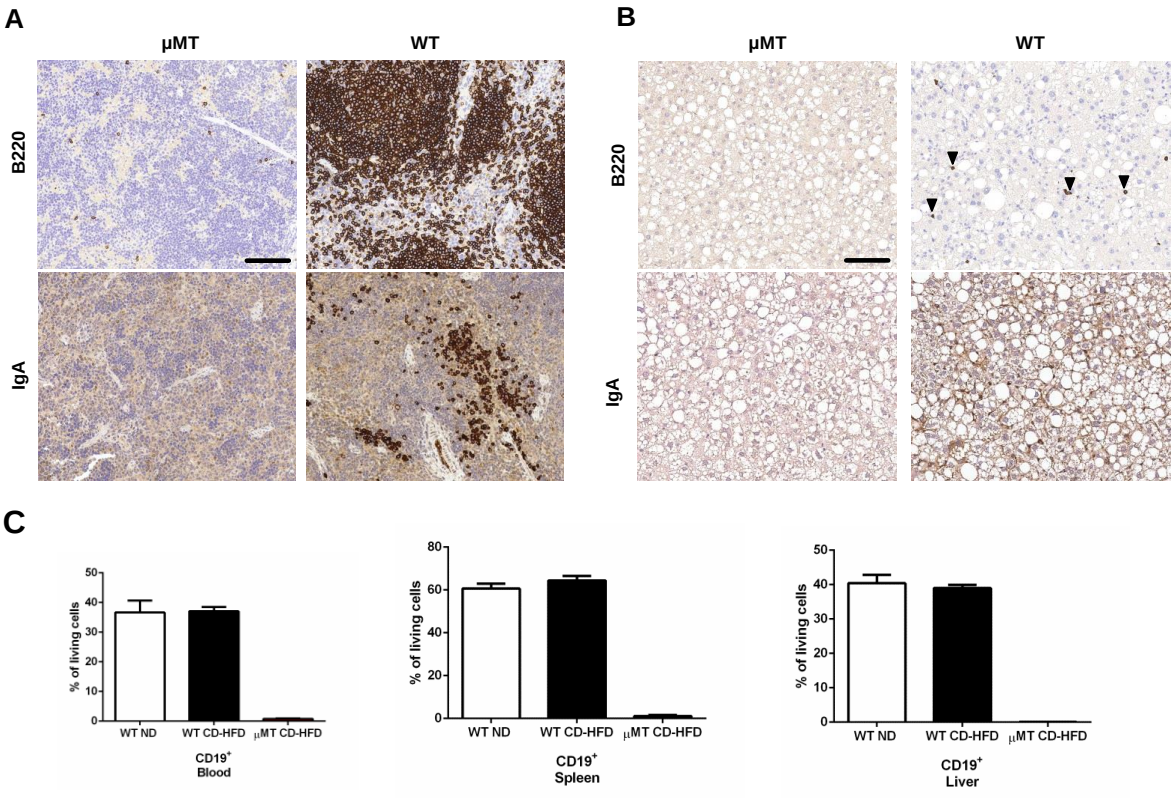

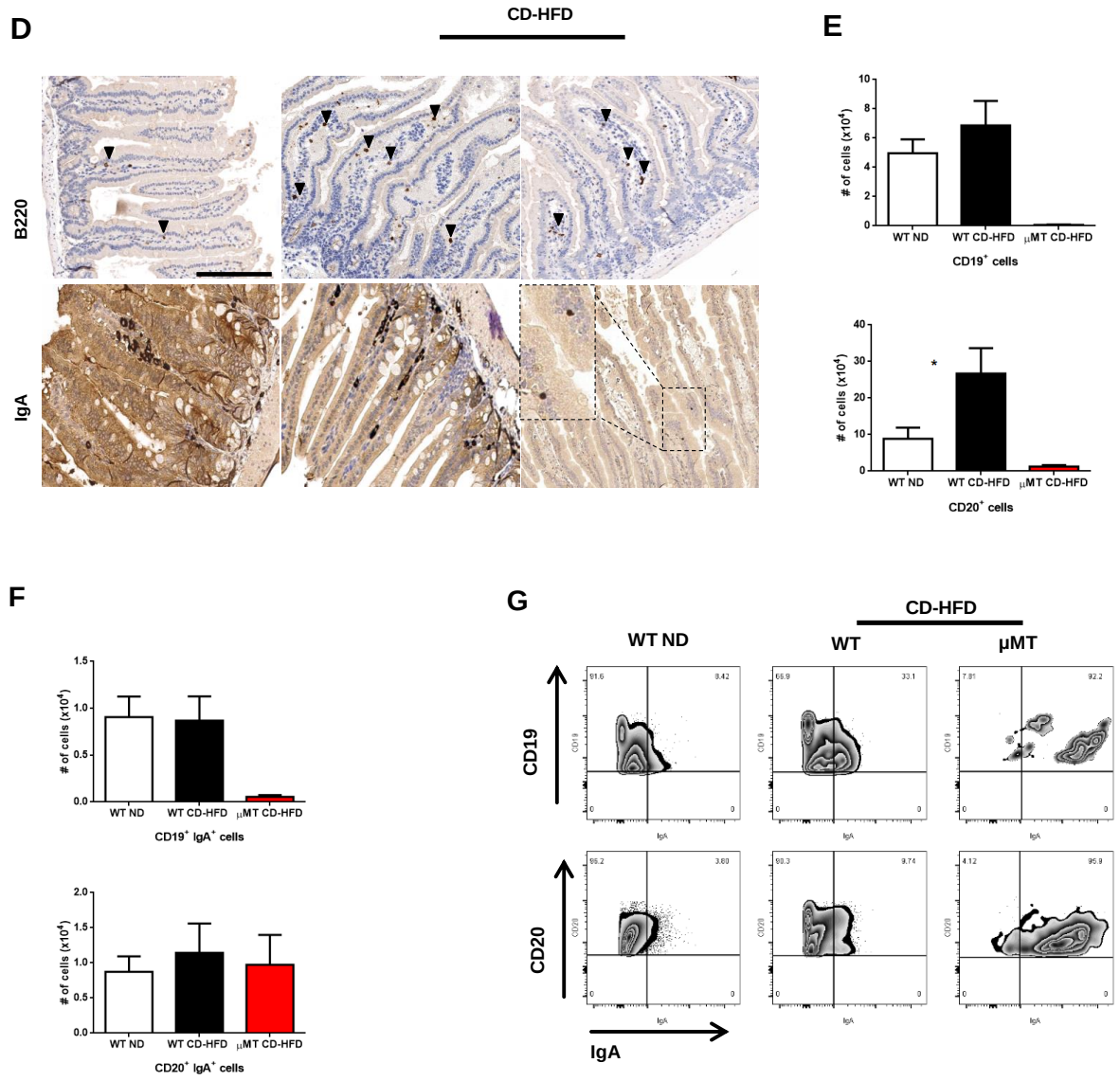

Figure 13. B cells in the lamina propria of the small intestine in WT and µMT mice

(A, B) Representative IHC of (A) spleen and (B) liver sections from 6-month-old WT and µMT mice. Upper row: B220. Lower row: IgA. **(C)** Quantification of flow cytometric analyses of 6-month-old WT ND, CD-HFD and µMT CD-HFD mice. From left to right: blood, spleen, liver, $CD19^+$ B cells. **(D)** Representative IHC of the small intestine derived from 6-month-old WT and µMT mice. Upper row: B220. Lower row: IgA. **(E, F)** Quantification of flow cytometric analyses of the lamina propia of the small intestine derived from 6-month-old WT ND, CD-HFD and µMT CD-HFD mice; **(E)** Upper graph: $CD19^+$ B cells. Lower graph: $CD20^+$ B cells, **(F)** Upper graph: $CD19^+$ IgA^+ B cells. Lower graph: $CD20^+$ IgA^+ B cells. **(G)** Representative zebra plots and quantifications of flow cytometric analyses comparing the lamina propria of the small intestine of 6-month-old WT ND, CD-HFD and µMT CD-HFD mice. The scale bar represents 100 µm. All data are presented as mean ± SEM. n=10 in each group.

6.2.2 Characterization of IgA^+ and IgM^+ B cell populations in the WT and μMT CD-HFD lamina propria small intestine

We wanted to further characterize the B cell populations in LP SI in WT ND, WT CD-HFD and μMT CD-HFD 6-month-old male mice. Flow cytometry revealed higher frequencies of $CD19^+$ and $CD20^+$ B cell populations in the WT CD-HFD LP SI when compared to WT ND, whereas in the LP SI of the μMT mice the dominant B cell population was $CD20^+$, as it was also shown above **(fig. 14A, B)**. Moreover, we observed higher frequencies in the WT CD-HFD LP SI of $CD19^+CD20^+$ B cells when compared to WT ND **(fig. 14A, B)**. The next step was to evaluate the immunoglobulin status of the populations of interest. In the WT CD-HFD LP SI, the frequencies of $CD19^+IgA^+$ and $CD19^+IgM^+$ cells were higher when compared to WT ND **(fig. 14C)**. Regarding the $CD20^+$ cells, the IgA^+ and IgM^+ cells had higher frequencies in the WT CD-HFD LP SI when compared with WT ND, whereas in the μMT CD-HFD LP SI, we observed higher frequencies of $CD20^+IgA^+$ cells when compared to WT ND and CD-HFD respectively **(fig. 14D)**. Finally, for the cell population $CD19^-CD20^-CD4^-CD8^-IgA^+$, which we regarded phenotypically as plasma cells, we noted higher frequencies in WT and μMT CD-HFD LP SI when compared to WT ND **(fig. 14E)**.

A

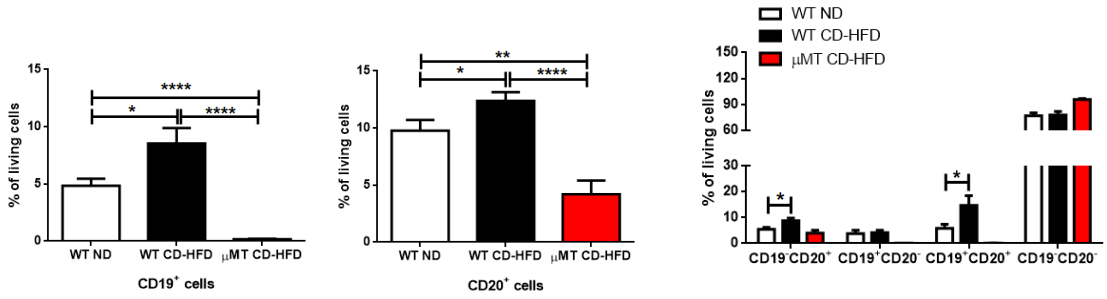

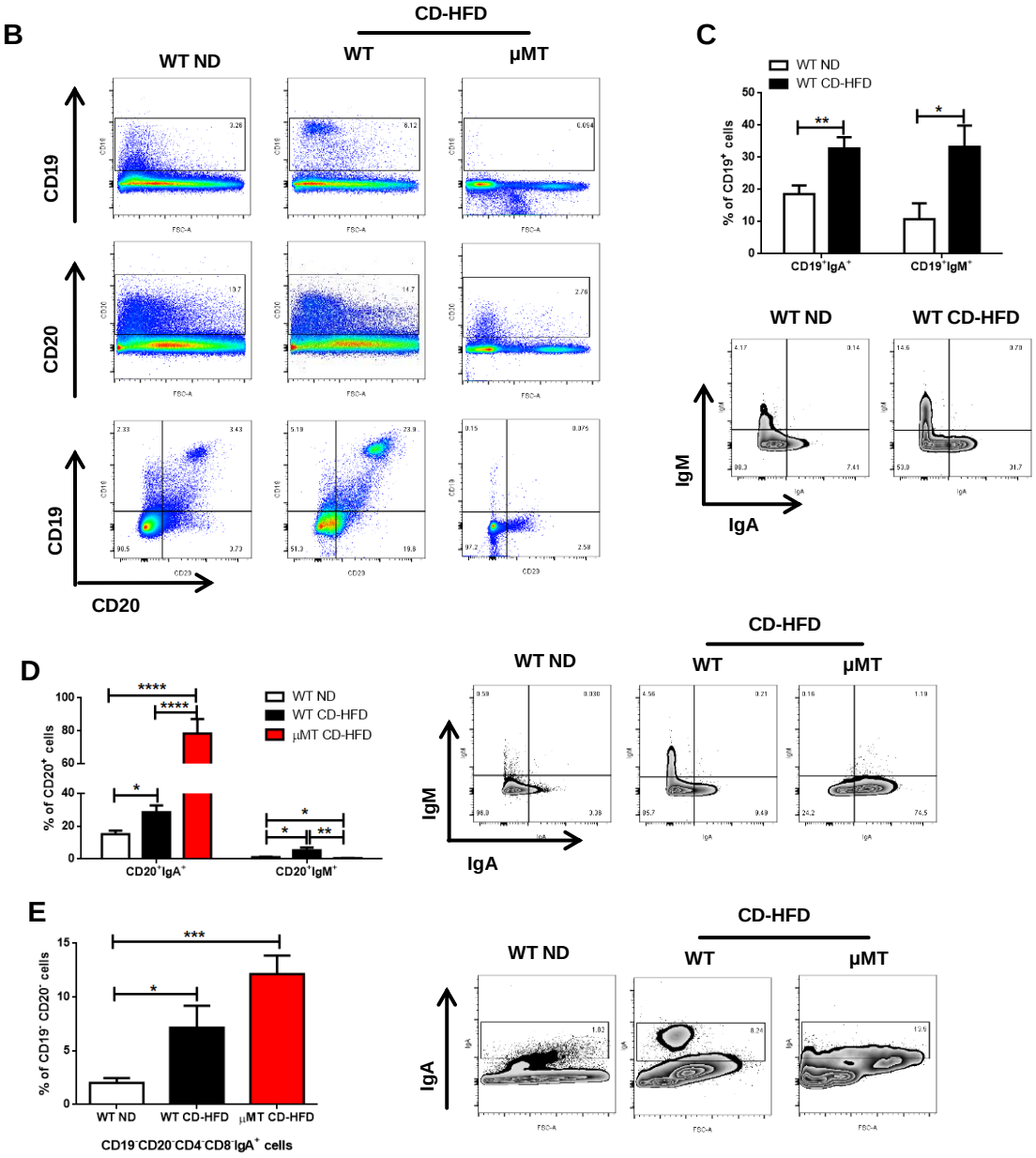

Figure 14. Frequencies of IgA$^+$ and IgM$^+$ B cells in the WT ND, CD-HFD and µMT CD-HFD lamina propria of the small intestine

(A, B) Frequencies and (B) representative pseudocolor plots of CD19$^{+/-}$ and CD20$^{+/-}$ B cell populations in the WT ND, CD-HFD and µMT CD-HFD LP SI. **(C)** Right: Frequencies of CD19$^+$IgA$^+$ and CD19$^+$IgM$^+$ B cells in the WT ND and CD-HFD LP SI. Left: representative zebra plots. **(D)** Right: Frequencies of CD20$^+$IgA$^+$ and CD20$^+$IgM$^+$ B cells in the WT ND, CD-HFD and µMT CD-HFD LP SI. Left: representative zebra plots. **(E)** Right: Frequencies of CD19$^-$CD20$^-$CD4$^-$CD8$^-$IgA$^+$ B cells in the WT ND, CD-HFD and µMT CD-HFD LP SI. Left: representative zebra plots. All data are presented as mean ± SEM. n=10 in each group.

6.2.3 Long term CD-HFD leads to metabolic syndrome and NASH in the absence of fibrosis in µMT CD-HFD mice

Contrary to JH$^{-/-}$ CD-HFD and similar to WT CD-HFD, µMT CD-HFD showed a constant rise in body weight compared to WT ND mice **(fig. 15A)**. H/E staining of

µMT CD-HFD liver sections showed the typical hallmarks of NASH **(fig. 15B, C)** and serum analysis revealed increased ALT **(fig. 15D)** levels in µMT CD-HFD compared to WT ND. µMT CD-HFD serum cholesterol and hepatic triglycerides were also increased **(fig. 15E, F)**. Consistently, Sudan red staining of µMT CD-HFD liver sections showed accumulation of large lipid droplets **(fig. 15G)**. Sirius red staining of µMT CD-HFD livers showed an absence of perisinusoidal fibrosis, accordingly to what has been previously reported [101] **(fig. 15H)**. Transcriptional analysis demonstrated that the deregulation of several genes involved in lipid metabolism observed in WT CD-HFD was not prevented in µMT CD-HFD mice **(fig. 15I)**. IPGTT test showed an impaired glucose response in µMT CD-HFD, similar to WT CD-HFD **(fig. 15J)**.

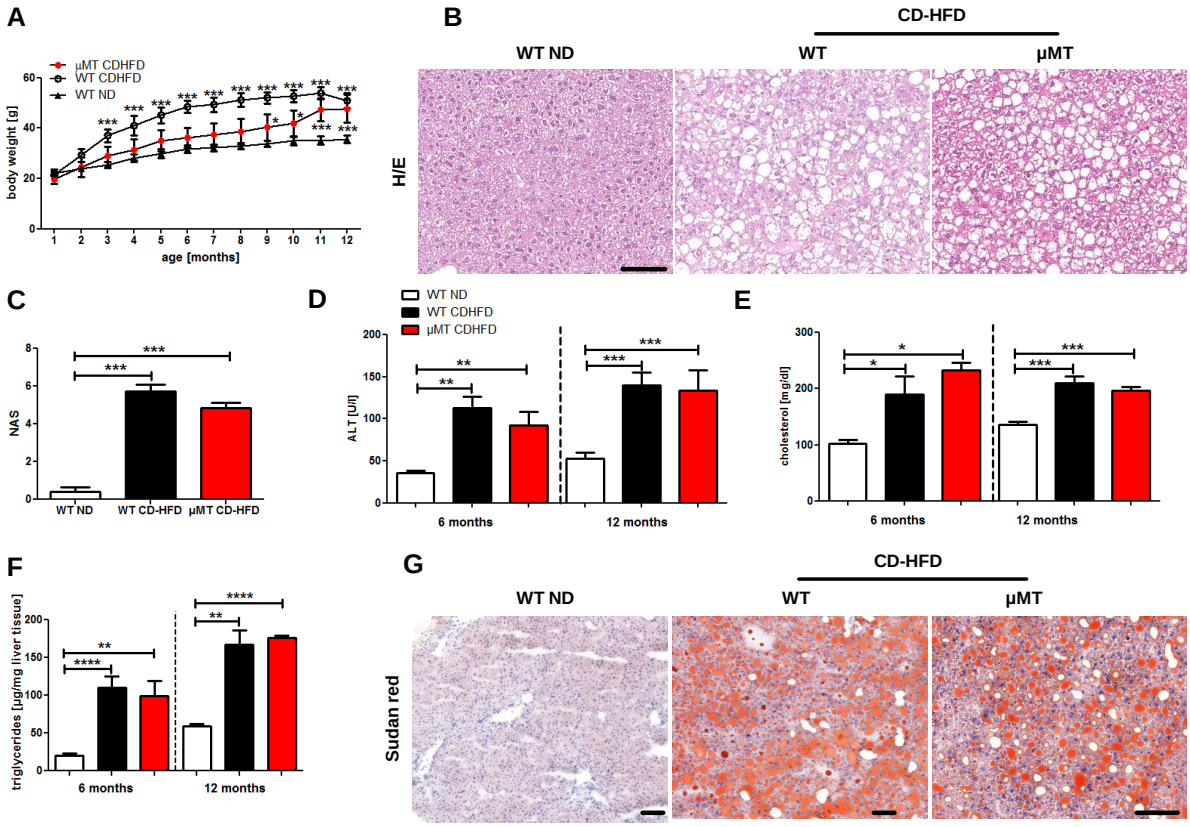

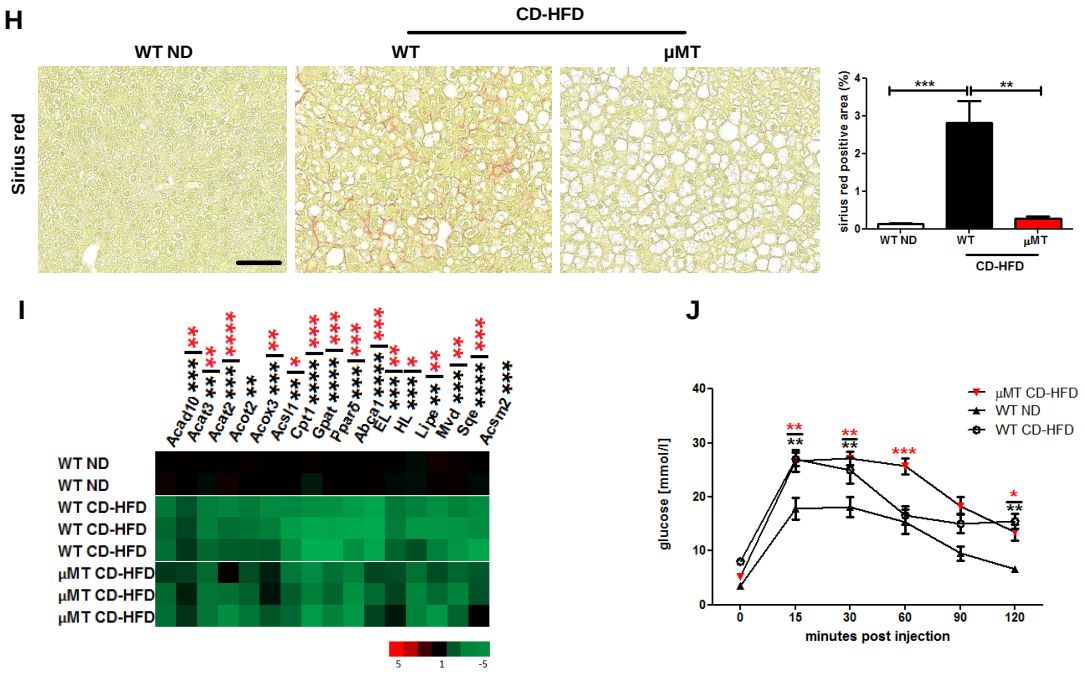

Figure 15. Intestinal B cells play a role in NASH development and in fibrosis in µMT CD-HFD mice
(A) Weight development in male WT ND, CD-HFD and µMT CD-HFD mice (n=20). **(B)** Representative H&E staining of 12-month-old, WT ND, WT CD-HFD and µMT CD-HFD mice illustrating NASH. **(C)** NAFLD score (NAS) for the three respective groups. **(D)** Quantification of serum ALT in male 6- and 12-month-old WT and µMT mice (n=10 each). **(E)** Quantification of serum cholesterol in male 6- and 12-month-old WT and µmT mice (n=10 each). **(F)** Quantification of hepatic triglycerides in male 6- and 12-month-old WT and µMT mice (n=6 each). **(G)** Representative Sudan red staining illustrating fat accumulation in livers of WT ND, WT CD-HFD and µMT CD-HFD mice. To the right, quantification of total Sudan red^{+} area (n=6 each). **(H)** Representative Sirius red staining illustrating the status of perisinusoidal fibrosis in livers of WT ND, WT CD-HFD and µMT CD-HFD mice. To the right, quantification of total Sirius red^{+} area (n=6 each). **(I)** Real-time PCR analysis for lipid metabolism genes on mRNA isolated from WT ND and CD-HFD and µMT CD-HFD livers. **(J)** Glucose tolerance test performed with 9-month-old male mice (n=6 each). The scale bar represents 100 µm. All data are presented as mean ± SEM.

6.2.4 Fat deposition in µMT CD-HFD mice

µMT CD-HFD liver-to-body weight ratio was not increased compared to ND **(fig. 16A)**. MRI analysis showed increase an in fat mass **(fig. 16B)**, as well as perigonadal white adipose tissue and inguinal white adipose tissue compared to WT ND, similar to WT CD-HFD **(fig. 16C)**.

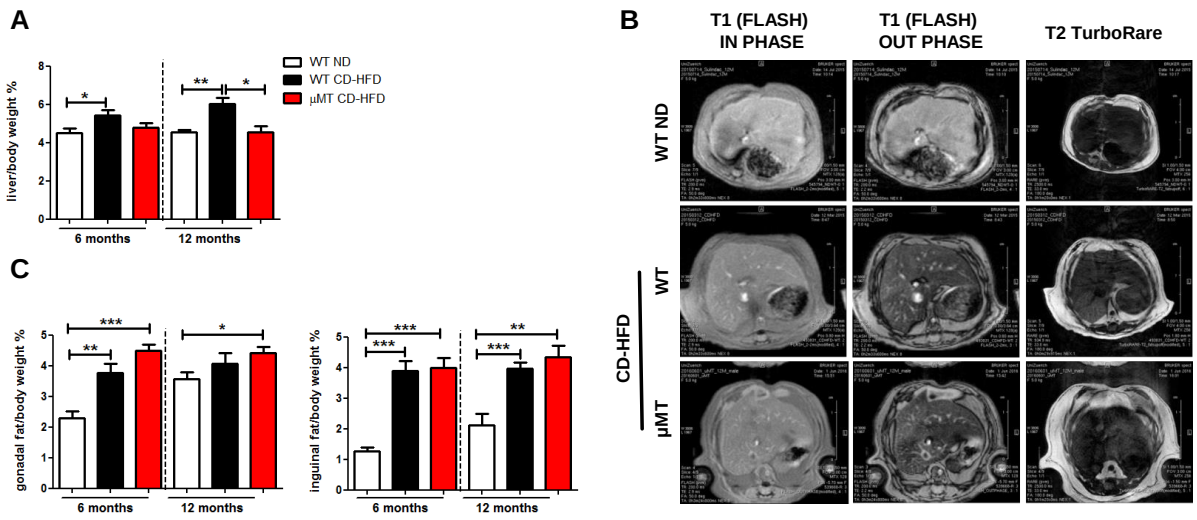

Figure 16. Fat deposition in µMT CD-HFD mice is not affected

(A) Quantitative analysis of liver-to-body weight ratio of WT ND, CD-HFD and µMT CD-HFD livers in 6- and 12-month-old mice (n=10 each). **(B)** MRI analyses of livers from 12-month-old WT ND, CD-HFD and µMT CD-HFD mice. T1 (fast low-angle shot [FLASH]) OUT phase: dark color indicative of steatosis. T2. TurboRare visualizes increase in subcutaneous and abdominal fat and hepatic lipid accumulation (bright regions) in CD-HFD mice. **(C)** Quantitative analysis of perigonadal white adipose tissue and inguinal white adipose tissue-to-body weight ratio of 6- and 12-month-old WT ND, CD-HFD and µMT CD-HFD mice (n=10 each). All data are presented as mean ± SEM.

6.2.5 Hepatic infiltration and activation of immune cells in µMT CD-HFD mice

FACS analysis showed an absence of $CD19^+$ B cells in the liver and a significant increase of hepatic CD3+ T cells in the µMT CD-HFD mice when compared to WT ND **(fig. 17A)** Moreover, FACS showed significantly more activated hepatic $CD4^+$ T cells in µMT CD-HFD mice compared to WT ND **(fig. 17B)** Accordingly, IHC showed an increase of $CD3^+$ T cells and $CD3^+$ foci in liver sections **(fig. 17C, D)**. Further IHC analysis revealed no $B220^+$ in the µMT CD-HFD livers, and increase of $F4/80^+$ and $MHCII^+$ cells similarly to WT CD-HFD **(fig. 17E, F)**.

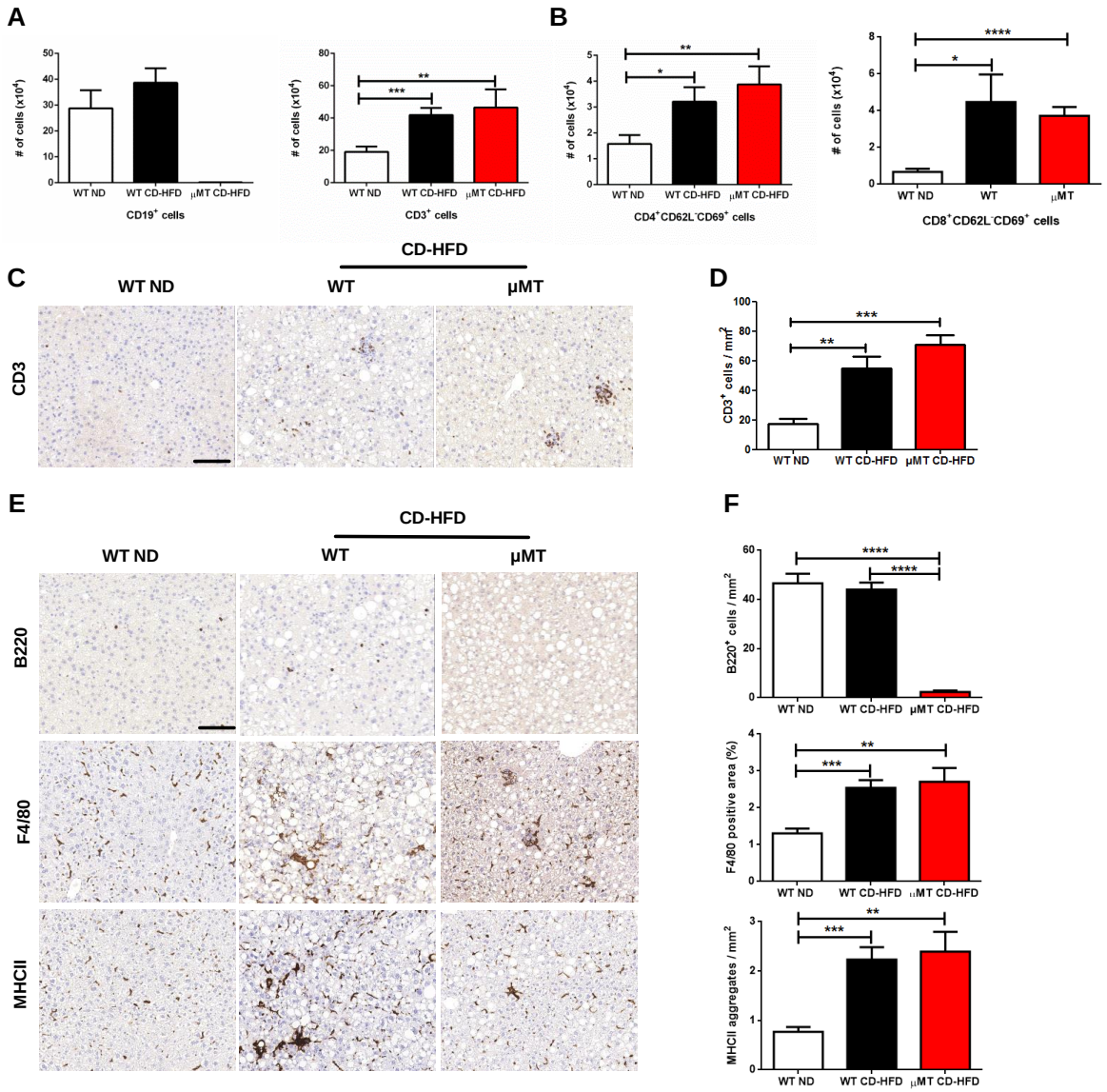

Figure 17. Presence of intestinal B cells, CD-HFD does not induce infiltration and activation of hepatic lymphocytes

(A,B) Quantifications of flow cytometric analyses comparing 6-month-old WT ND, CD-HFD and µMT CD-HFD mice (n≥6); **(A)** $CD19^+CD3^-$ B cells, $CD19^-CD3^+$ T cells and **(B)**, $CD69^+CD4+CD62L^-$ T cells.

(C-F) Representative histology and IHC on liver sections of 6-month-old WT ND, CD-HFD and µMT CD-HFD; **(C)** CD3 and quantification of $CD3^+$ T cells per mm^2 (n=6) **(D)**, **(E)** B220, F4/80 and MHCII and quantification of the respective cells per mm^2 (n=6) **(F)**. The scale bar represents 100 µm. All data are presented as mean ± SEM.

6.2.6 Lower incidence of HCC development in µMT CD-HFD mice

Of 40 µMT CD-HFD mice that were sacrificed at 12 months, only two developed tumors of an incidence of 5% **(fig. 18A, B)**.

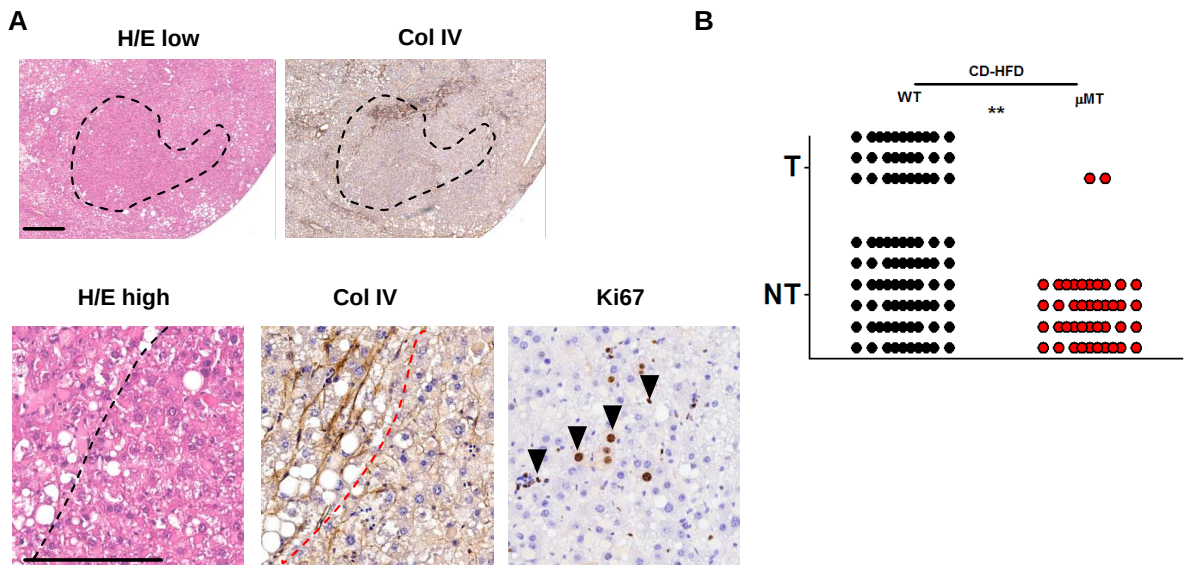

Figure 18. The presence of intestinal B cells is insufficient for NASH-driven HCC

(A) H/E and IHC of liver derived from 12-month-old µMT CD-HFD mice with HCC. Dashed lines depict HCC border. The scale bars represent H/E: 600µm (low) and 200 µm (high); collagen IV: 200 µm; Ki67: 200 µm (depicted by arrowheads). **(B)** Graph summarizing WT and µMT CD-HFD mice without tumor (NT) and with tumor (T). Symbols depict individual mice.

6.2.7 Therapeutic αCD20 treatment abrogates NASH in µMT CD-HFD mice but not glucose intolerance

Similar to our approach with WT CD-HFD, we followed the same B cell-depletion protocol in the µMT CD-HFD mice by treating them i.p. with the same antibody that depletes $CD20^+$ cells (section 1.5) **(fig. 19B, C)**. As it has been shown above for WT, at 4 months CD-HFD when the $CD20^+$ depletion has started, the µMT CD-HFD **(fig. 19A)** mice have already developed NASH **(fig. 19B)**. As previously (section 1.5), the treatment lasted for 6 weeks. The µMT CD-HFD αCD20 treated livers showed NASH abrogation as determined by H/E staining **(fig. 19C, D)**. Accordingly, ALT levels were reduced **(fig. 19E)** when compared to untreated µMT CD-HFD mice. Serum cholesterol remained high as in the CD-HFD untreated group **(fig. 19F)** whereas hepatic triglycerides were significantly decreased **(fig. 19G)**. Consistently, Sudan red staining in liver sections showed a strong decrease of large lipid droplets **(fig. 19H)**. Sirius red staining of µMT CD-HFD treated livers demonstrated an absence of perisinusoidal fibrosis similar to µMT CD-HFD, as shown above **(fig. 19H)**.

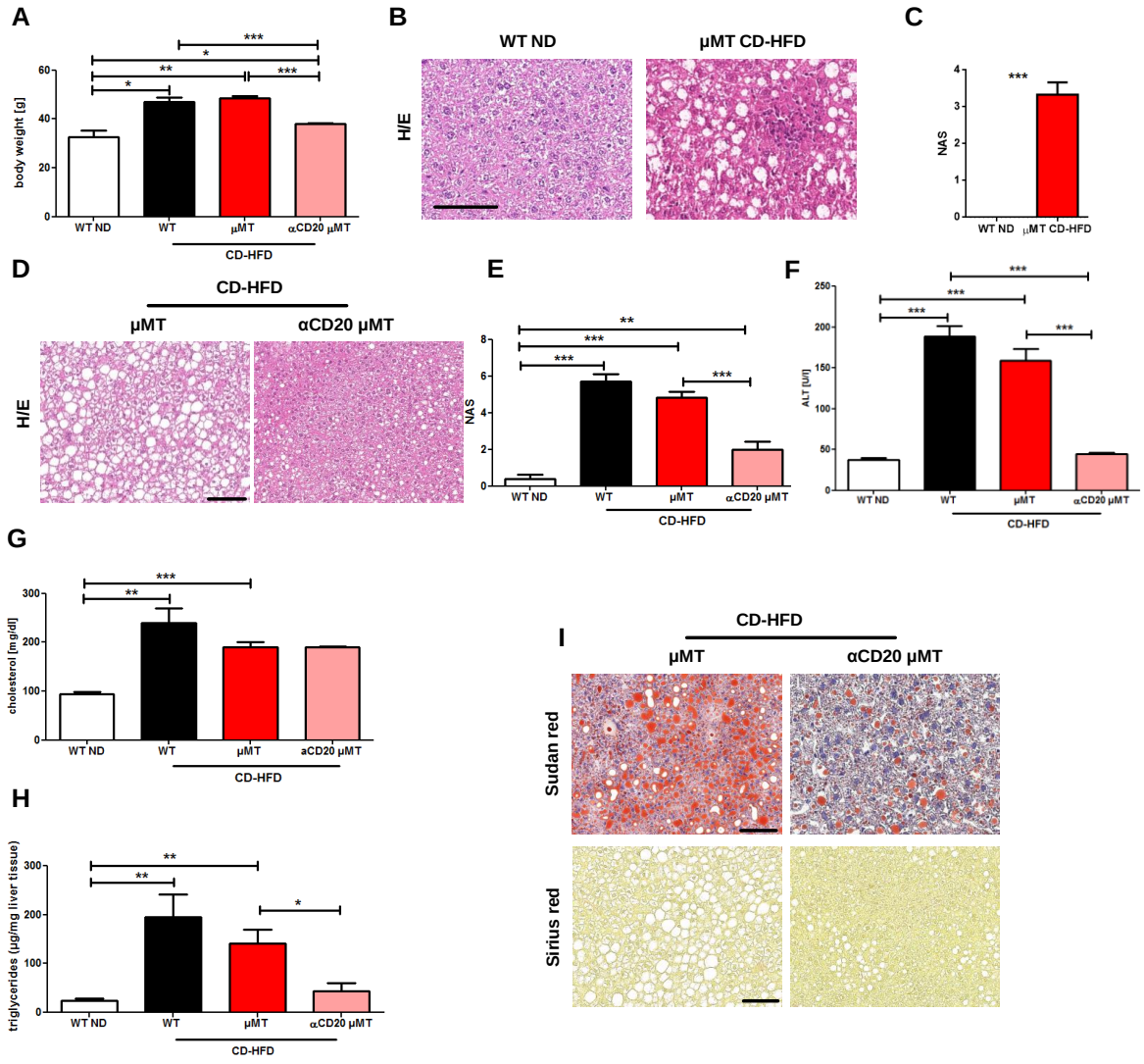

Figure 19. NASH development depends on the presence of intestinal B cells

(A) Body weight in male WT ND, CD-HFD, µMT CD-HFD and µMT αCD20 CD-HFD mice (n=5 each). **(B)** Representative H&E staining of 4-month-old WT ND and CD-HFD mice illustrating NASH. **(C)** NAFLD score (NAS) for the livers derived from 4-month-old WT ND and µMT CD-HFD mice (n=3 each). **(D)** Representative H&E staining of 6-month-old µMT CD-HFD and µMT αCD20 CD-HFD livers illustrating absence of NASH for the µMT αCD20 CD-HFD mice. **(E)** NAFLD score (NAS) for the livers derived from 6-month-old WT ND, CD-HFD, µMT CD-HFD and µMT αCD20 CD-HFD mice (n=5 each). **(F)** Quantification of serum ALT in the 6-month-old respective groups (n=5 each). **(G)** Quantification of serum cholesterol in the 6-month-old respective groups (n=5 each). **(H)** Quantification of hepatic triglycerides in the 6-month-old respective groups (n=5 each). **(I)** Upper row: Representative Sudan red staining illustrating fat accumulation in µMT CD-HFD and µMT αCD20 CD-HFD livers. Lower row: Representative Sirius red staining illustrating absence of perisinusoidal fibrosis in µMT CD-HFD and µMT αCD20 CD-HFD livers. The scale bar represents 100 µm. All data are presented as mean ± SEM.

6.2.8 Fat deposition in µMT αCD20 CD-HFD mice

In αCD20 µMT treated CD-HFD mice, liver-to-body weight ratio was reduced **(fig. 20A)**. Similar to the JH$^{-/-}$ CD-HFD mice, the inguinal white adipose tissue was significantly reduced but not the perigonadal white adipose tissue **(fig. 20B).**

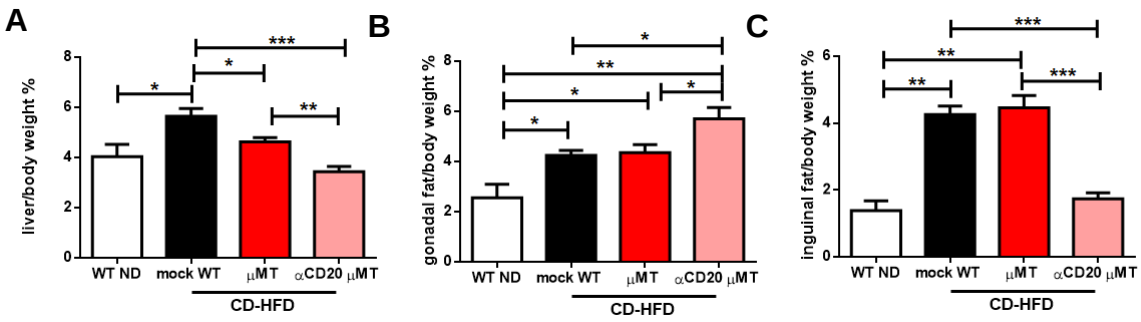

Figure 20. In αCD20 treated mice the fat deposition is affected

(A) Quantitative analysis of liver-to-body weight ratio of WT ND, CD-HFD, CD-HFD mock and αCD20 µMT CD-HFD livers in 6-month-old mice (n=5 each). **(B)** Quantitative analysis of perigonadal white adipose tissue and inguinal white adipose tissue-to-body weight ratio of the respective 6-month-old mice (n=5 each). All data are presented as mean ± SEM.

6.2.9 Hepatic infiltration and activation of immune cells is abolished in µMT CD-HFD mice under therapeutic αCD20 treatment

We observed a strong reduction of activated hepatic $CD4^+$ T cells in αCD20 treated µMT CD-HFD mice compared to µMT CD-HFD untreated **(fig. 21A)**. Accordingly IHC showed reduction of $CD3^+$ T cells and $CD3^+$ foci in liver sections **(fig. 21B, C)**. Further IHC analysis revealed absence of $B220^+$ cells in αCD20 µMT CD-HFD livers and reduction of $F4/80^+$ and $MHCII^+$ cells compared to µMT CD-HFD **(fig. 21D, E).**

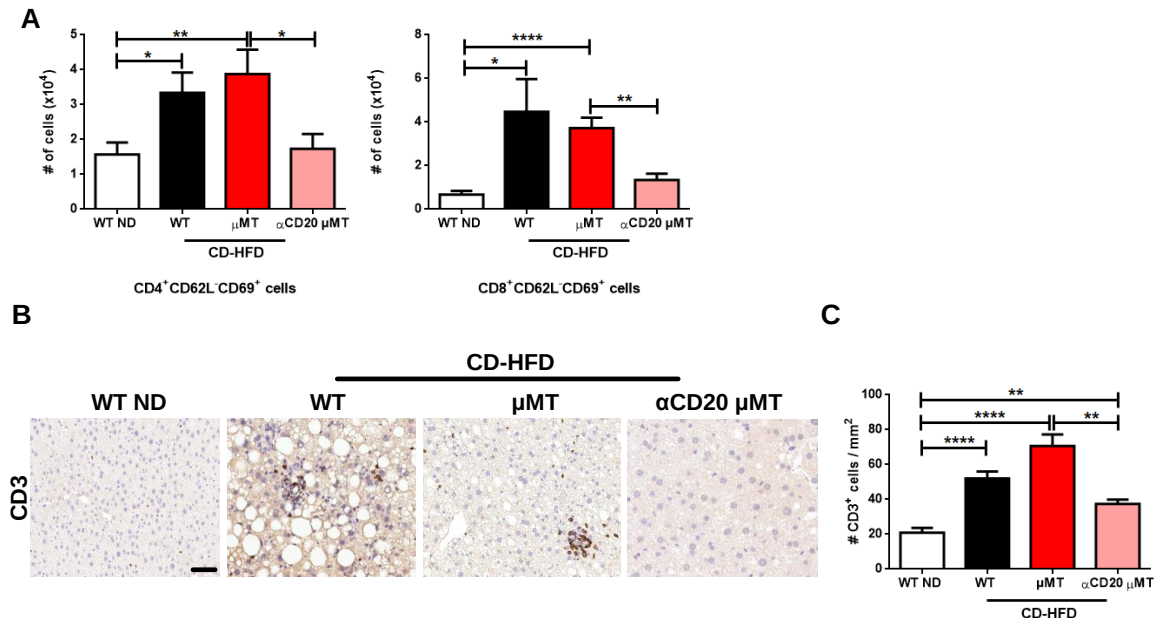

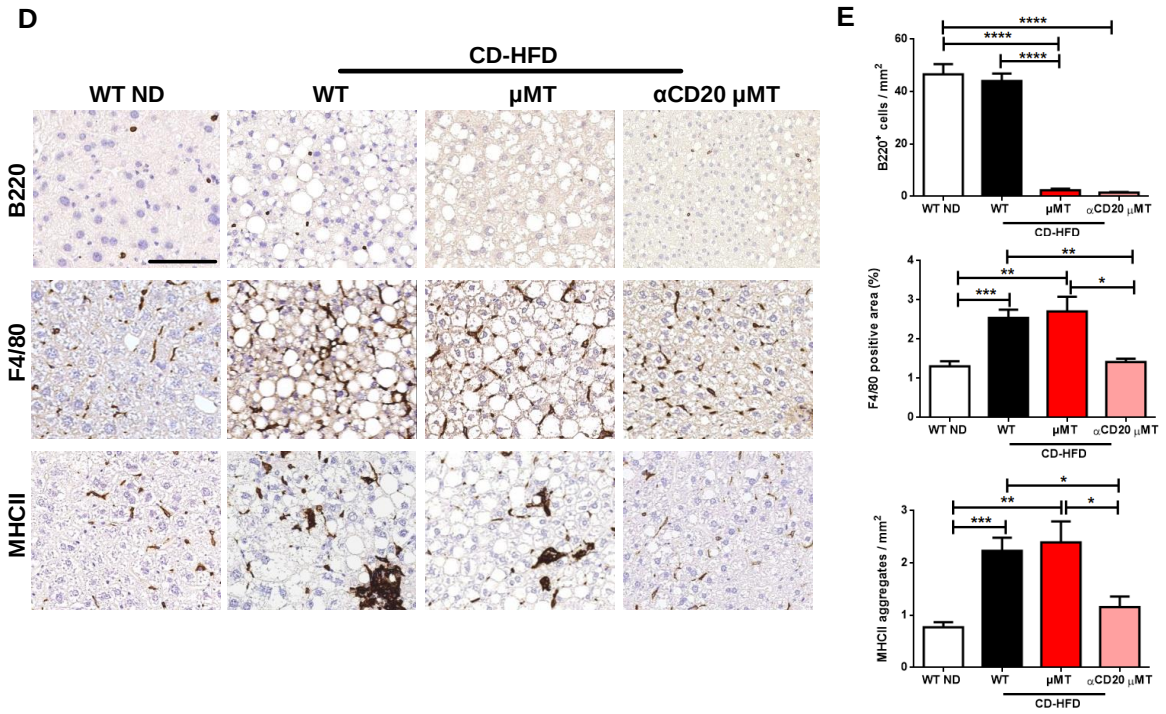

Figure 21. Therapeutic depletion of B cells leads to abrogation of infiltration and activation of lymphocytes in CD-HFD livers

(A) Quantification of flow cytometric analysis comparing 6-month-old WT ND, CD-HFD, μMT CD-HFD and αCD20 μMT CD-HFD mice (n≥4); $CD69^{+}CD4{+}CD62L^{-}$ T cells. **(B - E)** Representative histology and IHC on liver sections of the respective groups; **(C)** CD3 and quantification of $CD3^{+}$ T cells per mm^2 (n=5) **(D)**, B220, F4/80 and MHCII and quantification of the respective cells per mm^2 (n=5) **(E)**. The scale bar represents 100 μm. All data are presented as mean ± SEM.

6.3. Immunoglobulins are playing a role in NASH development

Since we had established that B cells are important for the development of NASH pathology, we wanted to identify their exact function was. As it has been discussed in the literature, B cells and immunoglobulins are suspected to be involved in metabolic syndrome and T2D[121,122], NASH development[102] and in liver fibrosis[123].

6.3.1 Immunoglobulins in CD-HFD-induced murine NASH

As noted above, we identified IgA^{+} cells in WT and μMT LP SI. In order to understand whether IgA is systemically secreted in μMT and how this compares to WT mice we proceeded to perform ELISA assays for IgA, IgM and IgG using as negative control $JH^{-/-}$ CD-HFD mice. In μMT CD-HFD mice we detected no secreted immunoglobulins in the serum whereas serum derived from WT CD-HFD mice there was a tendency for increased IgA levels when compared to WT ND serum **(fig. 22A)**.

Next, we measured secreted IgA and IgM in the lumen of the small intestine, where we observed higher levels for both immunoglobulins in WT CD-HFD mice when compared to WT ND **(fig. 22B)**. To our surprise we weren't able to identify IgA secretion in the μMT CD-HFD SI lumen **(fig. 22B)** but when we performed 16seq of IgA coated bacteria from faecal samples of the four above groups, we were able to detect IgA in μMT CD-HFD faeces (data not shown) which means that to some extent, IgA is secreted in the μMT gut lumen. In order to validate our FACS and IHC data, we also performed ELISA assays from tissue derived from the SI ileum **(fig. 22C)** where IgA and IgM were detected in the μMT CD-HFD gut with a tendency for increased levels in the WT CD-HFD gut when compared to WT ND.

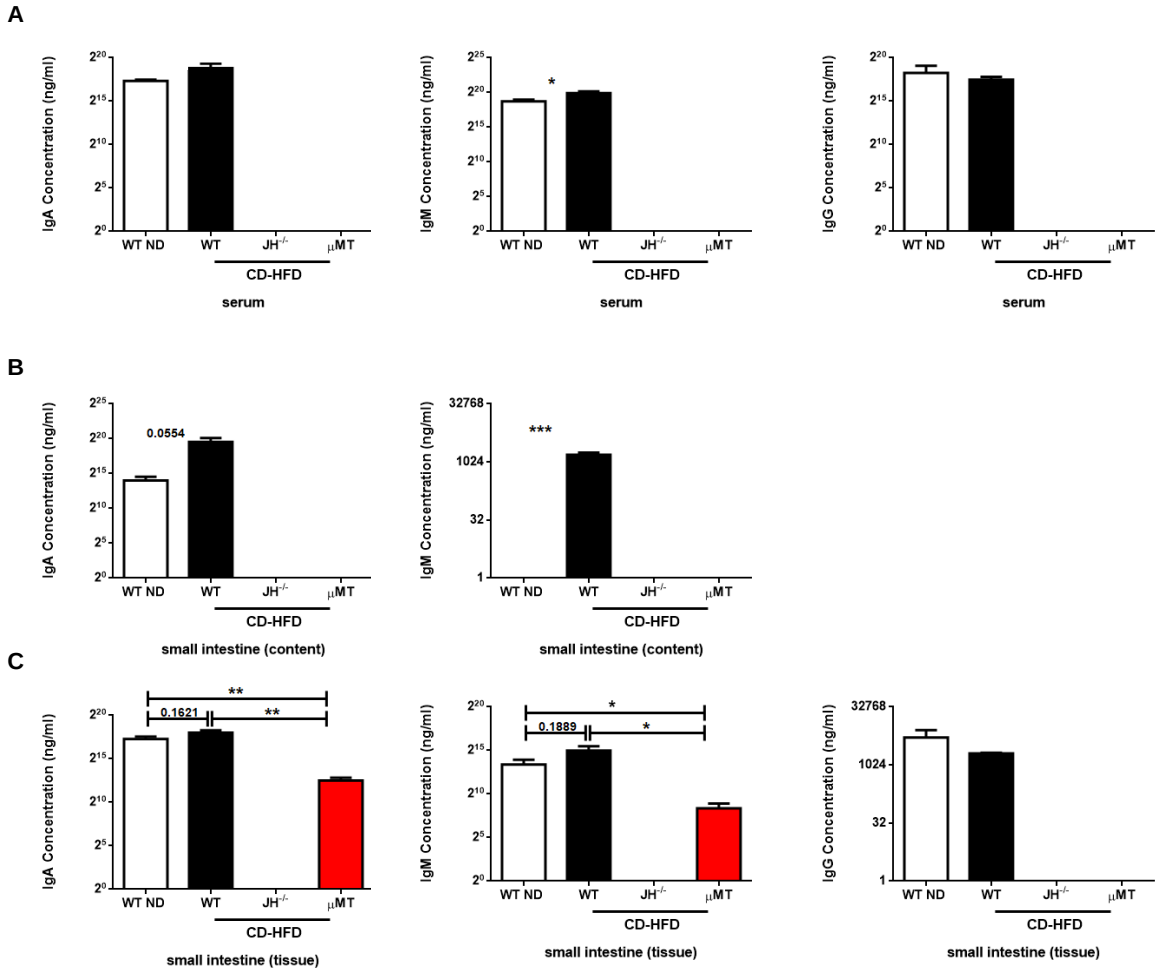

Figure 22. IgA and IgM immunoglobulins in WT and μMT CD-HFD mice

(A) Quantifications of ELISA assays for IgA, IgM and IgG immunoglobulins in the serum of WT ND, CD-HFD and $JH^{-/-}$ and μMT CD-HFD mice (n=4 each). **(B)** Quantifications of ELISA assays for IgA, IgM immunoglobulins in the lumen of the small intestine of WT ND, CD-HFD and $JH^{-/-}$ and μMT CD-HFD mice (n=4 each). **(C)** Quantifications

of ELISA assays for IgA, IgM and IgG immunoglobulins in the ileum of the small intestine of WT ND, CD-HFD and $JH^{-/-}$ and μMT CD-HFD mice (n≥3). All data are presented as mean ± SEM.

6.3.2 Low-affinity IgM and IgA in NASH and fibrosis development

Next, we put $IgA^{-/-}$ mice on CD-HFD for 6 months. Surprisingly the mice developed NASH, and using comprehensive ELISA and IHC analyses we consistently identified strong IgA present in the serum and the tissues (data not shown). Therefore we put $AID^{-/-}$ and AIDg23s mice on CD-HFD for 6 months. $AID^{-/-}$ mice have a complete defect in CSR but they can produce IgM that lacks SHM[192]. The AIDg23s mice have less SHM but normal amount of immunoglobulins in both serum and intestinal secretions[193]. As a result, the AIDg23s mice lack high-affinity immunoglobulins due to defects in SHM.

$AID^{-/-}$ and AIDg23s CD-HFD mice showed a constant increase in body weight, similar to WT CD-HFD, when compared to WT ND **(fig. 23A)**. H/E staining of $AID^{-/-}$ and AIDg23s CD-HFD liver sections showed NASH development **(fig. 23B, C)** and serum analysis revealed increased ALT **(fig. 23D)** when compared with WT ND. $AID^{-/-}$ and AIDg23s CD-HFD serum cholesterol and hepatic triglycerides were also increased **(fig. 23E, F)**. Sudan red staining of $AID^{-/-}$ and AIDg23s CD-HFD liver sections showed accumulation of large lipid droplets **(fig. 23G)**. Interestingly, Sirius red staining showed absent perisinusoidal hepatic fibrosis for the $AID^{-/-}$ CD-HFD but not for the AIDg23s CD-HFD **(fig. 23H, I)**.

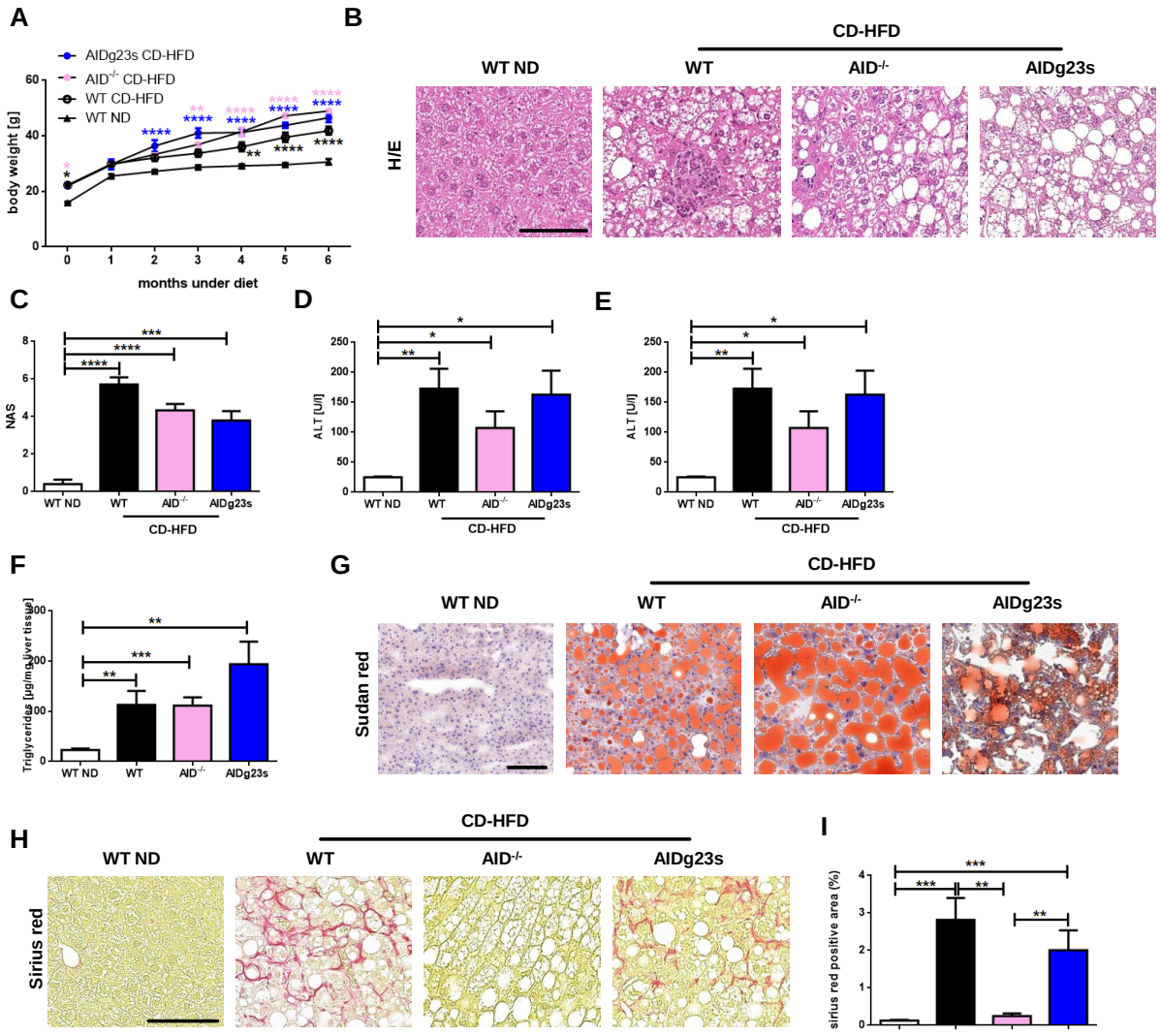

Figure 23. AID$^{-/-}$ and AIDg23s mice develop NASH under long-term CD-HFD

(A) Weight development in male WT ND, CD-HFD, AID$^{-/-}$ and AIDg23s CD-HFD mice (n≥4). **(B)** Representative H&E staining of 6-month-old WT ND, CD-HFD, AID$^{-/-}$ and AIDg23s CD-HFD male mice illustrating NASH. **(C)** NAFLD score (NAS) for the four respective groups. **(D)** Quantification of serum ALT in male 6-month-old WT ND, CD-HFD, AID$^{-/-}$ and AIDg23s CD-HFD mice (n≥4). **(E)** Quantification of serum cholesterol in male 6-month-old WT ND, CD-HFD, AID$^{-/-}$ and AIDg23s CD-HFD mice (n≥4). **(F)** Quantification of hepatic triglycerides in male 6-month-old WT ND, CD-HFD, AID$^{-/-}$ and AIDg23s CD-HFD mice (n≥4). **(G)** Representative Sudan red staining illustrating fat accumulation in livers of WT ND, CD-HFD, AID$^{-/-}$ and AIDg23s CD-HFD mice. **(H)** Representative Sirius red staining illustrating the status of perisinusoidal fibrosis in livers WT ND, CD-HFD, AID$^{-/-}$ and AIDg23s CD-HFD mice. **(I)** Quantification of total Sirius red^{+} area (n≥4). The scale bar represents 100 µm. All data are presented as mean ± SEM.

6.3.3 Secretion of immunoglobulins and their role in NASH and fibrosis development

In order to further evaluate the role secreted immunoglobulins and to confirm the results from our AID$^{-/-}$ and AIDg23s CD-HFD experiments, we put IgMi mice on CD-HFD for 6 months. IgMi mice develop normal B cells that exclusively express

membrane bound IgM and do not secrete immunoglobulins apart from IgG1[194]. IgMi CD-HFD showed an increasing body weight, similar to WT CD-HFD **(fig. 24A)**. H/E staining of IgMi CD-HFD liver sections demonstrated significantly less steatosis and NASH abrogation **(fig. 24B, C)**. Serum analysis revealed significantly less ALT **(fig. 24D)** and cholesterol levels **(fig. 24E)** compared to WT CD-HFD, as well as hepatic triglycerides **(fig. 24F)** and Sudan red staining on liver section **(fig. 24G)**. Sirius red staining on liver sections showed absent of perisinusoidal hepatic fibrosis, similar to AID$^{-/-}$ and contrary to AIDg23s CD-HFD mice **(fig. 24H, I)**.

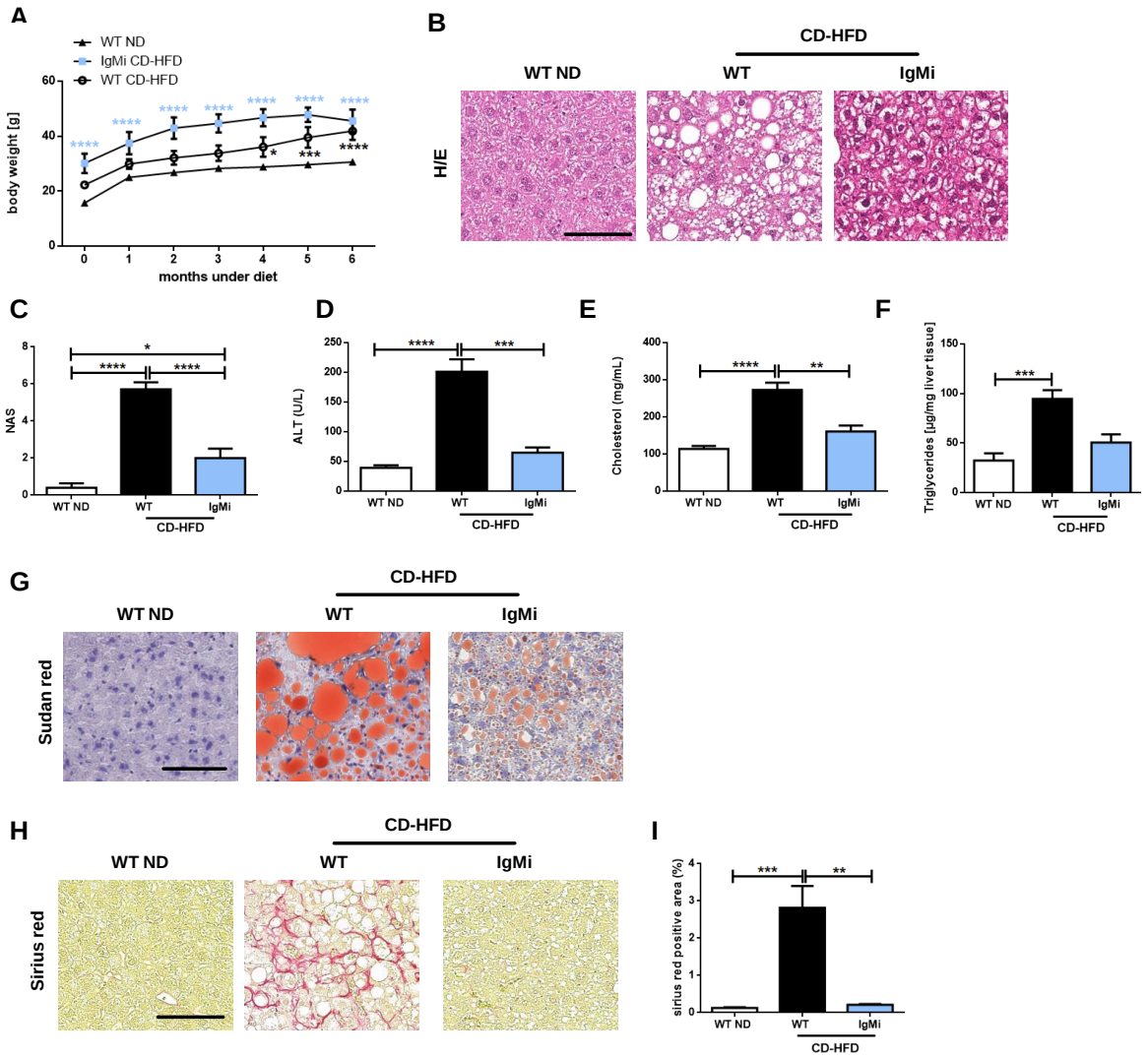

Figure 24. IgMi mice do not develop NASH or liver fibrosis under long-term CD-HFD

(A) Weight development in male WT ND, CD-HFD and IgMi CD-HFD mice (n=6 each). **(B)** Representative H&E staining of 6-month-old WT ND, CD-HFD and IgMi CD-HFD male. **(C)** NAFLD score (NAS) for the three respective groups. **(D)** Quantification of serum ALT in male 6-month-old WT ND, CD-HFD and IgMi CD-HFD mice (n=6 each). **(E)** Quantification of serum cholesterol in male 6-month-old WT ND, CD-HFD and IgMi CD-HFD mice (n=6 each). **(F)** Quantification of hepatic triglycerides in male 6-month-old WT ND, CD-HFD and IgMi CD-HFD mice (n=6 each). **(G)** Representative Sudan red staining illustrating fat accumulation in livers of WT ND,

CD-HFD and IgMi CD-HFD mice. **(H)** Representative Sirius red staining illustrating the status of perisinusoidal fibrosis in livers WT ND, CD-HFD and IgMi CD-HFD mice. **(I)** Quantification of total Sirius red^{+} area (n=6 each). The scale bar represents 100 µm. All data are presented as mean ± SEM.

6.3.4 Secreted immunoglobulins affect fat deposition

AID$^{-/-}$ and AIDg23s CD-HFD liver-to-body weight ratio was increased compared to WT ND but also reduced compared to WT CDHFD **(fig. 25A right)**. IgMi CD-HFD liver-to-body weight ratio was significantly reduced compared to WT CD-HFD **(fig. 25A left)**. Perigonadal white adipose tissue was significantly decreased in AID$^{-/-}$, AIDg23s and IgMi CD-HFD mice compared to WT CD-HFD **(fig. 25B)**. Inguinal white adipose tissue was significantly increased in AID$^{-/-}$, AIDg23s and IgMi CD-HFD mice compared to WT ND but also significantly reduced in AIDg23s CD-HFD compared to WT CD-HFD **(fig. 25C)**.

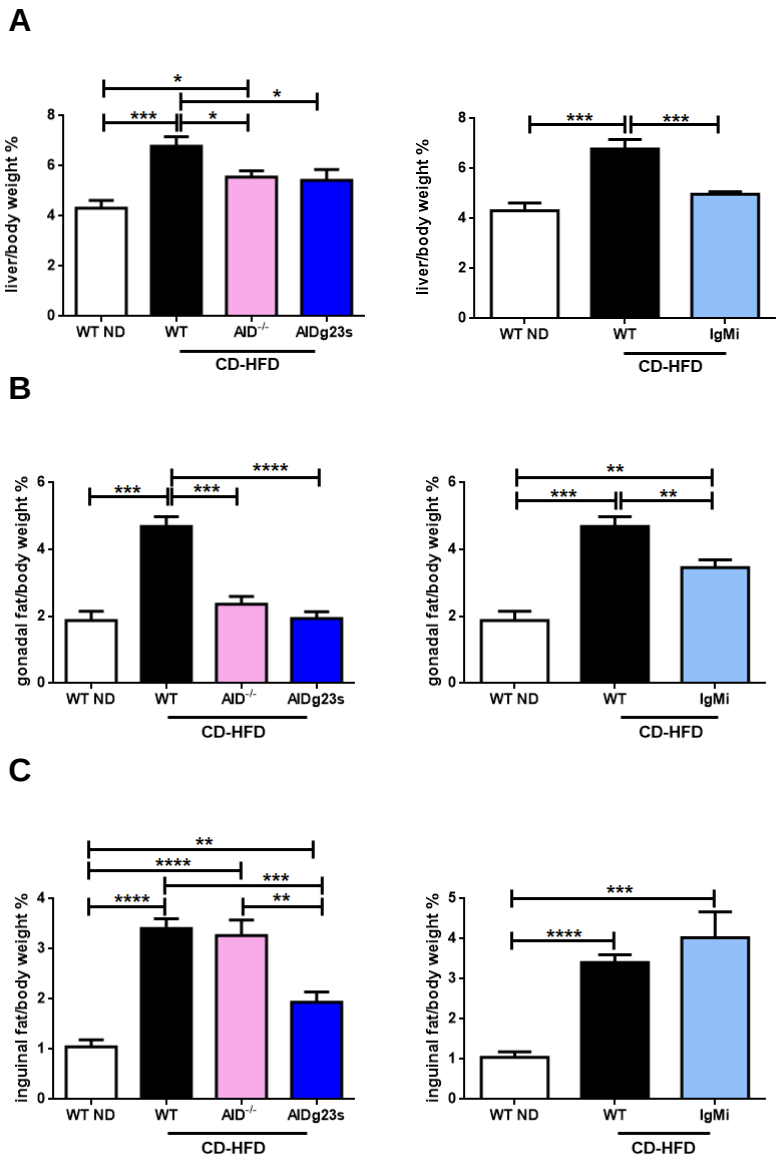

Figure 25. Fat deposition in AID$^{-/-}$, AIDg23s and IgMi CD-HFD mice

(A) Quantitative analysis of liver-to-body weight ratio of WT ND, CD-HFD, AID$^{-/-}$, AIDg23s and IgMi CD-HFD livers in 6-month-old male mice (n≥4). **(B)** Quantitative analysis of perigonadal white adipose tissue -to-body weight ratio of WT ND, CD-HFD, AID$^{-/-}$, AIDg23s and IgMi CD-HFD livers in 6-month-old male mice (n≥4). **(C)** Quantitative analysis of inguinal white adipose tissue-to-body weight ratio of WT ND, CD-HFD, AID$^{-/-}$, AIDg23s and IgMi CD-HFD livers in 6-month-old male mice (n≥4). All data are presented as mean ± SEM.

6.3.5 Differential hepatic infiltration of immune cells in AID$^{-/-}$, AIDg23s and IgMi CD-HFD mice

In AIDg23s CD-HFD the activated hepatic CD4$^+$ T cells were increased similar to WT CD-HFD when compared to WT ND, determined by FACS analysis **(fig. 26A, right)**. On the contrary, in IgMi CD-HFD group, liver FACS analysis showed significant reduction of activated CD4$^+$ T cells when compared to WT CD-HFD **(fig. 26A, left)**. IHC showed significant increase of CD3$^+$ T cells in AID$^{-/-}$ and AIDg23s CD-HFD mice when compared to WT ND **(fig. 26B, C)** but significant decrease in IgMi CD-HFD when compared to WT CD-HFD, accordingly with FACS analysis **(fig. 26B, C)**. Further IHC revealed no significant differences in B220$_+$ cells in AID$^{-/-}$, AIDg23s and IgMi CD-HFD livers **(fig. 26E, F, upper row)**. F4/80$^+$ and MHCII$^+$ cells were decreased in AID$^{-/-}$ and IgMi CD-HFD mice compared to WT CD-HFD but not in AIDg23s CD-HFD mice **(fig. 26E, F, middle and lower row)**.

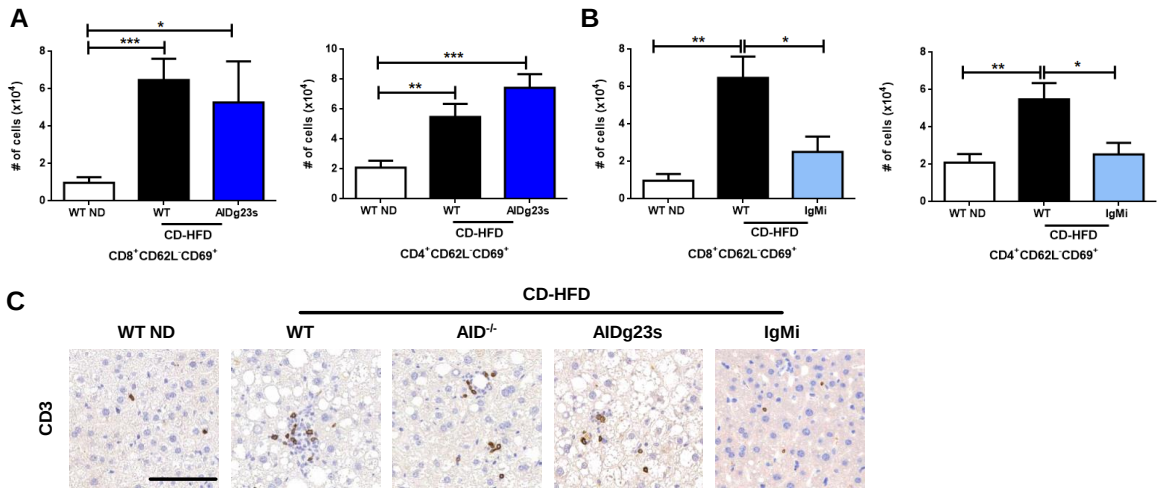

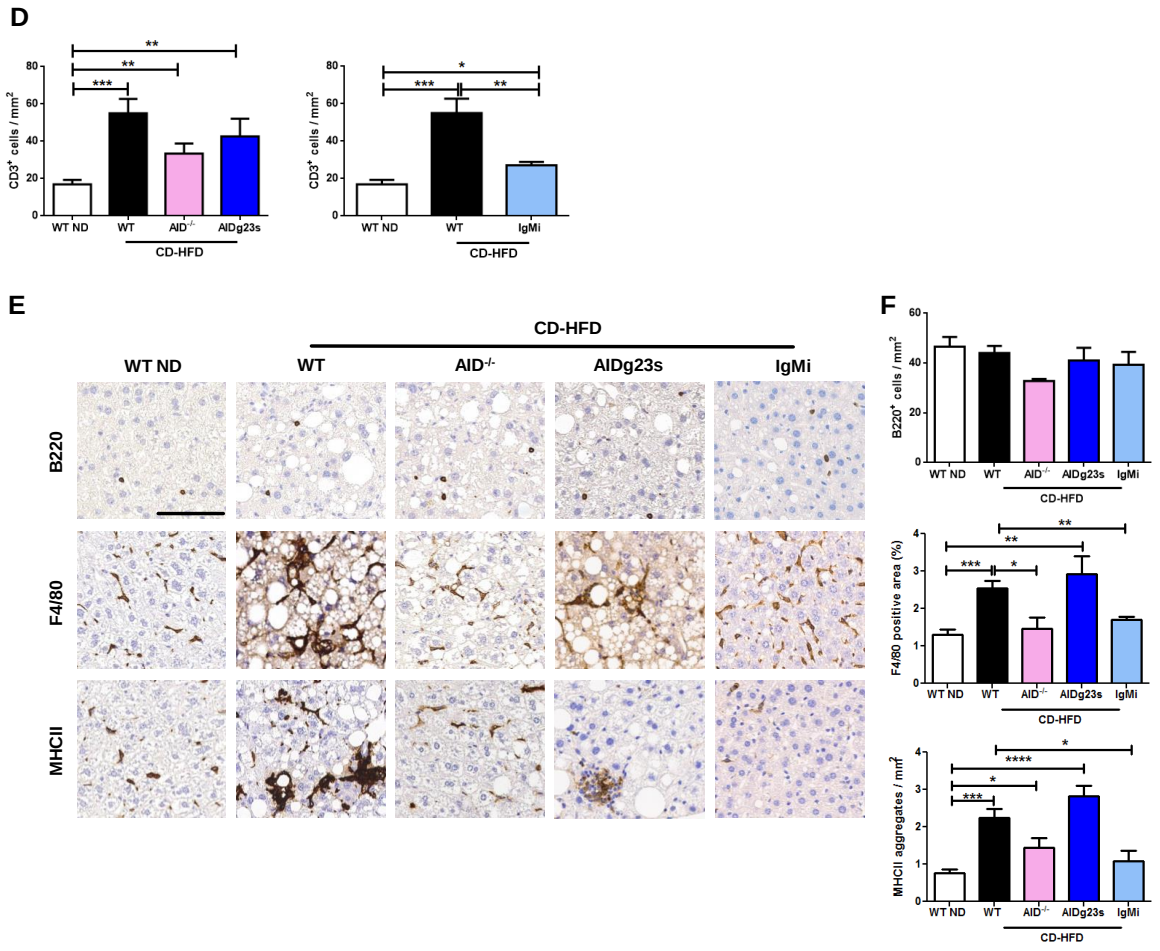

Figure 26. Absence of secreted IgA and IgM leads to abrogation of hepatic inflammation under CD-HFD
(A) Quantification of flow cytometric analysis comparing 6-month-old WT ND, CD-HFD, AIDg23s CD-HFD (right) (n≥3) and IgMi CD-HFD mice (left (n≥4); $CD69^{+}CD4{+}CD62L^{-}$ T cells. **(B, C)** Representative $CD3^{+}$ IHC on liver sections of the respective groups **(B)**. Quantification of $CD3^{+}$ T cells per mm^2 (n≥3) **(C)**. **(E, F)** Representative B220, F4/80 and MHCII IHC on liver sections **(E)** and quantification of the respective cells per mm^2 (n≥3) **(F)**. The scale bar represents 100 mm. All data are presented as mean ± SEM.

6.4. Microbiome is an important but not essential factor in NASH development.

The above data show that the presence of intestinal B cells and secreted immunoglobulins are sufficient NASH development and hepatic fibrosis under CD-HFD conditions. Next we wanted to investigate which antigens the immunoglobulins or the LP SI B cells directly target. Most likely antigens facing LP SI B cells are from components of the diet, the microbial cell wall and/or the microbial metabolism. Therefore we set up experiments to address the role of the microbiome in our model. Our first approach was to put WT male mice on CD-HFD treated with a wide

spectrum antibiotic mix in their drinking water (referred to from now on as WT ABX proph). In parallel we set up WT CD-HFD male cohorts started on antibiotics after four months on diet (referred to from now on as WT ABX ther). Finally, CD-HFD male WT mice were maintained under germ-free conditions (referred to from now on as GF). The above three experiments were terminated after six months of diet treatment.

6.4.1 Antibiotic treatment abrogates NASH and liver fibrosis but not glucose tolerance in CD-HFD mice in a prophylactic and therapeutic manner.

WT ABX proph and WT ABX ther mice showed a constant rise in body weight compared to WT ND mice, similar to WT CD-HFD mice **(fig. 27A, B)**. Both groups showed less steatosis as determined by Hematoxylin and Eosin (H/E) staining of liver sections and NAFLD activity score (NAS) **(fig. 27D)**. Liver damage was abrogated in both groups, as serum analysis revealed a reduction in ALT levels **(fig. 27E)**. Further evaluation of ALT levels of WT ABX ther group showed two subgroups: one with ALT<50 (U/L) and one with ALT>50 (U/L) **(fig. 27F)**. A regression analysis demonstrated a positive correlation of the ALT values with the body weight of the WT ABX ther mice, indicating a linear increase of the ALT values according to the body weight increase **(fig. 27G)**. WT ABX proph and WT ABX ther serum cholesterol remained high, similar to WT CD-HFD **(fig. 27H)**; hepatic triglycerides levels were decreased **(fig. 27I)** consistent with Sudan red staining that showed decrease of large lipid droplets in the livers of both groups **(fig. 27L)**. Further statistical analysis showed a linear correlation between the values ALT and the hepatic triglycerides **(fig. 27J)** as well as between the body weight and the hepatic triglycerides levels in the WT ABX ther group **(fig. 27K)**. Sirius red staining on liver sections of both ABX groups revealed absent perisinusoidal fibrosis, in contrast to WT CD-HFD livers **(fig. 27L)**. Metabolic analysis with an intraperitoneal glucose tolerance test (IPGTT) showed an impaired glucose response in both ABX groups **(fig. 27N, O)**.

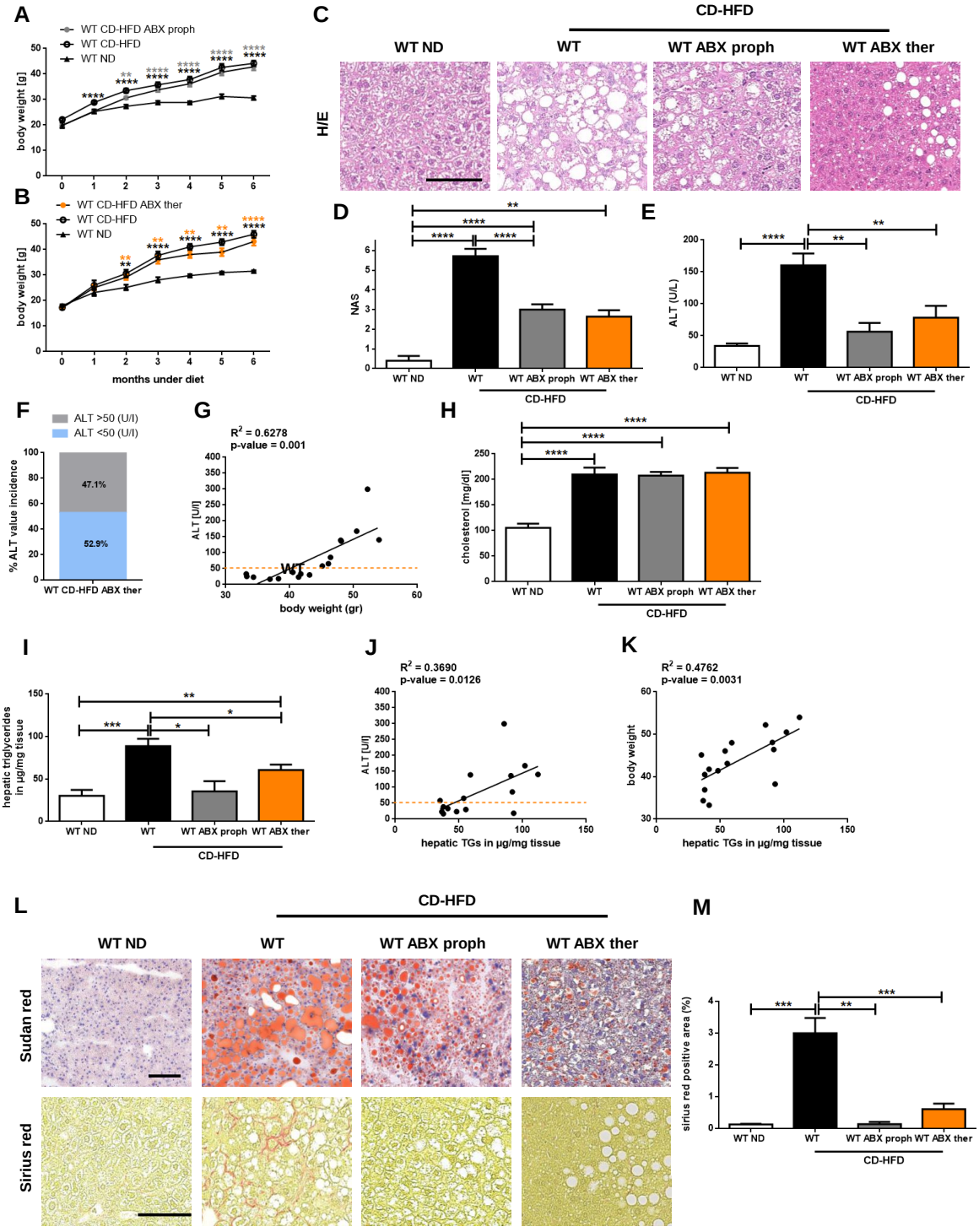
A
WT CD-HFD ABX proph
WT CD-HFD
WT ND
body weight [g]
B
WT CD-HFD ABX ther
WT CD-HFD
WT ND
body weight [g]
months under diet
C
CD-HFD
WT ND
WT
WT ABX proph
WT ABX ther
H/E
D
NAS
WT ND
WT
WT ABX proph
WT ABX ther
CD-HFD
E
ALT (U/L)
WT ND
WT
WT ABX proph
WT ABX ther
CD-HFD
F
ALT >50 (U/l)
ALT <50 (U/l)
% ALT value incidence
47.1%
52.9%
WT CD-HFD ABX ther
G
R2 = 0.6278
p-value = 0.001
ALT [U/l]
WT
body weight (gr)
H
cholesterol [mg/dl]
WT ND
WT
WT ABX proph
WT ABX ther
CD-HFD
I
hepatic triglycerides in µg/mg tissue
WT ND
WT
WT ABX proph
WT ABX ther
CD-HFD
J
R2 = 0.3690
p-value = 0.0126
ALT [U/l]
hepatic TGs in µg/mg tissue
K
R2 = 0.4762
p-value = 0.0031
body weight
hepatic TGs in µg/mg tissue
L
CD-HFD
WT ND
WT
WT ABX proph
WT ABX ther
Sudan red
Sirius red
M
sirius red positive area (%)
WT ND
WT
WT ABX proph
WT ABX ther
CD-HFD

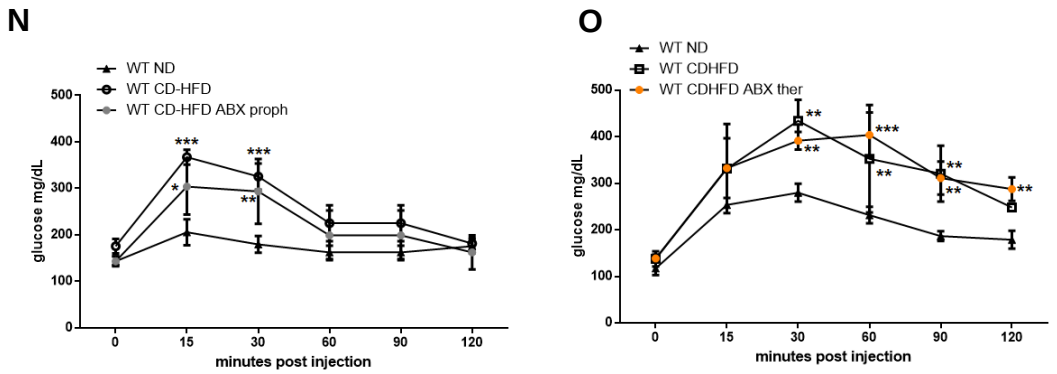

Figure 27. Microbiome modulation through wide spectrum antibiotics administration leads to abrogation NASH and hepatic fibrosis under CD-HFD

(A, B) Weight development in male WT ND, CD-HFD, WT ABX proph and ther mice (n>8). **(C)** Representative H&E staining of 6-month-old WT ND, CD-HFD, WT ABX proph and ther mice. **(D)** NAFLD score (NAS) for the three respective groups (n>8). **(E)** Quantification of serum ALT in male 6-month-old old WT ND, CD-HFD, WT ABX proph and ther mice (n>8). **(F)** Graph demonstrating the percentage of mice for 50 >ALT> 50U/L (n=17) (G) Linear regression of correlation between ALT values and body weight in male 6-month-old WT ND, CD-HFD, WT ABX proph and ther mice (n=17). **(H)** Quantification of serum cholesterol in male 6-month-old old WT ND, CD-HFD, WT ABX proph and ther mice (n>8). **(I)** Quantification of hepatic triglycerides of male 6-month-old WT ND, CD-HFD, WT ABX proph and ther mice (n>8). **(J)** Linear regression of correlation between ALT values and hepatic triglycerides in male 6-month-old WT ND, CD-HFD, WT ABX proph and ther mice (n=17). **(K)** Linear regression of correlation between ALT values and body weight in male 6-month-old WT ND, CD-HFD, WT ABX proph and ther mice (n=17). **(L)** Representative Sudan red (left) staining illustrating fat accumulation and Sirius red staining illustrating the status of perisinusoidal fibrosis (right) in livers of WT ND, CD-HFD, WT ABX proph and ther mice. **(M)** Quantification of total Sirius red^{+} area (n>8). **(N, O)** Glucose tolerance test performed with 6-month-old male WT ND, CD-HFD, WT ABX proph and ther mice (n>8). The scale bar represents 100 µm. All data are presented as mean ± SEM.

6.4.2 16s rRNA gene sequencing of faecal WT ND, CD-HFD and CD-HFD ABX samples

16s rRNA gene sequencing of faecal samples from mice after 6 months on diet revealed differences in the gut microbiome profile between WT ND and CD-HFD mice. In CD-HFD faecal samples, the phylum Firmicutes was more abundant in contrast to ND where the most abundant population was Bacteroidetes **(fig. 28A)**. Further taxonomical analysis revealed that in CD-HFD faeces, the highest proportion of sequences originated from *Allobaculum*, *Clostridiales* and *Lactobacillus,* as opposed to ND, where the highest proportion of sequences were from *Bacteroidetes* **(fig. 28B)**. The sequences of the most abundant four bacteria and their taxonomy are shown in **figures 28C** and **28D** respectively. WT CD-HFD ABX proph and ther had the same microbiome profile after 6 months of diet. The antibiotic cocktail we used depleted almost all bacteria apart from Lactococcus **(fig. 28E)**.

A

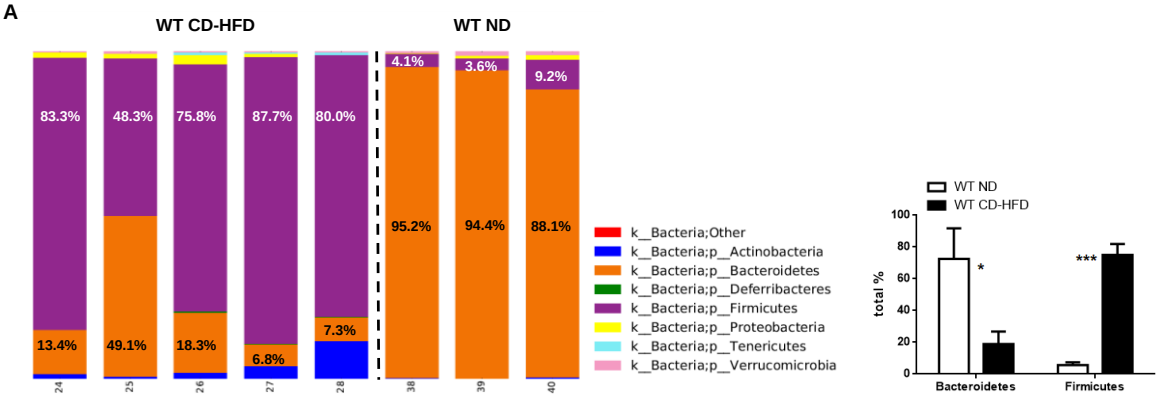

B

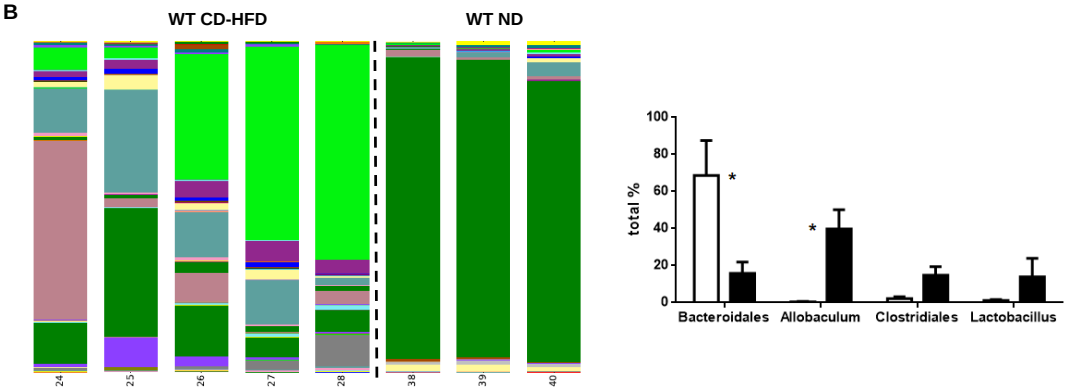

C

	WT CD-HFD					WT ND		
	24	**25**	**26**	**27**	**28**	**38**	**39**	**40**
	12.2%	39.0%	15.4%	6.0%	6.5%	91.1%	89.9%	85.1%
	6.7%	3.1%	38.0%	58.4%	64.7%	0.3%	0.3%	0.8%
	13.5%	31.0%	13.6%	13.4%	2.4%	0.7%	1.5%	4.2%
	53.9%	2.5%	8.6%	0.4%	4.0%	2.0%	0.7%	0.9%

D

	Kingdom	**Phylum**	**Class**	**Order**	**Family**	**Genus**
	Bacteria	Bacteroidetes	Bacteroidia	Bacteroidales		
	Bacteria	Firmicutes	Erysipelotrichi	Erysipelotrichales	Erysipelotrichaceae	Allobaculum
	Bacteria	Firmicutes	Clostridi	Clostridiales		
	Bacteria	Firmicutes	Bacilli	Lactobacillales	Lactobacillaceae	Lactobacillus

E

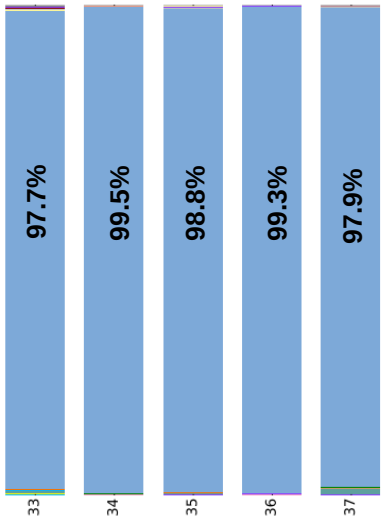

Kingdom	Bacteria
Phylum	Firmicutes
Class	Bacilli
Order	Lactobacillales
Family	Streptococcaceae
Genus	Lactococcus

Figure 28. Microbiota composition analysis on CD-HFD and antiobiotic treated CD-HFD male mice
(A, B) Faecal microbiota detected by PCR presented in bar graphs on the right and on the left plots of the microbiota relative abundances, Each bar on the left represents one mouse. Groups: WT ND and CD-HFD. **(C)** Table with relative abundances of selective bacteria for WT ND and CD-HFD. **(D)** Table with the taxonomy of the bacteria from the Table in C. **(E)** Faecal microbiota detected by PCR presented in bar graph on the right for the antibiotic group under CD-HFD; on the left a table with the taxonomy of *Lactococcus*. All data are presented as mean ± SEM

6.4.3 Sterile inflammation suffices to induce NASH, impaired glucose response and liver fibrosis in germ free C57BL/6 mice on CD-HFD

GF CD-HFD mice started to gain significant weight after one month on diet compared to GF ND mice **(fig. 29A)**. GF CD-HFD mice showed steatosis and hepatic inflammation as determined by Hematoxylin and Eosin (H/E) staining of liver sections and NAFLD activity score (NAS), similar to conventional (from now on referred as SPF) WT CD-HFD mice **(fig. 29B, C)**. Serum ALT analysis revealed liver damage in GF CD-HFD compared to GF ND mice already after three months of diet **(fig. 29D)**. GF CD-HFD serum cholesterol levels were significantly higher compared to GF ND **(fig. 29E)** and hepatic triglycerides were also high similar to SPF CD-HFD mice **(fig. 29F)**. Sudan red staining of liver sections showed an increase of large lipid droplets in GF CD-HFD mice compared to GF ND **(fig. 29G)**. Sirius red staining and quantification of liver sections showed perisinusoidal fibrosis in GF CD-HFD livers compared to GF ND **(fig. 29H)**. Contrary to SPF CD-HFD livers, the fibrosis of GF CD-HFD livers was in all cases characterized as mild (<2%) **(fig. 29I)**. Metabolic

analysis with an intraperitoneal glucose tolerance test (IPGTT) showed an impaired glucose response in GF CD-HFD mice **(fig. 29J)**.

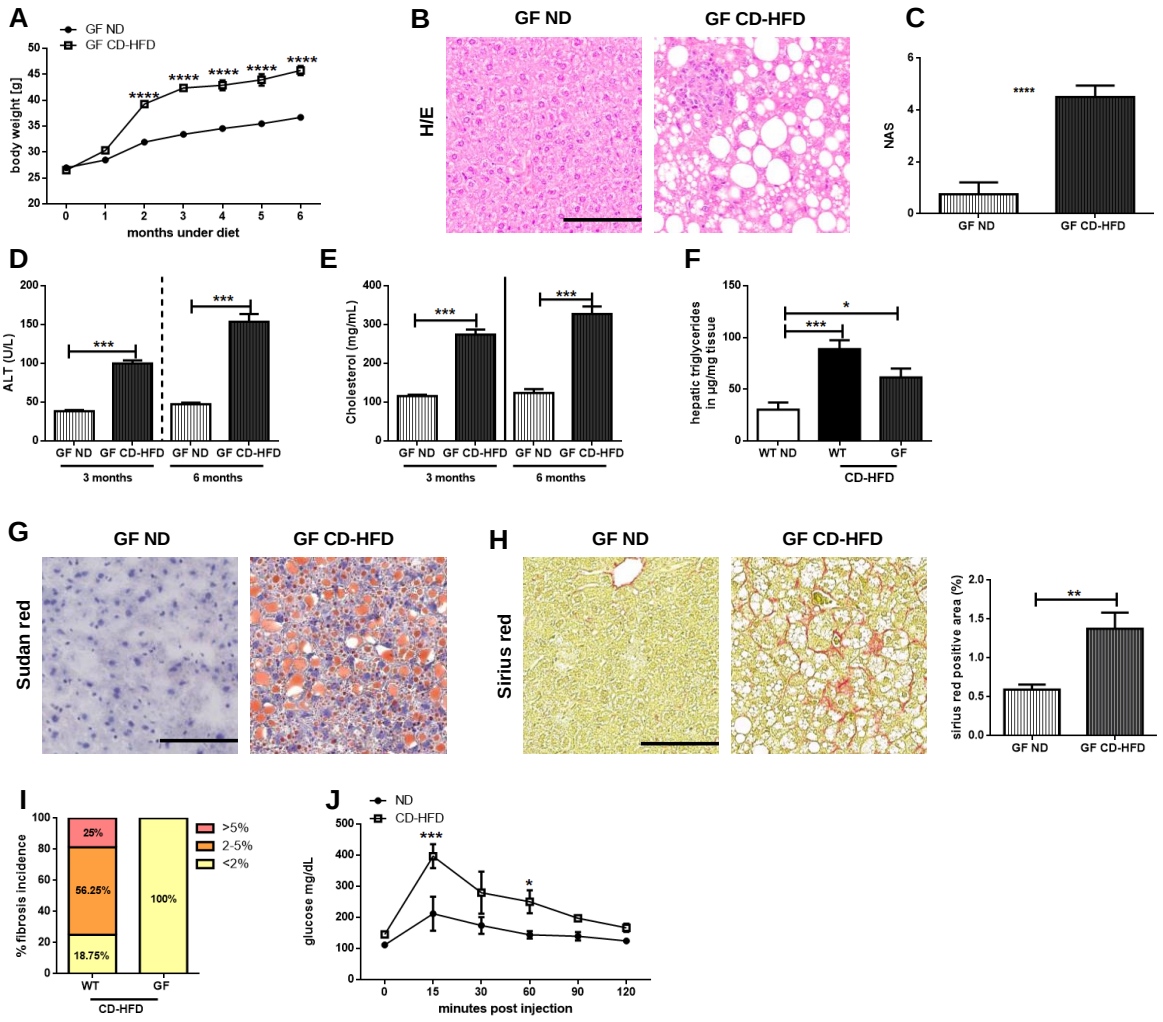

Figure 29. Germ free mice on long-term CD-HFD develop NASH and hepatic fibrosis

(A) Weight development in male GF ND and CD-HFD mice (n>6). **(B)** Representative H&E staining of 6-month-old GF ND and CD-HFD mice. **(C)** NAFLD score (NAS) for 6-month-old GF ND and CD-HFD mice (n>6). **(D)** Quantification of serum ALT in male 6-month-old old GF ND and CD-HFD mice (n>6). **(E)** Quantification of serum cholesterol of male 6-month-old old GF ND and CD-HFD mice (n>6). **(F)** Quantification of hepatic triglycerides in male 6-month-old GF ND and CD-HFD mice (n>6). **(G)** Representative Sudan red (left) staining illustrating fat accumulation fibrosis in livers of GF ND and CD-HFD mice. **(H)** Representative Sirius red staining illustrating the status of perisinusoidal fibrosis (left) in livers of GF ND and CD-HFD mice and quantification of total Sirius red^{+} area (n>6). **(I)** Incidence of fibrosis as it was quantified through total Sirius red^{+} area in WT ND and CD-HFD livers (n=10) and in male 6-month-old old GF ND and CD-HFD mice (n=6). The scale bar represents 100 µm. All data are presented as mean ± SEM.

6.4.4 Fat deposition in antibiotic treated and germ free C57BL/6 mice on CD-HFD

WT ABX proph and ther liver-to-body weight ratio was decreased compared to WT CD-HFD **(fig. 30A)** but it was increased for the GF CD-HFD mice compared to GF ND **(fig. 30B)**. Perigonadal white adipose tissue was increased compared to WT ND, similar to WT CD-HFD **(fig. 30C)** whereas no difference was observed between GF CD-HFD and ND mice **(fig. 30D)**. Inguinal white adipose tissue was reduced in both ABX groups compared to WT CD-HFD, but remained high compared to WT ND **(fig. 30E)**. In the GF mice, the inguinal fat was significantly increased in the CD-HFD group compared to ND **(fig. 30F)**.

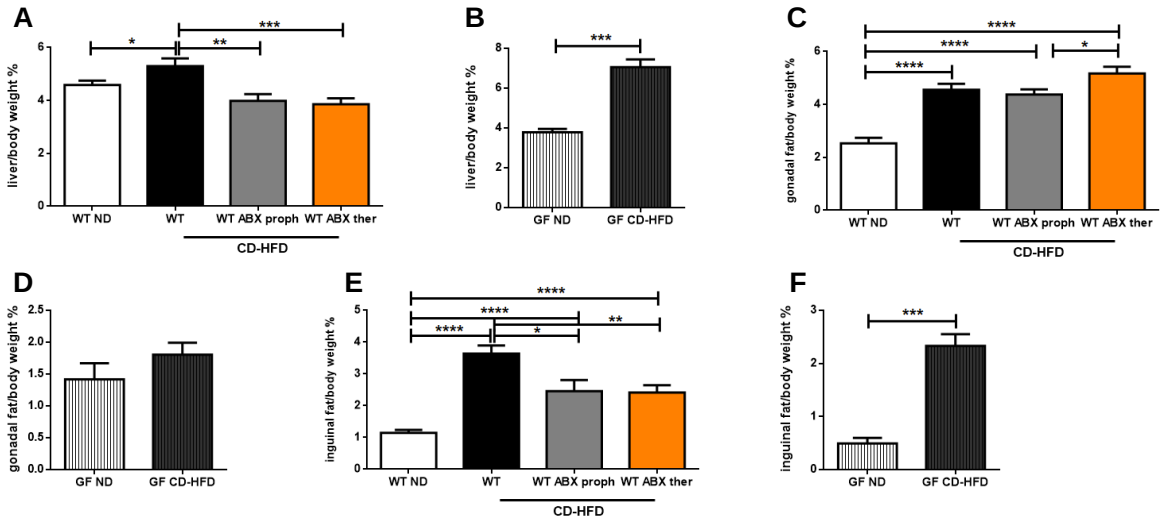

Figure 30. Microbiome modulation affects fat deposition in mice on CD-HFD

(A) Quantitative analysis of liver-to-body weight ratio of WT ND and CD-HFD, WT ABX proph and ther, GF ND and CD-HFD livers in 6-month-old mice (n>6). **(B)** Quantitative analysis of perigonadal white adipose tissue and inguinal white adipose tissue-to-body weight ratio of the respective 6-month-old mice (n>6). All data are presented as mean ± SEM.

6.4.5 Hepatic activation and infiltration of T cells in antibiotic treated and germ free C57BL/6 mice on CD-HFD

FACS analysis revealed fewer $CD3^+$ cells in the livers of WT ABX proph and ther mice compared to WT CD-HFD mice **(fig. 31A)** and more $CD3^+$ cells in GF CD-HFD livers compared to GF ND **(fig. 31B)**. FACS analysis also showed significantly fewer $CD4^+$ cells in WT ABX proph mice and a trend for reduced $CD4^+$ numbers in WT ABX ther compared to WT CD-HFD mice **(fig. 31C)**. The $CD4^+$ cells in GF CD-HFD mice were elevated compared to GF ND **(fig. 31D)** whereas there were significantly fewer $CD8^+$ cells in both ABX groups compared to WT CD-HFD **(fig. 31E)** but more

in GF CD-HFD livers compared to GF ND **(fig. 31F)**. Deeper evaluation, through FACS, of the T cell population showed fewer CD44+CD62L$^-$ CD4$^+$ and CD8$^+$ cells (memory cells) in both ABX groups compared to WT CD-HFD mice **(fig. 31G, I)** but more CD4$^+$ and CD8$^+$ memory cells in GF CD-HFD compared to GF ND (**fig. 31H, J)**. Hepatic activated CD4$^+$ and CD8$^+$ cells were decreased in both ABX groups compared to WT CD-HFD group **(fig. 31K, M)** but they were increased in GF CD-HFD mice compared to GF ND mice **(fig. 31L, N)**. CD3$^+$ IHC of liver sections showed more CD3$^+$ cells in GF CD-HFD mice compared to GF ND **(fig. 31O)** and fewer CD3$^+$ cells in the ABX groups compared to WT CD-HFD mice, consistent with the FACS analysis **(fig. 31P)**.

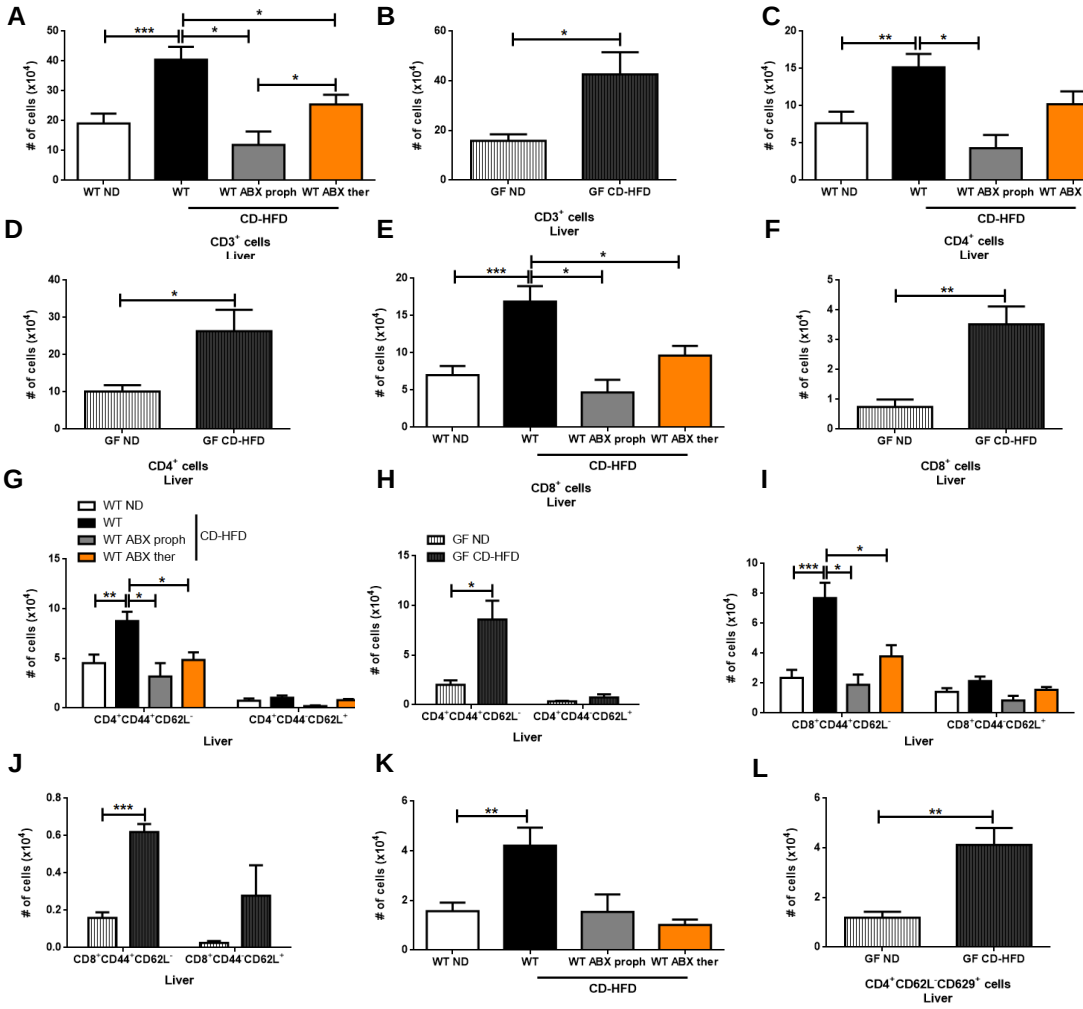

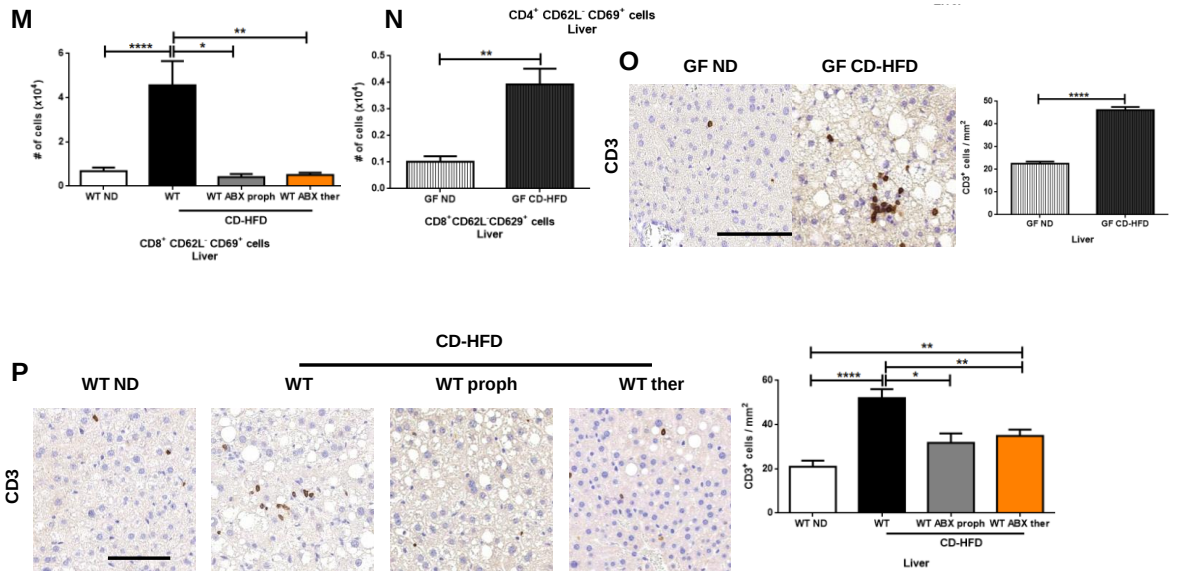

Figure 31. Antibiotic administration leads to reduced T-cell activation in the CD-HFD liver but microbiome presence is not necessary for the T-cell activation

(A-N) Quantification of flow cytometric analysis of livers 6-month-old WT ND and CD-HFD, WT ABX proph and ther (n>8), GF ND and CD-HFD (n>6); **(A, B)** $CD3^+$ cells, **(C, D)** $CD4^+$ cells, **(E, F)** $CD8^+$ cells, **(G, H)** $CD4^+CD44^+$ $CD62L^-$ and $CD4^+CD44^-CD62L^-$ cells, **(I, J)** $CD8^+CD44^+$ $CD62L^-$ and $CD8^+CD44^-CD62L^-$ cells **(K, L)** $CD4^+CD62L^-CD69^+$ cells, (**M, N)** $CD8^+CD62L^-CD69^+$ cells. **(O)** Representative $CD3^+$ IHC on liver sections of GF ND and CD-HFD mice (left) and quantification of $CD3^+$ T cells per mm^2 (n>6) (right). **(P)** Representative $CD3^+$ IHC on liver sections of WT ND and CD-HFD, WT ABX proph and ther mice (right) and quantification of $CD3^+$ T cells per mm^2 (n>8) (left). The scale bar represents 100 mm. All data are presented as mean ± SEM.

6.4.6 B cells and myeloid cells in the antibiotic treated and germ free C57BL/6 CD-HFD livers

In both CD-HFD ABX groups (proph and ther) we observed no increase in hepatic $B220^+$ cells as evaluated by IHC **(fig. 32A)** similar to GF CD-HFD mice **(fig. 32B)** compared to ND. Using IHC we noted a decrease in hepatic $F4/80^+$ cells in both CD-HFD ABX groups compared to CD-HFD mice **(fig. 32C upper row)**. In addition, $MHCII^+$ cells in the liver were decreased in both CD-HFD ABX groups compared to CD-HFD, even though $MHCII^+$ cells in the ABX proph group remained high compared to ND **(fig. 32C lower row)**. Interestingly, $F4/80^+$ cells in GF CD-HFD were at similar levels to GF ND **(fig. 32D upper row)** whereas $MHCII^+$ cells were higher in GF CD-HFD compared to GF ND **(fig. 32D lower row)**.

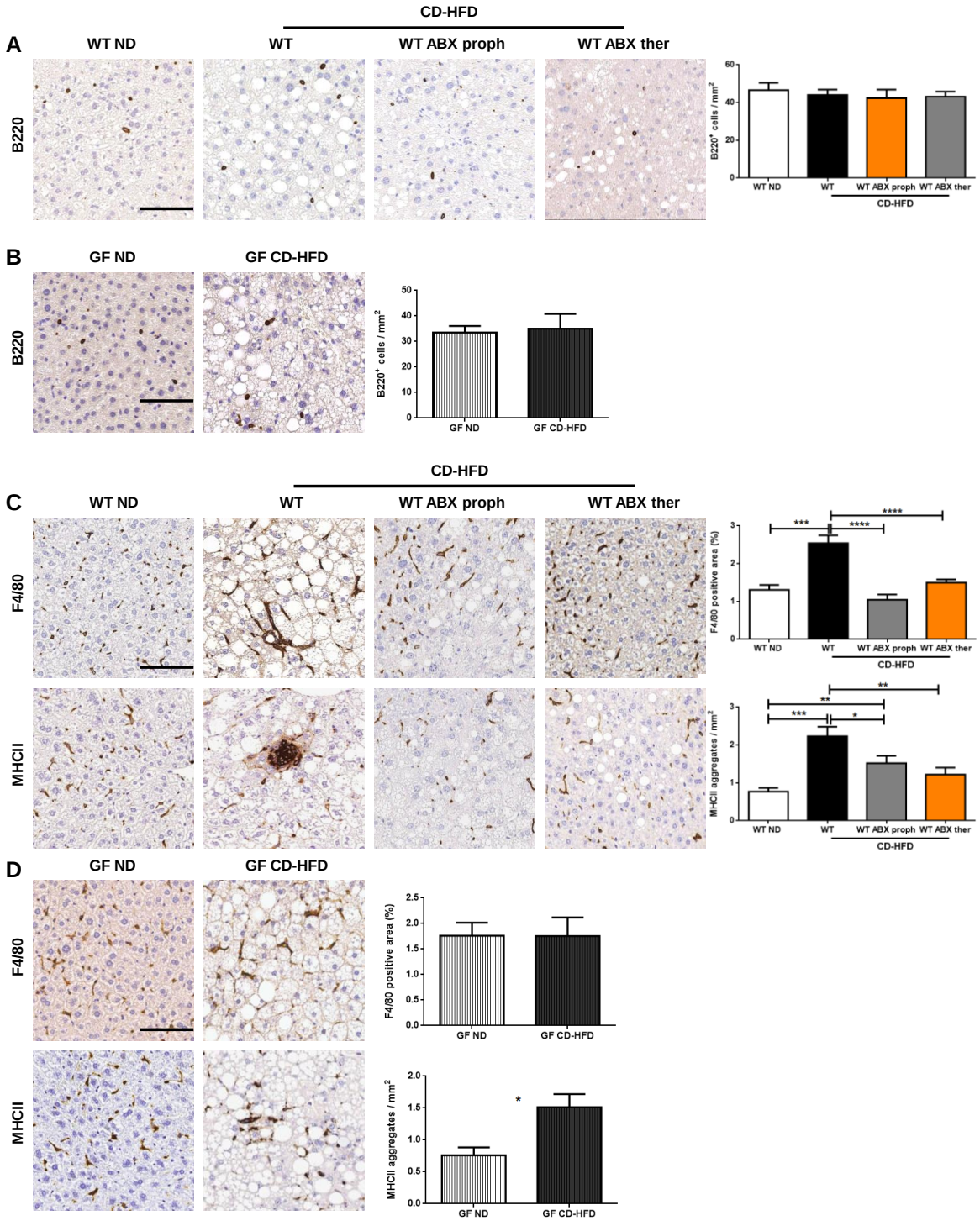

Figure 32. B cells are not affected by microbiome modulation in CD-HFD liver contrary to F4/80$^+$ and MHCII$^+$ cells

(A, B) Representative B220$^+$ IHC on liver sections of WT ND and CD-HFD, WT ABX and ther (left) and quantification of B220$^+$ T cells per mm^2 (n>8) (right) **(A)**, and GF ND and CDHFD (n>6) **(B)**. **(C, D)** Representative F4/80$^+$ (upper row) and MHCII$^+$ (lower row) IHC on liver sections of WT ND and CD-HFD, WT ABX and ther (left) and quantification of F4/80$^+$ and MHCII$^+$ cells per mm^2 (n>8) (right) **(C)**, and GF ND and CDHFD (n>6) **(D)**. The scale bar represents 100 mm. All data are presented as mean ± SEM

6.4.7 B cells of the small intestine lamina propria in germ free C57BL/6 mice on CD-HFD: a comparison with SPF C57BL/6 mice on CD-HFD

Next we evaluated through FACS the frequencies of different B-cell subpopulations in the lamina propria of the small intestine for GF ND and CD-HFD mice and in SPF ND and CD-HFD mice. No differences appeared in the $CD45^+$ compartment between the four groups **(fig. 33A)**. There were no differences in the $CD19^+$ and $CD20^+$ cells between GF ND and CD-HFD **(fig. 33B upper graph)** while in SPF mice, $CD19^+$ and $CD20^+$ cells appeared in higher frequencies in CD-HFD mice compared to ND **(fig. 33B lower graph)**. Further evaluation of $CD19^+$ and $CD20^+$ subpopulations showed no difference s between the ND and CD-HFD GF mice **(fig. 33C upper graph)** contrary to SPF mice where the frequencies of $CD19^+CD20^+$ and $CD19^-CD20^+$ were higher in CD-HFD compared to ND mice **(fig. 33C lower graph)**. In GF CD-HFD mice, $CD19^+IgD^+$ cells appeared in significant higher frequencies compared to GF ND **(fig. 33D upper graph)**. In SPF mice, there was no change in $CD19^+IgD^+$ cells between ND and CD-HFD, but $CD19^+IgA^+$ and $CD19^+IgM^+$ cells were more frequent in CD-HFD compared to ND **(fig. 33D lower graph)**. In GF mice, a trend was observed toward more $CD20^+IgD^+$ cells in CD-HFD compared to ND GF mice **(fig. 33E upper graph)**. In SPF mice, $CD20^+IgA^+$ and $CD20^+IgM^+$ cells were in higher frequencies in CD-HFD compared to ND **(fig. 33E lower graph)**. Further gating revealed a trend in higher numbers of $CD19^+CD20^+IgD^+$ frequencies in CD-HFD compared to ND GF mice **(fig. 33F upper graph)** whereas in SPF mice, there was a trend towards higher frequencies for $CD19^+CD20^+IgD^+$ and $CD19^+CD20^+IgM^+$ cells in CD-HFD mice compared to ND **(fig. 33F lower graph)**. $CD19^+CD20^-IgD^+$ cells appeared in higher frequencies in GF CD-HFD compared to GF ND **(fig. 33G upper graph)** similar to SPF CD-HFD mice compared to ND **(fig. 33G lower graph)**. In GF CD-HFD mice there was a reduction in $CD19^-CD20^+IgM^+$ cells in CD-HFD compared to ND mice **(fig. 33H upper graph)** and in SPF CD-HFD mice there was a trend toward higher frequencies in $CD19^-CD20^+IgD^+$ **(fig. 33H lower graph)**. In GF CD-HFD mice there were no differences in $CD19^-CD20^-IgA^+$, $CD19^-CD20^-IgD^+$ and $CD19^-CD20^-IgM^+$ frequencies compared to ND **(fig. 33I upper graph)** contrary to SPF mice where $CD19^-CD20^-IgA^+$ were found at higher frequencies in CD-HFD, and $CD19^-CD20^-IgD^+$ had a trend for higher frequencies in CD-HFD mice compared to ND mice **(fig. 33I lower graph)**.

We then proceeded with further FACS analysis in order to evaluate the activation status and the potential capacity for antigen presentation of B cells in the lamina propria of the small intestine, in both GF and SPF conditions. $MHCII^+IgA^+$ and $MHCII^+IgM^+$ cells were observed in significantly lower frequencies in GF CD-HFD mice compared to ND, whereas there was a trend toward higher frequencies in $MHCII^+IgD^+$ in GF CD-HFD compared to ND **(fig. 33J upper graph)**. In SPF mice, $MHCII^+IgD^+$ and $MHCII^+IgM^+$ were significantly more frequent in CD-HFD compared to ND **(fig. 33J lower graph)**. Further gating revealed higher frequencies of $MHCII^+CD19^+$ cells in GF CD-HFD compared to ND **(fig. 33K upper graph)** similar to SPF mice; in addition in SPF mice there was a trend toward higher $MHCII^+CD20^+$ cells in CD-HFD compared to ND **(fig. 33K lower graph)**. In GF mice, $MHCII^+CD19^+IgD^+$ cells were significantly more frequent in CD-HFD compared to ND, contrary to $MHCII^+CD19^+IgA^+$ cells, which were significantly lower **(fig. 33L upper graph)**. $MHCII^+CD19^+IgD^+$ cells were also significantly more frequent in SPF CD-HFD mice compared to ND **(fig. 33L lower graph)**. In GF mice, $MHCII^+CD20^+IgA^+$ and $MHCII^+CD20^+IgM^+$ cells were significantly less frequent in CD-HFD whereas $MHCII^+CD20^+IgD^+$ cells showed a trend toward higher frequencies compared to ND **(fig. 33M upper graph)**. In SPF mice, $MHCII^+CD20^+IgD^+$ cells were observed at significantly higher frequencies in CD-HFD compared to ND **(fig. 33M lower graph)**. $MHCII^+CD19^+CD20^+IgA^+$ cells showed a trend toward lower frequencies in CD-HFD compared to ND. On the other hand, $MHCII^+CD19^+CD20^+IgD^+$ cells were more frequent in GF CD-HGF compared to ND **(fig. 33N upper graph)**, similar to SPF mice **(fig. 33N lower graph)**. $MHCII^+CD19^-CD20^+IgM^+$ cells were less frequent, $MHCII^+CD19^-CD20^+IgA^+$ cells showed a trend toward less frequencies and $MHCII^+CD19^-CD20^+IgD^+$ a trend toward higher frequencies in GF CD-HFD compared to ND **(fig. 33O upper graph)**. In SPF mice, $MHCII^+CD19^-CD20^+IgD^+$ were more frequent in CD-HFD compared to ND **(fig. 33O lower graph)**. Finally, $MHCII^+CD19^+CD20^-IgA^+$ and $MHCII^+CD19^+CD20^-IgM^+$ cells were significantly lower and trended toward lower frequencies respectively in GF CD-HFD mice compared to ND, whereas $MHCII^+CD19^+CD20^-IgD^+$ cells were significantly higher in GF CD-HFD compared to ND **(fig. 33P upper graph)**. Similar to GF mice, in SPF mice $MHCII^+CD19^+CD20^-IgD^+$ cells were found at significantly higher frequencies in CD-HFD compared to ND, as well as $MHCII^+CD19^+CD20^-IgM^+$ cells **(fig. 33P lower graph)**. Summarizing, we observed significant differences

between GF ND and CD-HFD in $MHCII^{+}IgD^{+}$ populations, similar to SPF mice. As expected, we didn´t observe any differences in IgA^{+} and IgM^{+} populations between ND and CD-HFD germ free mice, a result that is attributed to lack of microbiota.

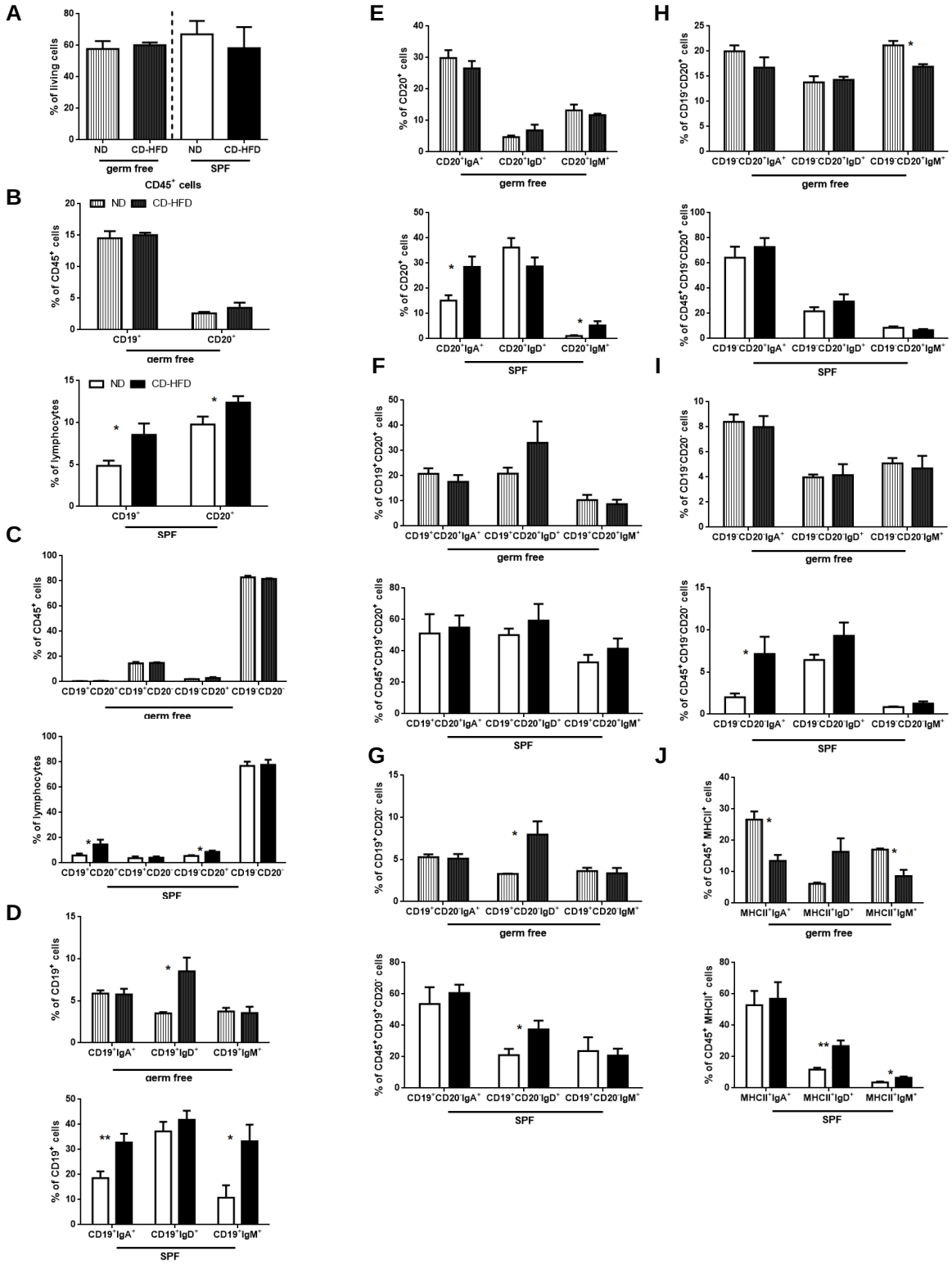

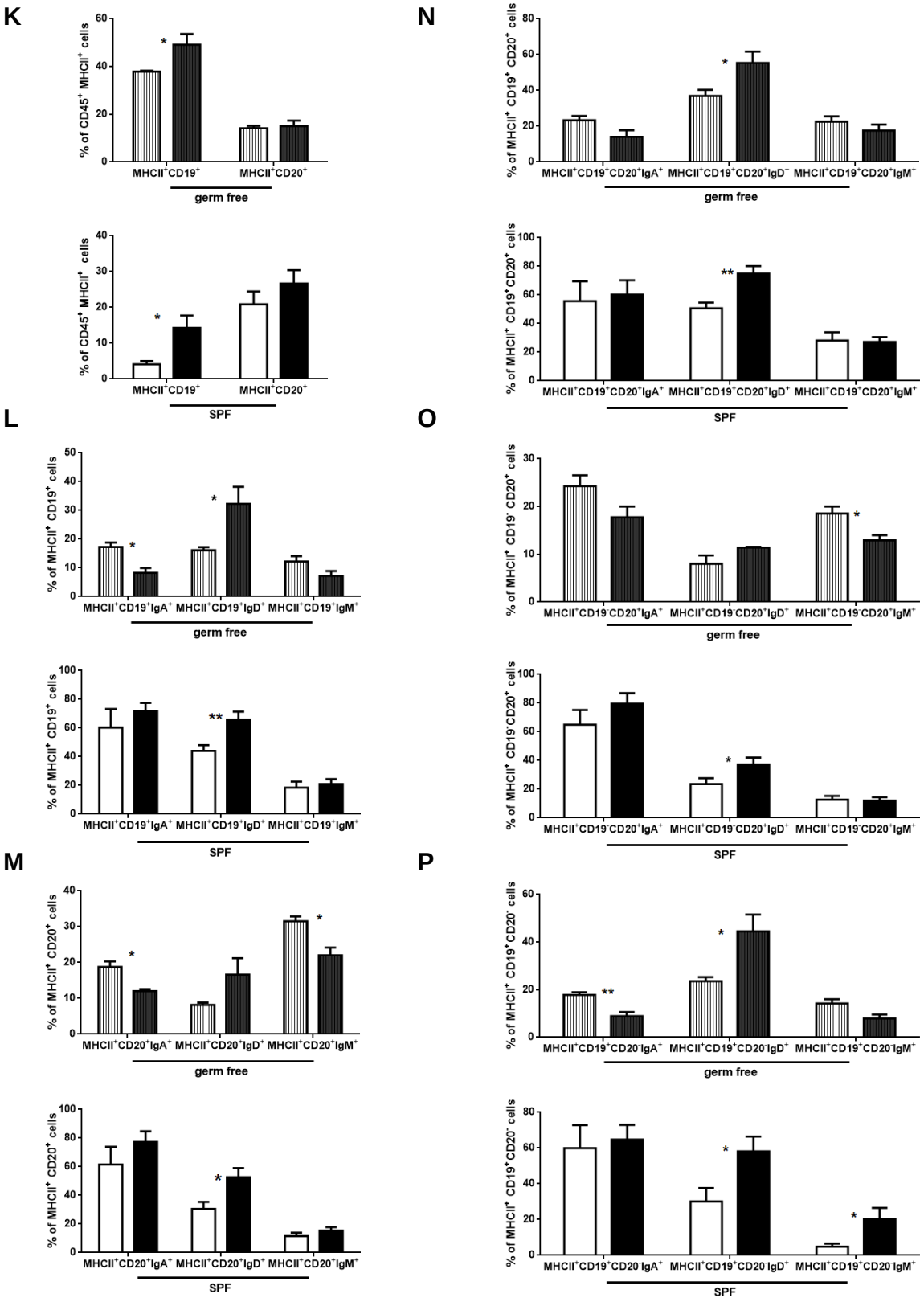
K
% of CD45+ MHCII+ cells
MHCII+CD19+
MHCII+CD20+
germ free
% of CD45+ MHCII+ cells
MHCII+CD19+
MHCII+CD20+
SPF
N
% of MHCII+ CD19+ CD20+ cells
MHCII+CD19+CD20+IgA+
MHCII+CD19+CD20+IgD+
MHCII+CD19+CD20+IgM+
germ free
% of MHCII+ CD19+CD20+ cells
MHCII+CD19+CD20+IgA+
MHCII+CD19+CD20+IgD+
MHCII+CD19+CD20+IgM+
SPF
L
% of MHCII+ CD19+ cells
MHCII+CD19+IgA+
MHCII+CD19+IgD+
MHCII+CD19+IgM+
germ free
% of MHCII+ CD19+ cells
MHCII+CD19+IgA+
MHCII+CD19+IgD+
MHCII+CD19+IgM+
SPF
O
% of MHCII+ CD19-CD20+ cells
MHCII+CD19-CD20+IgA+
MHCII+CD19-CD20+IgD+
MHCII+CD19-CD20+IgM+
germ free
% of MHCII+ CD19-CD20+ cells
MHCII+CD19-CD20+IgA+
MHCII+CD19-CD20+IgD+
MHCII+CD19-CD20+IgM+
SPF
M
% of MHCII+ CD20+ cells
MHCII+CD20+IgA+
MHCII+CD20+IgD+
MHCII+CD20+IgM+
germ free
% of MHCII+ CD20+ cells
MHCII+CD20+IgA+
MHCII+CD20+IgD+
MHCII+CD20+IgM+
SPF
P
% of MHCII+ CD19+CD20- cells
MHCII+CD19+CD20-IgA+
MHCII+CD19+CD20-IgD+
MHCII+CD19+CD20-IgM+
germ free
% of MHCII+ CD19+CD20- cells
MHCII+CD19+CD20-IgA+
MHCII+CD19+CD20-IgD+
MHCII+CD19+CD20-IgM+
SPF

Figure 33. B cells in the lamina propria of the small intestine in germ free and SPF conditions on CD-HFD **(A-P)** Frequencies of flow cytometric analysis of lamina propria of the small intestine of 6-month-old SPF ND and CD-HFD and GF ND and CD-HFD (n>6); **(A)** CD45+ cells, **(B)** $CD19^+$ and $CD20^+$cells (SPF, upper graph) (GF, lower graph), **(C)** $CD19^+CD20^+$, $CD19^+CD20^-$, $CD19^-CD20^+$ and $CD19^-CD20^-$ cells, **(D)** $CD19^+IgA^+$, $CD19^+IgD^+$ and $CD19^+IgM^+$cells, **(E)** $CD20^+IgA^+$, $CD20^+IgD^+$ and $CD20^+IgM^+$cells, **(F)** $CD19^+CD20^+IgA^+$, $CD19^+CD20^+IgD^+$, $CD19^+CD20^+IgM^+$ cells, **(G)** $CD19^+CD20^-IgA^+$, $CD19^+CD20^-IgD^+$ and $CD19^+CD20^-IgM^+$ cells, **(H)** $CD19^-CD20^+IgA^+$, $CD19^-CD20^+IgD^+$ and $CD19^-CD20^+IgM^+$ cells, **(I)** $CD19^-CD20^-IgA^+$, $CD19^-CD20^-IgD^+$ and $CD19^-CD20^-IgM^+$ cells, **(J)** $MHCII^+IgA^+$, $MHCII^+IgD^+$and $MHCII^+IgM^+$ cells, **(K)** $MHCII^+CD19^+$ and $MHCII^+CD20^+$ cells, **(L)** $MHCII^+CD19^+IgA^+$, $MHCII^+CD19^+IgD^+$ and $MHCII^+CD19^+IgM^+$cells, **(M)** $MHCII^+CD20^+IgA^+$, $MHCII^+CD20^+IgD^+$ and $MHCII^+CD20^+IgM^+$cells, **(N)** $MHCII^+CD19^+CD20^+IgA^+$, $MHCII^+CD19^+CD20^+IgD^+$, $MHCII^+CD19^+CD20^+IgM^+$ cells, **(O)** $MHCII^+CD19^-CD20^+IgA^+$, $MHCII^+CD19^-CD20^+IgD^+$ and $MHCII^+CD19^-CD20^+IgM^+$ cells, **(P)** $MHCII^+CD19^+CD20^-IgA^+$, $MHCII^+CD19^+CD20^-IgD^+$ and $MHCII^+CD19^+CD20^-IgM^+$ cells. All data are presented as mean ± SEM.

7. Discussion

From previous studies in our lab, it was shown that immune cells are important players in NASH development and in NASH-to-HCC transition in a CD-HFD mouse NASH model[88]. Amongst others, it was shown that the activation of intrahepatic $CD8^+$ T cells and NKT cells facilitated NASH-to-HCC transition and that mice lacking mature B and T cells ($Rag1^{-/-}$) did not develop NASH, nor HCC, while fed a long-term CD-HFD[88].

To date, the exact role of B cells in NASH development and subsequent HCC development remains unclear. It was recently shown in mice that accumulation of liver-resident IgA^+ $PDL1^+$ cells in the context of chronic inflammation and NASH is involved in the suppression of $CD8^+$ T-cell responses inducing HCC[102]. In obesity, it has been shown in a CCl4 mouse model that B cells can drive $CD4^+$ T-cell activation in the adipose tissue[100] and that they are involved in the development of fibrosis in an antibody-independent manner[101]. With regard to gut-liver axis, it has been reported that in the liver there are IgA^+ B cells that can drive antigen specific responses in a T-cell dependent and T-cell independent manner[103]. The authors argued that these IgA^+ B cells migrate from the small intestine to the liver through the portal vein system and it is unlikely that IgA CSR occurs in the liver, contrary to what has been proposed by Shalapour et al[102].

Our data show that in a CD-HFD mouse NASH model, B cells are playing an important role in NASH development. $JH^{-/-}$ mice that are lacking mature B cells did not develop NASH or HCC on a long-term CDHFD (fig. 6-9), contrary to WT CD-HFD mice, as it has been described here and also in 2014 by Wolf et al[88]. $JH^{-/-}$ CD-HFD mice, while obese, demonstrated significantly reduced serum ALT and cholesterol levels and also showed no impairment in insulin response after glucose challenge, contrary to WT CD-HFD mice, indicating that B cells are important also for the metabolic syndrome which is usually associated with NASH pathology in humans, as well[63].

µMT mice are largely B-cell deficient mice harbouring only IgA^+ B cells in the lamina propria (LP) of their small intestine, as reported here (fig. 13, 14) and by Macpherson et al, 2001[191]. On long term CD-HFD, µMT mice demonstrated obesity, metabolic syndrome and NASH development in the absence of perisinusoidal fibrosis with a

significantly lower HCC incidence compared to WT CD-HFD mice (fig. 15-18). Contrary to what has been reported by Macpherson et al[191], we didn't observe IgA expression in the serum of μMT mice (fig. 22) but only in the lamina propria of the small intestine (fig. 13, 14). Therefore we concluded that the intestinal B cell response suffices for the induction of NASH but is less important for the development of hepatic fibrosis, something that we hypothesized is the main reason for the low HCC incidence in μMT CD-HFD mice. $JH^{-/-}$ CD-HFD did not develop hepatic fibrosis either (fig. 6H). Moreover, the results suggest that the pathways from NASH to hepatic fibrosis to HCC is not linear, something that has also been suggested for the human situation[83]. In addition, the data indicate that LP B cells and secondary lymphoid organs (SLOs) B cells are playing different roles in the pathology; the former are involved in NASH development whereas the latter are involved in hepatic fibrosis in NASH.

μMT mice similar to $JH^{-/-}$, do not have structured SLOs (fig. 13A) since mature B cells are necessary for the correct architecture of SLOs [195]. The development of IgA^{+} B cells in the μMT involves an alternative B cell ontogeny pathway, where expression of membrane IgM or IgD at an early stage is not a requirement[191]. In addition it has also been reported that gut IgA CSR can occur in the absence of CD40 responses and that it is independent of the germinal centre (GC) reaction[196]. The authors of the latter study, Bergqvist et al, were unable to successfully show that gut IgA CSR can indeed occur in the LP, something that has been reported in an earlier and more detailed study by Fagarasan et al[197], thus concluding that LP is not a site for IgA CSR[196]. Moreover, two studies have shown that LTβR signalling on LP stromal cells is required for the presence of B cells in the LP and for IgA production, emphasizing the sufficiency of the LP environment for the generation of IgA plasma cells and implying that the presence of structured SLOs is not necessary for IgA induction[198,199]. μMT, like $JH^{-/-}$ mice have defective GC reaction and therefore no appropriate CD40 responses[200] between T and B cells in the SLOs. We could show that blocking CD40-CD40L interactions through the administration of an i.p. injected antibody (clone: MR1) in μMT CD-HFD mice 4 months on diet with established liver damage, as demonstrated by serum ALT, had no effect on NASH development (data not shown) as expected.

Efficient therapeutic depletion of B cells, using an αCD20 antibody from GenTech (clone: 5D2), in WT and μMT mice 4 months on CD-HFD was successful in abrogating the NASH phenotype (fig. 10, 12, 19, 21) confirming the important role of B cells in NASH development. We repeated the B cell depletion experiment using Rituximab on WT CD-HFD mice, with similar approach to the αCD20 (5D2) depletion. Rituximab depleted the SLOs and circulating B cells but it didn't deplete the LP B cells of the small intestine (data not shown). The Rituximab CD-HFD treated mice developed NASH in the absence of perisinusoidal hepatic fibrosis similar to μMT CD-HFD mice, thus strengthen our argument about the differential role of B cells in NASH and hepatic fibrosis development. We observed the same effect when we used the 5D2 clone to deplete B cells in a Western-Diet NASH mouse model, a diet high in saturated fat, trans-fat, and sugar[201]; the fibrotic phenotype was abrogated and the serum ALT values were lower compared to the untreated group (data not shown) verifying the crucial role of B-cells in NASH pathology in an independent NASH model. αCD20 treatment is not currently considered an option for NASH treatment as it carries the danger of inducing severe side effects due to immunosuppresion. Nevertheless, preliminary data from NAFLD patients receiving αCD20 treatment for rheumatoid arthritis, showed that 5/11 patients experienced a decrease in their serum ALT values after 6 months of anti-B cell therapy (data not shown) corroborating our *in vivo* studies. However an in-depth analysis will be required for definitive conclusions and is currently ongoing.

Human studies have shown higher serum IgG titers in about 40% of adults with NAFLD/NASH and 60% of children with NASH[98,99]. Elevated serum immunoglobulins are observed in specific liver diseases, such as autoimmune hepatitis (raised IgG), primary biliary cirrhosis (raised IgM) and alcoholic liver disease (higher IgA)[117,118]. It has also been reported that there is an increase of serum IgA levels in patients with metabolic syndrome, T2D[121,122] and NAFLD patients[123]. Moreover, it has been suggested that IgA could potentially be used as a marker of advanced fibrosis[123]. These observations are in agreement with our findings from the $JH^{-/-}$, the μMT and the B cell depletion experiments.

Our CD-HFD experiments with $AID^{-/-}$, AIDg23s and IgMi mice illuminated further the role of secreted immunoglobulins in NASH development and fibrosis. $AID^{-/-}$ mice having a complete defect in CSR, yet can still produce low-affinity IgM[192]. $AID^{-/-}$ mice

on CD-HFD developed obesity and NASH (fig. 23, 26) in the absence of hepatic fibrosis. AIDg23s mice can produce low-affinity IgA and IgM[193], and while on CD-HFD they developed obesity, NASH and hepatic fibrosis (fig. 23, 26). IgMi mice do not secrete immunoglobulins apart from IgG1[194], and when on CD-HFD they developed obesity but they abrogated NASH and hepatic fibrosis (fig. 24, 26).

Taken together **(table 8)**, we concluded that low-affinity secreted IgA is important for perisinusoidal fibrosis in NASH liver while local intestinal IgA B-cell response suffices for NASH development as it was shown from the μMT data. On the other hand, the $AID^{-/-}$ data indicate that low-affinity IgM secretion should also suffice for NASH development. IgM and IgA share a number of similarities, as both can be secreted at mucosal surfaces [191]. IgM and IgA are more closely related than IgG and IgE while μ and α chains share a characteristic secretory segment in their loci[202]. Also, IgM- and IgA-secreting plasma cells are derived from the peritoneal lymphocyte compartment[203,204]. In addition, Pinto et al have shown that human IgA and IgM, but not IgG, plasma cells isolated from the bone marrow and the colon LP express a functional BCR and that can directly respond to antigenic stimulation[205]. Considering that αCD20 treatment does not affect long-lived plasma cells, the most likely B-cell populations mediating NASH in our CD-HFD mouse model are short-lived plasma cells or unconventional Ig-secreting B cells. Of note, our data show that the B-cell populations present in the lamina propria of μMT small intestine are $CD20^{+}CD19^{-}IgA^{+}$ and $CD20^{-}CD19^{-}IgA^{+}$ cells (long-lived plasma cells), which means the population that most likely is responsible for driving the pathology is a $CD20^{+}CD19^{-}IgA^{+}$ cell. The role of IgA secretion in NASH-related hepatic fibrosis still needs further evaluation with more functional experiments and a detailed analysis of the molecular biology of the individual fibrogenic events.

Table 8. A summary of our experimental groups for the role of B cells in NASH development and in fibrosis

Exp. Mouse Group	B cells & Igs	NASH	Hepatic Fibrosis	HCC
WT CD-HFD	LP & SLOs B cells, IgA, IgM, IgG	yes	yes	yes (~25%)
JH$^{-/-}$ CD-HFD	no	no	no	no
μMT CD-HFD	only LP IgA B cells	yes	no	low incidence (5%)
αCD20 (clone 5D2) CD-HFD	only long-lived plasma cells	no	no	-
Rituximab CD-HFD	only long-lived plasma cells & LP B cells	yes	no	-
AID$^{-/-}$ CD-HFD	low affinity IgM	yes	no	-
AIDg23s CD-HFD	low affinity IgM & IgA	yes	yes	-
IgMi CD-HFD	only IgG	no	no	-

What remains an open question in this study is the role of B cells in fat accumulation and distribution. Here we described that in WT CD-HFD the gonadal and inguinal (subcutaneous) fat are increased in WT CD-HFD and that in JH$^{-/-}$ CD-HFD mice the subcutaneous fat -to-body weight ratio is decreased compared to WT CD-HFD mice (fig. 7). On the contrary, in μMT CD-HFD mice, gonadal and inguinal fat remained as high as in the WT CD-HFD mice but after αCD20 treatment μMT CD-HFD mice displayed a decrease in the inguinal fat compared to the untreated mice (fig. 20), similar to αCD20 WT CD-HFD treated mice. Interestingly enough, AID$^{-/-}$, AIDg23s and IgMi on CD-HFD showed a decrease in the gonadal fat compared to the WT CD-HFD but not in the inguinal fat. AIDg23s also showed a decrease in the inguinal fat compared to WT CD-HFD, but it remained significantly higher compared to WT ND mice. AID$^{-/-}$, AIDg23s and IgMi CD-HFD mice displayed obesity and, in the case of the IgMi, the gonadal fat was decreased whereas the inguinal was unaffected (fig. 25).

The description of the differential fat deposition in the different experimental groups does not illuminate a particular mechanism of action of B cells in adiposity but it highlights the need for further investigation. For future experiments, the mesenteric fat should also be taken into account, as well as the fat around the kidneys (known

as perirenal fat) and the renal sinus fat which is the fat around the renal arteries (a condition known as fatty kidney). These latter three types of fat are also important in obesity, metabolic syndrome and T2D. Emerging evidence suggest that B cells play a role in obesity-induced adipose tissue inflammation and insulin resistance. It has been suggested that B cells accumulate in the visceral adipose tissue and modulate T cells in an MHC-dependent manner, thereby promoting the impairment of metabolic parameters, probably through B-cell antigen presentation to T cells [206]. Accumulation of B cells in adipose tissue has also been reported elsewhere[207] and that in human obese individuals, plasma cell density is higher in the visceral fat compared to subcutaneous fat[208]. In another human study it was reported that in obese subjects, B cells in the subcutaneous fat are present in higher numbers than T cells, and form crown-like structures contributing to inflammation[209].

Mucosal membranes provide a dynamic interface where gut microbiota in the lumen interact with the gut immune system and in particular the IgA^+ B cells, modulating gut homeostasis[185]. There is a growing evidence indicating that gut microbiota are playing an important role in obesity[135-141] and chronic liver diseases such as NAFLD[143] and NASH[144,145]. Ongoing clinical trials that target the gut-liver axis in chronic liver disease involve the use of different approaches of microbiome modulation, including the use of antibiotics[127].

Our data show that modulation of microbiome through the administration of a wide spectrum antibiotic cocktail ameliorated NASH phenotype in a prophylactic and therapeutic manner (fig. 27, 31, 32). In addition, hepatic fibrosis was abrogated in both antibiotic groups but not the insulin response (fig. 27). When the antibiotics were administrated therapeutically we observed two groups of mice: almost 50% had serum ALT values lower than 50U/L and 50% higher than 50 U/L (fig. 27F). Further analysis revealed that there is a strong correlation of the ALT values with the body weight (fig. 27G) and the hepatic triglycerides (fig. 27J) despite the fact that these mice showed no hepatic activation of T cells (fig. 31) and no hepatic infiltration of $F4/80^+$ and $MHCII^+$ cells (fig. 32). These observations indicate that in the therapeutic antibiotic CD-HFD mice, the higher serum ALT values were most likely due to hepatic lipid accumulation and not due to infiltration of immune cells in the liver.

16s rRNA sequencing of faecal material from WT ND, WT CD-HFD revealed a distinct microbiome profile for the CD-HFD mice with the phylum Firmicutes being more abundant (fig. 28), disturbing the Firmicutes/Bacteriodes ratio. Studies in obesity indicate that Firmicutes demonstrate higher relative abundance compared to the micobiota of lean individuals in mice[136] and humans[210,211]. In our antibiotic treated CD-HFD mice the only bacterium which was not depleted was of the genus *Lactococcus*. *Lactococcus* has been proposed to act as probiotic with a potential beneficial function in obesity[212] and NAFLD[213,214]. Our data thus far do not provide any mechanistic insights into this issue, but we hypothesize that NASH abrogation in the antibiotic CD-HFD mice could potentially be due to the dominant, protective presence of *Lactococcus*. Ongoing experiments on this topic will provide more detailed information and will determine whether our hypothesis is true.

Surprisingly, our germ free mice on long-term CD-HFD developed NASH, hepatic fibrosis and impaired insulin response (fig. 29, 31, 32). Bäckhed et al, through colonization and western-diet experiments, have shown that germ free mice gain less weight than conventional mice and were protected against diet-induced obesity[215,216]. Rabot et al reached the same conclusion by using HFD[217], contrary to our observations with HFD experiments in germ free mice (data not shown). On the other hand, Bindels et al have noted that C57BL/6 germ free mice on a western diet were more resistant to obesity compared to C3H/HeN germ free mice on western diet[218]. Nevertheless, both strains gained weight, with the germ free C57BL/6 mice gaining less weight compared to SPF. It was also noted that the energy intake was the same for the two strains when compared with SPF[218].

In our study we describe for the first time CD-HFD-induced obesity and NASH in germ free mice, and to our knowledge it is the first time CD-HFD and HFD have been given to germ free mice for as long as 6 months. We also observed an increase in serum ALT values in germ free mice already after 3 months on diet. The reason why we are the first to describe NASH in a germ free dietary mouse model, despite studies that have been published stating the opposite, could be the specifics of our experimental design. Bindels et al have shown that the mouse strain can affect the kinetics of weight gain in germ free mice on diet[218] and we are the first to perform a germ free diet experiment for as long as 6 months (24 weeks), whereas most studies stop the experiment around week 8 on diet. Taking into account that

the mouse strain we have used is C57BL/6 and that we observed a delay in the weight gain of our germ free CD-HFD mice (they started to increase their body weight significantly after week 4-5) (fig, 29A), this might mean that we were able to observe the phenotype precisely because we kept the mice on diet for 6 months.

The mucosal immune system is essential for regulating the symbiotic relationship between the host and gut microbiota and vice versa: the intestinal bacteria develop and regulate the gut immune system while the gut immune system affects the bacterial composition[219,220].

It has been reported that chronic liver disease may be associated with increased intestinal permeability[219]. Obesity and metabolic syndrome can lead to leaky gut in mice[131] and in humans[221], and it has been shown that NAFLD patients have increased intestinal permeability with more disrupted tight junctions compared to healthy individuals[222]. Hayes et al have recently shown that the presence of commensal microbiota is important for the maturation of the colonic barrier structure and permeability[223] while Ukena et al have shown improvement of the barrier integrity in germ free mice upon bacterial colonization[224]. Our germ free studies show that sterile inflammation suffices to induce NASH, and further analysis on the intestinal barrier integrity is needed to clarify whether leaky gut is an important factor for the development of NASH pathology.

Germ free animals display severe immune defects, more pronounced in the gut, and are more susceptible to infection[225]. In the germ free gut, GALT (gut-associated lymphoid tissue) is underdeveloped with fewer and smaller Peyer's patches and mesenteric lymph nodes and with reduced mucus thickness[226,227]. B cells in germ free mice produce less secretory IgA, which is essential for maintaining gut homeostasis and barrier integrity[228]. They also have fewer T_H1 cells[229], fewer $CD4^+$ cells, including T_H17 cells[230] and decreased numbers of regulatory T cells[231].

The germ free mice on CD-HFD have shown differences in their B -cell immune profile of the lamina propria (LP) small intestine when compared to germ free ND and SPF on CD-HFD (fig. 33). Contrary to SPF LP on CD-HFD, the germ free CD-HFD mice do not have higher frequencies of $CD19^+$ and $CD20^+$ cells, and they also fail to display higher frequencies of IgA^+ and IgM^+ B cells due to CD-HFD, as the SPF mice do. What the germ free CD-HFD group has in common with the SPF CD-

HFD is that both groups show significantly higher frequencies of $CD19^{+}CD20^{-}IgD^{+}$ cells compared to their respective ND controls. Another feature the germ free and SPF mice on CD-HFD share is that both groups have higher frequencies of $MHCII^{+}IgD^{+}$, $MHCII^{+}CD19^{+}$, $MHCII^{+}CD19^{+}CD20^{-}IgD^{+}$ and $MHCII^{+}CD19^{+}CD20^{+}IgD^{+}$ cells compared to their respective ND controls, showing that in both conditions LP B cells get activated and potentially have the capacity to present antigen, most likely to $CD4^{+}$ cells.

B cells present antigen through MHCII to $CD4^{+}$ T cells primed by dendritic cells, and this cognate B cell /T cell interaction promotes B cell proliferation and differentiation either into extrafollicular plasma cells or germinal centre (GC) B cells[232,233]. B cells undergo SHM and through this process B cells are generated that either are non-secreting memory B cells or antibody-secreting plasma cells[172,234]. Usually, antigen-presenting B cells are IgM^{-} and IgD^{-}, but studies have shown that memory B cells can be maintained in a post-GC phase as precursors for plasma cells upon antigen challenge[172,180]. It has also been suggested that virus-specific long-term Ab memory leads to continuous differentiation of memory B cell into short-lived plasma cells[235].

All of our CD-HFD experimental groups that abrogated NASH ($JH^{-/-}$ mice, αCD20 therapeutic depletion IgMi mice, antibiotic treatment, both prophylactic and therapeutic) shared a common immunological hepatic profile (fig. 8, 12, 17, 21, 26, 31). In these groups, there was reduced infiltration and activation of $CD4^{+}$ and $CD8^{+}$ T cells and decreased numbers of $F4/80^{+}$ and $MHCII^{+}$ cells. SPF WT CD-HFD mice shared the same features of hepatic T cell activation with μMT, AIDg23s and the germ free mice (fig. 17, 26, 31) and the only difference is that we didn't observe more $F4/80^{+}$ cells in the germ free CD-HFD compared to their ND controls. In addition, $AID^{-/-}$ CDHFD mice showed no increase in $F4/80^{+}$ and $MHCII^{+}$ cells in their livers. Taken together, we conclude that the intestinal B cell response can drive hepatic inflammation, most likely through the gut-liver axis, and that IgA expression suffices for the activation of T cells in the liver and for $F4/80^{+}$ cell infiltration. In addition, microbiome signals are necessary for $F4/80^{+}$ cell infiltration in the CD-HFD livers and most likely the T-cell activation in the germ free CDHFD livers is due to signals driven by the hepatic lipid accumulation and the possible deregulation of lipid metabolism.

Our data illuminate a novel cellular mechanism for NASH development in a dietary mouse model **(fig. 34)**. The key factor is the LP intestinal B-cell response that communicates with the liver through the gut-liver axis, inducing liver inflammation and eventually NASH. Our data indicate that one possible mechanism of action is the secretion of immunoglobulins (IgA and IgM) but it cannot be excluded that the LP intestinal B cells might also contribute to NASH through antigen presentation. We were able to show that B cells get activated also under germ free conditions and that might also play a role in NASH development - this will be tested by depleting B cells therapeutically in germ free CD-HFD mice. Further experiments are currently ongoing with MHCIIfl/fl CD19cre CD-HFD mice to test the hypothesis that B-cell antigen presentation might play a role in NASH development.

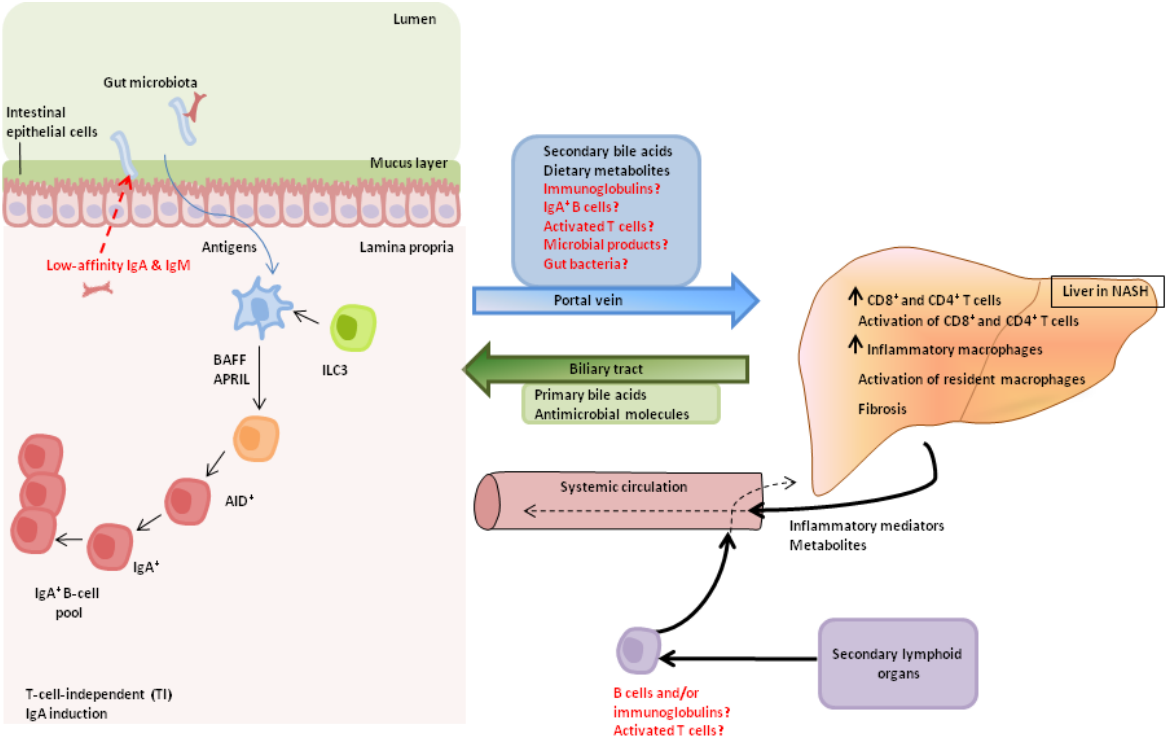

Figure 34: Potential mechanism of action of B cells in a dietary NASH mouse model. Our data suggest that T-cell-independent (TI) IgA induction pathway in the lamina propria of the small intestine (see also figure b) suffices to induce NASH in a CD-HFD dietary NASH mouse model. Low affinity IgA (and IgM) immunoglobulins can influence the flow of antigens from the lumen to the lamina propria through the intestinal epithelium but it might also be that they can educate the gut microbrial profile (red, dashed-line arrow on the left), thus influencing the translocation of metabolites from the small intestine to the liver through the portal vein. Dietary metabolites and secondary bile acids reach the liver through the portal vein but other possible candidates might also transport such as secreted immunoglobulins, IgA^+ B cells, activated T cells, altered microbial products and perhaps specific gut bacteria, inducing metabolic and inflammatory hepatic changes. Nevertheless, our results clearly show that sterile inflammation suffices to induce NASH and fibrosis and that modulation of the microbiome is an

important but not an essential factor for NASH development. Moreover, our data suggest that LP B cells are not involved in the induction of fibrosis therefore SLOs B cells and/or (low affinity) secreted immunoglobulins and perhaps activated T cells might transport to the liver through systemic circulation (that extends the gut-liver axis) and may induce hepatic fibrosis in NASH livers and in addition may contribute in NASH development. The communication between gut and liver is bidirectional: through the bile tract the liver transports primary bile acids and antimicrobial molecules to the intestinal lumen maintaining gut eubiosis by controlling unrestricted bacterial overgrowth. In addition, through systemic circulation inflammatory mediators and metabolites transport from the liver to the intestine. (adapted from Honda & Littman, *Nature*, 2016[185], Tripathi et al, *Nature Gastroenterolgy & Hepatology*, 2018[236], Anstee et al, *Nature Gastroenterolgy & Hepatology*, 2019[83])

8. References

1 Caballero, B. The global epidemic of obesity: an overview. *Epidemiol Rev* **29**, 1-5, doi:10.1093/epirev/mxm012 (2007).

2 Swinburn, B. A. *et al.* The global obesity pandemic: shaped by global drivers and local environments. *Lancet* **378**, 804-814, doi:10.1016/S0140-6736(11)60813-1 (2011).

3 Ogden, C. L., Carroll, M. D., Fryar, C. D. & Flegal, K. M. Prevalence of Obesity Among Adults and Youth: United States, 2011-2014. *NCHS Data Brief*, 1-8 (2015).

4 Imes, C. C. & Burke, L. E. The Obesity Epidemic: The United States as a Cautionary Tale for the Rest of the World. *Curr Epidemiol Rep* **1**, 82-88, doi:10.1007/s40471-014-0012-6 (2014).

5 Befort, C. A., Nazir, N. & Perri, M. G. Prevalence of obesity among adults from rural and urban areas of the United States: findings from NHANES (2005-2008). *J Rural Health* **28**, 392-397, doi:10.1111/j.1748-0361.2012.00411.x (2012).

6 Lovejoy, J. C. The menopause and obesity. *Prim Care* **30**, 317-325 (2003).

7 Christakis, N. A. & Fowler, J. H. The spread of obesity in a large social network over 32 years. *N Engl J Med* **357**, 370-379, doi:10.1056/NEJMsa066082 (2007).

8 Wardle, J. *et al.* Gender differences in food choice: the contribution of health beliefs and dieting. *Ann Behav Med* **27**, 107-116 (2004).

9 Yang, W., Kelly, T. & He, J. Genetic epidemiology of obesity. *Epidemiol Rev* **29**, 49-61, doi:10.1093/epirev/mxm004 (2007).

10 Kanter, R. & Caballero, B. Global gender disparities in obesity: a review. *Adv Nutr* **3**, 491-498, doi:10.3945/an.112.002063 (2012).

11 Troiano, R. P. *et al.* Physical activity in the United States measured by accelerometer. *Med Sci Sports Exerc* **40**, 181-188, doi:10.1249/mss.0b013e31815a51b3 (2008).

12 Varo, J. J. *et al.* Distribution and determinants of sedentary lifestyles in the European Union. *Int J Epidemiol* **32**, 138-146 (2003).

13 Monteiro, C. A., Conde, W. L. & Popkin, B. M. The burden of disease from undernutrition and overnutrition in countries undergoing rapid nutrition transition: a view from Brazil. *Am J Public Health* **94**, 433-434 (2004).

14 Popkin, B. M. Nutrition Transition and the Global Diabetes Epidemic. *Curr Diab Rep* **15**, 64, doi:10.1007/s11892-015-0631-4 (2015).

15 Popkin, B. M. An overview on the nutrition transition and its health implications: the Bellagio meeting. *Public Health Nutr* **5**, 93-103 (2002).

16 Blüher, M. Obesity: global epidemiology and pathogenesis. *Nat Rev Endocrinol* **15**, 288-298, doi:10.1038/s41574-019-0176-8 (2019).

17 Alberti, K. G. *et al.* Harmonizing the metabolic syndrome: a joint interim statement of the International Diabetes Federation Task Force on Epidemiology and Prevention; National Heart, Lung, and Blood Institute; American Heart Association; World Heart Federation; International Atherosclerosis Society; and International Association for the Study of Obesity. *Circulation* **120**, 1640-1645, doi:10.1161/CIRCULATIONAHA.109.192644 (2009).

18 Esser, N., Legrand-Poels, S., Piette, J., Scheen, A. J. & Paquot, N. Inflammation as a link between obesity, metabolic syndrome and type 2 diabetes. *Diabetes Res Clin Pract* **105**, 141-150, doi:10.1016/j.diabres.2014.04.006 (2014).

19 Pickup, J. C., Mattock, M. B., Chusney, G. D. & Burt, D. NIDDM as a disease of the innate immune system: association of acute-phase reactants and interleukin-6 with metabolic syndrome X. *Diabetologia* **40**, 1286-1292, doi:10.1007/s001250050822 (1997).

20 Yudkin, J. S., Stehouwer, C. D., Emeis, J. J. & Coppack, S. W. C-reactive protein in healthy subjects: associations with obesity, insulin resistance, and endothelial dysfunction: a potential role for cytokines originating from adipose tissue? *Arterioscler Thromb Vasc Biol* **19**, 972-978 (1999).

21 Bastard, J. P. *et al.* Elevated levels of interleukin 6 are reduced in serum and subcutaneous adipose tissue of obese women after weight loss. *J Clin Endocrinol Metab* **85**, 3338-3342, doi:10.1210/jcem.85.9.6839 (2000).

22 Haffner, S. *et al.* Intensive lifestyle intervention or metformin on inflammation and coagulation in participants with impaired glucose tolerance. *Diabetes* **54**, 1566-1572 (2005).

23 Bruun, J. M., Helge, J. W., Richelsen, B. & Stallknecht, B. Diet and exercise reduce low-grade inflammation and macrophage infiltration in adipose tissue but not in skeletal muscle in severely obese subjects. *Am J Physiol Endocrinol Metab* **290**, E961-967, doi:10.1152/ajpendo.00506.2005 (2006).

24 Belalcazar, L. M. *et al.* Lifestyle intervention and/or statins for the reduction of C-reactive protein in type 2 diabetes: from the look AHEAD study. *Obesity (Silver Spring)* **21**, 944-950, doi:10.1002/oby.20431 (2013).

25 Chawla, A., Nguyen, K. D. & Goh, Y. P. Macrophage-mediated inflammation in metabolic disease. *Nat Rev Immunol* **11**, 738-749, doi:10.1038/nri3071 (2011).
26 Shoelson, S. E., Lee, J. & Goldfine, A. B. Inflammation and insulin resistance. *J Clin Invest* **116**, 1793-1801, doi:10.1172/JCI29069 (2006).
27 Dinarello, C. A. Immunological and inflammatory functions of the interleukin-1 family. *Annu Rev Immunol* **27**, 519-550, doi:10.1146/annurev.immunol.021908.132612 (2009).
28 Esser, N. *et al.* Obesity phenotype is related to NLRP3 inflammasome activity and immunological profile of visceral adipose tissue. *Diabetologia* **56**, 2487-2497, doi:10.1007/s00125-013-3023-9 (2013).
29 Stienstra, R. *et al.* Inflammasome is a central player in the induction of obesity and insulin resistance. *Proc Natl Acad Sci U S A* **108**, 15324-15329, doi:10.1073/pnas.1100255108 (2011).
30 Vandanmagsar, B. *et al.* The NLRP3 inflammasome instigates obesity-induced inflammation and insulin resistance. *Nat Med* **17**, 179-188, doi:10.1038/nm.2279 (2011).
31 Zhou, R., Tardivel, A., Thorens, B., Choi, I. & Tschopp, J. Thioredoxin-interacting protein links oxidative stress to inflammasome activation. *Nat Immunol* **11**, 136-140, doi:10.1038/ni.1831 (2010).
32 Wen, H. *et al.* Fatty acid-induced NLRP3-ASC inflammasome activation interferes with insulin signaling. *Nat Immunol* **12**, 408-415, doi:10.1038/ni.2022 (2011).
33 L'homme, L. *et al.* Unsaturated fatty acids prevent activation of NLRP3 inflammasome in human monocytes/macrophages. *J Lipid Res* **54**, 2998-3008, doi:10.1194/jlr.M037861 (2013).
34 Schroder, K., Zhou, R. & Tschopp, J. The NLRP3 inflammasome: a sensor for metabolic danger? *Science* **327**, 296-300, doi:10.1126/science.1184003 (2010).
35 McLaughlin, T., Abbasi, F., Lamendola, C. & Reaven, G. Heterogeneity in the prevalence of risk factors for cardiovascular disease and type 2 diabetes mellitus in obese individuals: effect of differences in insulin sensitivity. *Arch Intern Med* **167**, 642-648, doi:10.1001/archinte.167.7.642 (2007).
36 Karelis, A. D., St-Pierre, D. H., Conus, F., Rabasa-Lhoret, R. & Poehlman, E. T. Metabolic and body composition factors in subgroups of obesity: what do we know? *J Clin Endocrinol Metab* **89**, 2569-2575, doi:10.1210/jc.2004-0165 (2004).
37 Reaven, G. All obese individuals are not created equal: insulin resistance is the major determinant of cardiovascular disease in overweight/obese individuals. *Diab Vasc Dis Res* **2**, 105-112, doi:10.3132/dvdr.2005.017 (2005).
38 Sims, E. A. Are there persons who are obese, but metabolically healthy? *Metabolism* **50**, 1499-1504, doi:10.1053/meta.2001.27213 (2001).
39 Wildman, R. P. *et al.* The obese without cardiometabolic risk factor clustering and the normal weight with cardiometabolic risk factor clustering: prevalence and correlates of 2 phenotypes among the US population (NHANES 1999-2004). *Arch Intern Med* **168**, 1617-1624, doi:10.1001/archinte.168.15.1617 (2008).
40 Koster, A. *et al.* Body fat distribution and inflammation among obese older adults with and without metabolic syndrome. *Obesity (Silver Spring)* **18**, 2354-2361, doi:10.1038/oby.2010.86 (2010).
41 Stefan, N. *et al.* Identification and characterization of metabolically benign obesity in humans. *Arch Intern Med* **168**, 1609-1616, doi:10.1001/archinte.168.15.1609 (2008).
42 Phillips, C. M. & Perry, I. J. Does inflammation determine metabolic health status in obese and nonobese adults? *J Clin Endocrinol Metab* **98**, E1610-1619, doi:10.1210/jc.2013-2038 (2013).
43 Kim, J. Y. *et al.* Obesity-associated improvements in metabolic profile through expansion of adipose tissue. *J Clin Invest* **117**, 2621-2637, doi:10.1172/JCI31021 (2007).
44 Parekh, N., Chandran, U. & Bandera, E. V. Obesity in cancer survival. *Annu Rev Nutr* **32**, 311-342, doi:10.1146/annurev-nutr-071811-150713 (2012).
45 Park, J., Euhus, D. M. & Scherer, P. E. Paracrine and endocrine effects of adipose tissue on cancer development and progression. *Endocr Rev* **32**, 550-570, doi:10.1210/er.2010-0030 (2011).
46 Park, J., Morley, T. S., Kim, M., Clegg, D. J. & Scherer, P. E. Obesity and cancer--mechanisms underlying tumour progression and recurrence. *Nat Rev Endocrinol* **10**, 455-465, doi:10.1038/nrendo.2014.94 (2014).
47 Zhang, Y. *et al.* Stromal progenitor cells from endogenous adipose tissue contribute to pericytes and adipocytes that populate the tumor microenvironment. *Cancer Res* **72**, 5198-5208, doi:10.1158/0008-5472.CAN-12-0294 (2012).
48 Zheng, Q. *et al.* Leptin receptor maintains cancer stem-like properties in triple negative breast cancer cells. *Endocr Relat Cancer* **20**, 797-808, doi:10.1530/ERC-13-0329 (2013).
49 Park, E. J. *et al.* Dietary and genetic obesity promote liver inflammation and tumorigenesis by enhancing IL-6 and TNF expression. *Cell* **140**, 197-208, doi:10.1016/j.cell.2009.12.052 (2010).

50 Nieman, K. M. *et al.* Adipocytes promote ovarian cancer metastasis and provide energy for rapid tumor growth. *Nat Med* **17**, 1498-1503, doi:10.1038/nm.2492 (2011).
51 Tessitore, L. *et al.* Adipocyte expression and circulating levels of leptin increase in both gynaecological and breast cancer patients. *Int J Oncol* **24**, 1529-1535 (2004).
52 Park, J. & Scherer, P. E. Adipocyte-derived endotrophin promotes malignant tumor progression. *J Clin Invest* **122**, 4243-4256, doi:10.1172/JCI63930 (2012).
53 Wolin, K. Y., Carson, K. & Colditz, G. A. Obesity and cancer. *Oncologist* **15**, 556-565, doi:10.1634/theoncologist.2009-0285 (2010).
54 Howe, L. R., Subbaramaiah, K., Hudis, C. A. & Dannenberg, A. J. Molecular pathways: adipose inflammation as a mediator of obesity-associated cancer. *Clin Cancer Res* **19**, 6074-6083, doi:10.1158/1078-0432.CCR-12-2603 (2013).
55 Renehan, A. G., Tyson, M., Egger, M., Heller, R. F. & Zwahlen, M. Body-mass index and incidence of cancer: a systematic review and meta-analysis of prospective observational studies. *Lancet* **371**, 569-578, doi:10.1016/S0140-6736(08)60269-X (2008).
56 De Pergola, G. & Silvestris, F. Obesity as a major risk factor for cancer. *J Obes* **2013**, 291546, doi:10.1155/2013/291546 (2013).
57 Treuting, P. M. & Dintzis, S. M. ***Comparative Anatomy and Histology: A Mouse and Human Atlas***. (2012).
58 Argo, C. K. & Caldwell, S. H. Epidemiology and natural history of non-alcoholic steatohepatitis. *Clin Liver Dis* **13**, 511-531, doi:10.1016/j.cld.2009.07.005 (2009).
59 Browning, J. D. *et al.* Prevalence of hepatic steatosis in an urban population in the United States: impact of ethnicity. *Hepatology* **40**, 1387-1395, doi:10.1002/hep.20466 (2004).
60 Szczepaniak, L. S. *et al.* Magnetic resonance spectroscopy to measure hepatic triglyceride content: prevalence of hepatic steatosis in the general population. *Am J Physiol Endocrinol Metab* **288**, E462-468, doi:10.1152/ajpendo.00064.2004 (2005).
61 Bedogni, G. *et al.* Prevalence of and risk factors for nonalcoholic fatty liver disease: the Dionysos nutrition and liver study. *Hepatology* **42**, 44-52, doi:10.1002/hep.20734 (2005).
62 Byrne, C. D. & Targher, G. NAFLD: a multisystem disease. *J Hepatol* **62**, S47-64, doi:10.1016/j.jhep.2014.12.012 (2015).
63 Younossi, Z. *et al.* Global burden of NAFLD and NASH: trends, predictions, risk factors and prevention. *Nat Rev Gastroenterol Hepatol* **15**, 11-20, doi:10.1038/nrgastro.2017.109 (2018).
64 Ng, M. *et al.* Global, regional, and national prevalence of overweight and obesity in children and adults during 1980-2013: a systematic analysis for the Global Burden of Disease Study 2013. *Lancet* **384**, 766-781, doi:10.1016/S0140-6736(14)60460-8 (2014).
65 Anderson, E. L. *et al.* The Prevalence of Non-Alcoholic Fatty Liver Disease in Children and Adolescents: A Systematic Review and Meta-Analysis. *PLoS One* **10**, e0140908, doi:10.1371/journal.pone.0140908 (2015).
66 Musso, G., Gambino, R. & Cassader, M. Non-alcoholic fatty liver disease from pathogenesis to management: an update. *Obes Rev* **11**, 430-445, doi:10.1111/j.1467-789X.2009.00657.x (2010).
67 Hossain, N., Kanwar, P. & Mohanty, S. R. A Comprehensive Updated Review of Pharmaceutical and Nonpharmaceutical Treatment for NAFLD. *Gastroenterol Res Pract* **2016**, 7109270, doi:10.1155/2016/7109270 (2016).
68 Edmison, J. & McCullough, A. J. Pathogenesis of non-alcoholic steatohepatitis: human data. *Clin Liver Dis* **11**, 75-104, ix, doi:10.1016/j.cld.2007.02.011 (2007).
69 Caldwell, S. H. *et al.* Cryptogenic cirrhosis: clinical characterization and risk factors for underlying disease. *Hepatology* **29**, 664-669, doi:10.1002/hep.510290347 (1999).
70 Caldwell, S. H. & Hespenheide, E. E. Subacute liver failure in obese women. *Am J Gastroenterol* **97**, 2058-2062, doi:10.1111/j.1572-0241.2002.05922.x (2002).
71 Bugianesi, E. *et al.* Expanding the natural history of nonalcoholic steatohepatitis: from cryptogenic cirrhosis to hepatocellular carcinoma. *Gastroenterology* **123**, 134-140 (2002).
72 Ong, J. *et al.* Cryptogenic cirrhosis and posttransplantation nonalcoholic fatty liver disease. *Liver Transpl* **7**, 797-801, doi:10.1053/jlts.2001.24644 (2001).
73 Younossi, Z. M. *et al.* Nonalcoholic fatty liver disease in lean individuals in the United States. *Medicine (Baltimore)* **91**, 319-327, doi:10.1097/MD.0b013e3182779d49 (2012).
74 Conus, F., Rabasa-Lhoret, R. & Péronnet, F. Characteristics of metabolically obese normal-weight (MONW) subjects. *Appl Physiol Nutr Metab* **32**, 4-12, doi:10.1139/H07-926 (2007).
75 Younossi, Z. M., Otgonsuren, M., Venkatesan, C. & Mishra, A. In patients with non-alcoholic fatty liver disease, metabolically abnormal individuals are at a higher risk for mortality while metabolically normal individuals are not. *Metabolism* **62**, 352-360, doi:10.1016/j.metabol.2012.08.005 (2013).

76 McPherson, S. *et al.* Evidence of NAFLD progression from steatosis to fibrosing-steatohepatitis using paired biopsies: implications for prognosis and clinical management. *J Hepatol* **62**, 1148-1155, doi:10.1016/j.jhep.2014.11.034 (2015).
77 Singh, S. *et al.* Fibrosis progression in nonalcoholic fatty liver vs nonalcoholic steatohepatitis: a systematic review and meta-analysis of paired-biopsy studies. *Clin Gastroenterol Hepatol* **13**, 643-654.e641-649; quiz e639-640, doi:10.1016/j.cgh.2014.04.014 (2015).
78 Angulo, P. *et al.* Liver Fibrosis, but No Other Histologic Features, Is Associated With Long-term Outcomes of Patients With Nonalcoholic Fatty Liver Disease. *Gastroenterology* **149**, 389-397.e310, doi:10.1053/j.gastro.2015.04.043 (2015).
79 Anstee, Q. M. & Day, C. P. The genetics of NAFLD. *Nat Rev Gastroenterol Hepatol* **10**, 645-655, doi:10.1038/nrgastro.2013.182 (2013).
80 Romeo, S. *et al.* Genetic variation in PNPLA3 confers susceptibility to nonalcoholic fatty liver disease. *Nat Genet* **40**, 1461-1465, doi:10.1038/ng.257 (2008).
81 Zeybel, M. *et al.* Multigenerational epigenetic adaptation of the hepatic wound-healing response. *Nat Med* **18**, 1369-1377, doi:10.1038/nm.2893 (2012).
82 Hardy, T. *et al.* Plasma DNA methylation: a potential biomarker for stratification of liver fibrosis in non-alcoholic fatty liver disease. *Gut* **66**, 1321-1328, doi:10.1136/gutjnl-2016-311526 (2017).
83 Anstee, Q. M., Reeves, H. L., Kotsiliti, E., Govaere, O. & Heikenwälder, M. From NASH to HCC: Current concepts and future challenges. *Nat Rev Gastroenterol Hepatol* a***cc. 04/19*** (2019).
84 Nonalcoholic steatohepatitis clinical research network. *Hepatology* **37**, 244, doi:10.1002/hep.510370203 (2003).
85 Kleiner, D. E. *et al.* Design and validation of a histological scoring system for nonalcoholic fatty liver disease. *Hepatology* **41**, 1313-1321, doi:10.1002/hep.20701 (2005).
86 Brown, G. T. & Kleiner, D. E. Histopathology of nonalcoholic fatty liver disease and nonalcoholic steatohepatitis. *Metabolism* **65**, 1080-1086, doi:10.1016/j.metabol.2015.11.008 (2016).
87 Reeves, H. L., Zaki, M. Y. & Day, C. P. Hepatocellular Carcinoma in Obesity, Type 2 Diabetes, and NAFLD. *Dig Dis Sci* **61**, 1234-1245, doi:10.1007/s10620-016-4085-6 (2016).
88 Wolf, M. J. *et al.* Metabolic activation of intrahepatic CD8+ T cells and NKT cells causes nonalcoholic steatohepatitis and liver cancer via cross-talk with hepatocytes. *Cancer Cell* **26**, 549-564, doi:10.1016/j.ccell.2014.09.003 (2014).
89 Rakhra, K. *et al.* CD4(+) T cells contribute to the remodeling of the microenvironment required for sustained tumor regression upon oncogene inactivation. *Cancer Cell* **18**, 485-498, doi:10.1016/j.ccr.2010.10.002 (2010).
90 Kang, T. W. *et al.* Senescence surveillance of pre-malignant hepatocytes limits liver cancer development. *Nature* **479**, 547-551, doi:10.1038/nature10599 (2011).
91 Ma, C. *et al.* NAFLD causes selective CD4(+) T lymphocyte loss and promotes hepatocarcinogenesis. *Nature* **531**, 253-257, doi:10.1038/nature16969 (2016).
92 Fu, J. *et al.* Increased regulatory T cells correlate with CD8 T-cell impairment and poor survival in hepatocellular carcinoma patients. *Gastroenterology* **132**, 2328-2339, doi:10.1053/j.gastro.2007.03.102 (2007).
93 Gao, Q. *et al.* Intratumoral balance of regulatory and cytotoxic T cells is associated with prognosis of hepatocellular carcinoma after resection. *J Clin Oncol* **25**, 2586-2593, doi:10.1200/JCO.2006.09.4565 (2007).
94 Hoechst, B. *et al.* Myeloid derived suppressor cells inhibit natural killer cells in patients with hepatocellular carcinoma via the NKp30 receptor. *Hepatology* **50**, 799-807, doi:10.1002/hep.23054 (2009).
95 Lanthier, N. Targeting Kupffer cells in non-alcoholic fatty liver disease/non-alcoholic steatohepatitis: Why and how? *World J Hepatol* **7**, 2184-2188, doi:10.4254/wjh.v7.i19.2184 (2015).
96 Reid, D. T. *et al.* Kupffer Cells Undergo Fundamental Changes during the Development of Experimental NASH and Are Critical in Initiating Liver Damage and Inflammation. *PLoS One* **11**, e0159524, doi:10.1371/journal.pone.0159524 (2016).
97 Bieghs, V. & Trautwein, C. The innate immune response during liver inflammation and metabolic disease. *Trends Immunol* **34**, 446-452, doi:10.1016/j.it.2013.04.005 (2013).
98 Kurien, B. T. & Scofield, R. H. Autoimmunity and oxidatively modified autoantigens. *Autoimmun Rev* **7**, 567-573, doi:10.1016/j.autrev.2008.04.019 (2008).
99 Nobili, V. *et al.* Oxidative stress parameters in paediatric non-alcoholic fatty liver disease. *Int J Mol Med* **26**, 471-476 (2010).

100 DeFuria, J. *et al.* B cells promote inflammation in obesity and type 2 diabetes through regulation of T-cell function and an inflammatory cytokine profile. *Proc Natl Acad Sci U S A* **110**, 5133-5138, doi:10.1073/pnas.1215840110 (2013).
101 Novobrantseva, T. I. *et al.* Attenuated liver fibrosis in the absence of B cells. *J Clin Invest* **115**, 3072-3082, doi:10.1172/JCI24798 (2005).
102 Shalapour, S. *et al.* Inflammation-induced IgA+ cells dismantle anti-liver cancer immunity. *Nature* **551**, 340-345, doi:10.1038/nature24302 (2017).
103 Moro-Sibilot, L. *et al.* Mouse and Human Liver Contain Immunoglobulin A-Secreting Cells Originating From Peyer's Patches and Directed Against Intestinal Antigens. *Gastroenterology* **151**, 311-323, doi:10.1053/j.gastro.2016.04.014 (2016).
104 Kubes, P. & Mehal, W. Z. Sterile inflammation in the liver. *Gastroenterology* **143**, 1158-1172, doi:10.1053/j.gastro.2012.09.008 (2012).
105 Davis, B. K., Wen, H. & Ting, J. P. The inflammasome NLRs in immunity, inflammation, and associated diseases. *Annu Rev Immunol* **29**, 707-735, doi:10.1146/annurev-immunol-031210-101405 (2011).
106 Arrese, M., Cabrera, D., Kalergis, A. M. & Feldstein, A. E. Innate Immunity and Inflammation in NAFLD/NASH. *Dig Dis Sci* **61**, 1294-1303, doi:10.1007/s10620-016-4049-x (2016).
107 Feldstein, A. E. Novel insights into the pathophysiology of nonalcoholic fatty liver disease. *Semin Liver Dis* **30**, 391-401, doi:10.1055/s-0030-1267539 (2010).
108 Peverill, W., Powell, L. W. & Skoien, R. Evolving concepts in the pathogenesis of NASH: beyond steatosis and inflammation. *Int J Mol Sci* **15**, 8591-8638, doi:10.3390/ijms15058591 (2014).
109 Zhang, C. Y., Yuan, W. G., He, P., Lei, J. H. & Wang, C. X. Liver fibrosis and hepatic stellate cells: Etiology, pathological hallmarks and therapeutic targets. *World J Gastroenterol* **22**, 10512-10522, doi:10.3748/wjg.v22.i48.10512 (2016).
110 Wynn, T. A. Common and unique mechanisms regulate fibrosis in various fibroproliferative diseases. *J Clin Invest* **117**, 524-529, doi:10.1172/JCI31487 (2007).
111 Pinzani, M. Pathophysiology of Liver Fibrosis. *Dig Dis* **33**, 492-497, doi:10.1159/000374096 (2015).
112 Pinzani, M., Rombouts, K. & Colagrande, S. Fibrosis in chronic liver diseases: diagnosis and management. *J Hepatol* **42 Suppl**, S22-36, doi:10.1016/j.jhep.2004.12.008 (2005).
113 Vernon, G., Baranova, A. & Younossi, Z. M. Systematic review: the epidemiology and natural history of non-alcoholic fatty liver disease and non-alcoholic steatohepatitis in adults. *Aliment Pharmacol Ther* **34**, 274-285, doi:10.1111/j.1365-2036.2011.04724.x (2011).
114 Germani, G., Hytiroglou, P., Fotiadu, A., Burroughs, A. K. & Dhillon, A. P. Assessment of fibrosis and cirrhosis in liver biopsies: an update. *Semin Liver Dis* **31**, 82-90, doi:10.1055/s-0031-1272836 (2011).
115 Clapper, J. R. *et al.* Diet-induced mouse model of fatty liver disease and nonalcoholic steatohepatitis reflecting clinical disease progression and methods of assessment. *Am J Physiol Gastrointest Liver Physiol* **305**, G483-495, doi:10.1152/ajpgi.00079.2013 (2013).
116 TOMASI, T. B. & TISDALE, W. A. SERUM GAMMA-GLOBULINS IN ACUTE AND CHRONIC LIVER DISEASES. *Nature* **201**, 834-835 (1964).
117 Husby, G. *et al.* Serum immunoglobulins and organ non-specific antibodies in diseases of the liver. *Scand J Gastroenterol* **12**, 297-304 (1977).
118 Martin, D. M., Vroon, D. H. & Nasrallah, S. M. Value of serum immunoglobulins in the diagnosis of liver disease. *Liver* **4**, 214-218 (1984).
119 Iturriaga, H., Pereda, T., Estévez, A. & Ugarte, G. Serum immunoglobulin A changes in alcoholic patients. *Ann Clin Res* **9**, 39-43 (1977).
120 van de Wiel, A., van Hattum, J., Schuurman, H. J. & Kater, L. Immunoglobulin A in the diagnosis of alcoholic liver disease. *Gastroenterology* **94**, 457-462 (1988).
121 Rodríguez-Segade, S., Camiña, M. F., Paz, J. M. & Del Río, R. Abnormal serum immunoglobulin concentrations in patients with diabetes mellitus. *Clin Chim Acta* **203**, 135-142 (1991).
122 Gonzalez-Quintela, A. *et al.* Serum levels of immunoglobulins (IgG, IgA, IgM) in a general adult population and their relationship with alcohol consumption, smoking and common metabolic abnormalities. *Clin Exp Immunol* **151**, 42-50, doi:10.1111/j.1365-2249.2007.03545.x (2008).
123 McPherson, S., Henderson, E., Burt, A. D., Day, C. P. & Anstee, Q. M. Serum immunoglobulin levels predict fibrosis in patients with non-alcoholic fatty liver disease. *J Hepatol* **60**, 1055-1062, doi:10.1016/j.jhep.2014.01.010 (2014).

124 Verma, S., Jensen, D., Hart, J. & Mohanty, S. R. Predictive value of ALT levels for non-alcoholic steatohepatitis (NASH) and advanced fibrosis in non-alcoholic fatty liver disease (NAFLD). *Liver Int* **33**, 1398-1405, doi:10.1111/liv.12226 (2013).
125 Saadeh, S. *et al.* The utility of radiological imaging in nonalcoholic fatty liver disease. *Gastroenterology* **123**, 745-750 (2002).
126 Brandl, K., Kumar, V. & Eckmann, L. Gut-liver axis at the frontier of host-microbial interactions. *Am J Physiol Gastrointest Liver Physiol* **312**, G413-G419, doi:10.1152/ajpgi.00361.2016 (2017).
127 Wiest, R., Albillos, A., Trauner, M., Bajaj, J. S. & Jalan, R. Targeting the gut-liver axis in liver disease. *J Hepatol* **67**, 1084-1103, doi:10.1016/j.jhep.2017.05.007 (2017).
128 Brun, P. *et al.* Increased intestinal permeability in obese mice: new evidence in the pathogenesis of nonalcoholic steatohepatitis. *Am J Physiol Gastrointest Liver Physiol* **292**, G518-525, doi:10.1152/ajpgi.00024.2006 (2007).
129 Erridge, C., Attina, T., Spickett, C. M. & Webb, D. J. A high-fat meal induces low-grade endotoxemia: evidence of a novel mechanism of postprandial inflammation. *Am J Clin Nutr* **86**, 1286-1292, doi:10.1093/ajcn/86.5.1286 (2007).
130 Etienne-Mesmin, L., Vijay-Kumar, M., Gewirtz, A. T. & Chassaing, B. Hepatocyte Toll-Like Receptor 5 Promotes Bacterial Clearance and Protects Mice Against High-Fat Diet-Induced Liver Disease. *Cell Mol Gastroenterol Hepatol* **2**, 584-604, doi:10.1016/j.jcmgh.2016.04.007 (2016).
131 Cani, P. D. *et al.* Metabolic endotoxemia initiates obesity and insulin resistance. *Diabetes* **56**, 1761-1772, doi:10.2337/db06-1491 (2007).
132 Laugerette, F. *et al.* Emulsified lipids increase endotoxemia: possible role in early postprandial low-grade inflammation. *J Nutr Biochem* **22**, 53-59, doi:10.1016/j.jnutbio.2009.11.011 (2011).
133 Rajilić-Stojanović, M., Smidt, H. & de Vos, W. M. Diversity of the human gastrointestinal tract microbiota revisited. *Environ Microbiol* **9**, 2125-2136, doi:10.1111/j.1462-2920.2007.01369.x (2007).
134 Zhu, B., Wang, X. & Li, L. Human gut microbiome: the second genome of human body. *Protein Cell* **1**, 718-725, doi:10.1007/s13238-010-0093-z (2010).
135 John, G. K. & Mullin, G. E. The Gut Microbiome and Obesity. *Curr Oncol Rep* **18**, 45, doi:10.1007/s11912-016-0528-7 (2016).
136 Turnbaugh, P. J. *et al.* An obesity-associated gut microbiome with increased capacity for energy harvest. *Nature* **444**, 1027-1031, doi:10.1038/nature05414 (2006).
137 Khan, M. J., Gerasimidis, K., Edwards, C. A. & Shaikh, M. G. Role of Gut Microbiota in the Aetiology of Obesity: Proposed Mechanisms and Review of the Literature. *J Obes* **2016**, 7353642, doi:10.1155/2016/7353642 (2016).
138 Turnbaugh, P. J. *et al.* A core gut microbiome in obese and lean twins. *Nature* **457**, 480-484, doi:10.1038/nature07540 (2009).
139 Schwiertz, A. *et al.* Microbiota and SCFA in lean and overweight healthy subjects. *Obesity (Silver Spring)* **18**, 190-195, doi:10.1038/oby.2009.167 (2010).
140 Collado, M. C., Isolauri, E., Laitinen, K. & Salminen, S. Distinct composition of gut microbiota during pregnancy in overweight and normal-weight women. *Am J Clin Nutr* **88**, 894-899 (2008).
141 Duncan, S. H. *et al.* Human colonic microbiota associated with diet, obesity and weight loss. *Int J Obes (Lond)* **32**, 1720-1724, doi:10.1038/ijo.2008.155 (2008).
142 Betrapally, N. S., Gillevet, P. M. & Bajaj, J. S. Gut microbiome and liver disease. *Transl Res* **179**, 49-59, doi:10.1016/j.trsl.2016.07.005 (2017).
143 Boursier, J. & Diehl, A. M. Implication of gut microbiota in nonalcoholic fatty liver disease. *PLoS Pathog* **11**, e1004559, doi:10.1371/journal.ppat.1004559 (2015).
144 Zhu, L. *et al.* Characterization of gut microbiomes in nonalcoholic steatohepatitis (NASH) patients: a connection between endogenous alcohol and NASH. *Hepatology* **57**, 601-609, doi:10.1002/hep.26093 (2013).
145 Mouzaki, M. *et al.* Bile Acids and Dysbiosis in Non-Alcoholic Fatty Liver Disease. *PLoS One* **11**, e0151829, doi:10.1371/journal.pone.0151829 (2016).
146 Llopis, M. *et al.* Intestinal microbiota contributes to individual susceptibility to alcoholic liver disease. *Gut* **65**, 830-839, doi:10.1136/gutjnl-2015-310585 (2016).
147 Okubo, H. *et al.* Involvement of resistin-like molecule β in the development of methionine-choline deficient diet-induced non-alcoholic steatohepatitis in mice. *Sci Rep* **6**, 20157, doi:10.1038/srep20157 (2016).
148 He, W. *et al.* Bacterial colonization leads to the colonic secretion of RELMbeta/FIZZ2, a novel goblet cell-specific protein. *Gastroenterology* **125**, 1388-1397 (2003).

149 Okubo, H. *et al.* Lactobacillus casei strain Shirota protects against nonalcoholic steatohepatitis development in a rodent model. *Am J Physiol Gastrointest Liver Physiol* **305**, G911-918, doi:10.1152/ajpgi.00225.2013 (2013).
150 Spencer, M. D. *et al.* Association between composition of the human gastrointestinal microbiome and development of fatty liver with choline deficiency. *Gastroenterology* **140**, 976-986, doi:10.1053/j.gastro.2010.11.049 (2011).
151 Michail, S. *et al.* Altered gut microbial energy and metabolism in children with non-alcoholic fatty liver disease. *FEMS Microbiol Ecol* **91**, 1-9, doi:10.1093/femsec/fiu002 (2015).
152 Zeisel, S. H. Dietary choline deficiency causes DNA strand breaks and alters epigenetic marks on DNA and histones. *Mutat Res* **733**, 34-38, doi:10.1016/j.mrfmmm.2011.10.008 (2012).
153 Hill, C. *et al.* Expert consensus document. The International Scientific Association for Probiotics and Prebiotics consensus statement on the scope and appropriate use of the term probiotic. *Nat Rev Gastroenterol Hepatol* **11**, 506-514, doi:10.1038/nrgastro.2014.66 (2014).
154 Million, M. & Raoult, D. The role of the manipulation of the gut microbiota in obesity. *Curr Infect Dis Rep* **15**, 25-30, doi:10.1007/s11908-012-0301-5 (2013).
155 Million, M. *et al.* Obesity-associated gut microbiota is enriched in Lactobacillus reuteri and depleted in Bifidobacterium animalis and Methanobrevibacter smithii. *Int J Obes (Lond)* **36**, 817-825, doi:10.1038/ijo.2011.153 (2012).
156 Million, M. *et al.* Comparative meta-analysis of the effect of Lactobacillus species on weight gain in humans and animals. *Microb Pathog* **53**, 100-108, doi:10.1016/j.micpath.2012.05.007 (2012).
157 Hwang, I. *et al.* Alteration of gut microbiota by vancomycin and bacitracin improves insulin resistance via glucagon-like peptide 1 in diet-induced obesity. *FASEB J* **29**, 2397-2411, doi:10.1096/fj.14-265983 (2015).
158 Parekh, P. J., Balart, L. A. & Johnson, D. A. The Influence of the Gut Microbiome on Obesity, Metabolic Syndrome and Gastrointestinal Disease. *Clin Transl Gastroenterol* **6**, e91, doi:10.1038/ctg.2015.16 (2015).
159 Cho, I. *et al.* Antibiotics in early life alter the murine colonic microbiome and adiposity. *Nature* **488**, 621-626, doi:10.1038/nature11400 (2012).
160 Cox, L. M. *et al.* Altering the intestinal microbiota during a critical developmental window has lasting metabolic consequences. *Cell* **158**, 705-721, doi:10.1016/j.cell.2014.05.052 (2014).
161 Pieper, K., Grimbacher, B. & Eibel, H. B-cell biology and development. *J Allergy Clin Immunol* **131**, 959-971, doi:10.1016/j.jaci.2013.01.046 (2013).
162 Nutt, S. L., Hodgkin, P. D., Tarlinton, D. M. & Corcoran, L. M. The generation of antibody-secreting plasma cells. *Nat Rev Immunol* **15**, 160-171, doi:10.1038/nri3795 (2015).
163 Fairfax, K. A., Kallies, A., Nutt, S. L. & Tarlinton, D. M. Plasma cell development: from B-cell subsets to long-term survival niches. *Semin Immunol* **20**, 49-58, doi:10.1016/j.smim.2007.12.002 (2008).
164 Jung, D., Giallourakis, C., Mostoslavsky, R. & Alt, F. W. Mechanism and control of V(D)J recombination at the immunoglobulin heavy chain locus. *Annu Rev Immunol* **24**, 541-570, doi:10.1146/annurev.immunol.23.021704.115830 (2006).
165 Schroeder, H. W. & Cavacini, L. Structure and function of immunoglobulins. *J Allergy Clin Immunol* **125**, S41-52, doi:10.1016/j.jaci.2009.09.046 (2010).
166 Early, P., Huang, H., Davis, M., Calame, K. & Hood, L. An immunoglobulin heavy chain variable region gene is generated from three segments of DNA: VH, D and JH. *Cell* **19**, 981-992 (1980).
167 Retter, I. *et al.* Sequence and characterization of the Ig heavy chain constant and partial variable region of the mouse strain 129S1. *J Immunol* **179**, 2419-2427 (2007).
168 Honjo, T., Reth, M., Radbruch, A. & Alt, F. *Molecular Biology of B cells, 2nd edition*. (2015).
169 Aoki-Ota, M., Torkamani, A., Ota, T., Schork, N. & Nemazee, D. Skewed primary Igκ repertoire and V-J joining in C57BL/6 mice: implications for recombination accessibility and receptor editing. *J Immunol* **188**, 2305-2315, doi:10.4049/jimmunol.1103484 (2012).
170 Eisen, H. N. & Reilly, E. B. Lambda chains and genes in inbred mice. *Annu Rev Immunol* **3**, 337-365, doi:10.1146/annurev.iy.03.040185.002005 (1985).
171 Panda, S. & Ding, J. L. Natural antibodies bridge innate and adaptive immunity. *J Immunol* **194**, 13-20, doi:10.4049/jimmunol.1400844 (2015).
172 McHeyzer-Williams, L. J. & McHeyzer-Williams, M. G. Antigen-specific memory B cell development. *Annu Rev Immunol* **23**, 487-513, doi:10.1146/annurev.immunol.23.021704.115732 (2005).
173 Adler, L. N. *et al.* The Other Function: Class II-Restricted Antigen Presentation by B Cells. *Front Immunol* **8**, 319, doi:10.3389/fimmu.2017.00319 (2017).

174 Reth, M. Antigen receptors on B lymphocytes. *Annu Rev Immunol* **10**, 97-121, doi:10.1146/annurev.iy.10.040192.000525 (1992).
175 Dal Porto, J. M. *et al.* B cell antigen receptor signaling 101. *Mol Immunol* **41**, 599-613, doi:10.1016/j.molimm.2004.04.008 (2004).
176 Blum, J. S., Wearsch, P. A. & Cresswell, P. Pathways of antigen processing. *Annu Rev Immunol* **31**, 443-473, doi:10.1146/annurev-immunol-032712-095910 (2013).
177 van Kasteren, S. I. & Overkleeft, H. S. Endo-lysosomal proteases in antigen presentation. *Curr Opin Chem Biol* **23**, 8-15, doi:10.1016/j.cbpa.2014.08.011 (2014).
178 Rolink, A. G. *et al.* Mutations affecting either generation or survival of cells influence the pool size of mature B cells. *Immunity* **10**, 619-628 (1999).
179 Chen, X. & Jensen, P. E. MHC class II antigen presentation and immunological abnormalities due to deficiency of MHC class II and its associated genes. *Exp Mol Pathol* **85**, 40-44, doi:10.1016/j.yexmp.2008.03.011 (2008).
180 Shimoda, M., Li, T., Pihkala, J. P. & Koni, P. A. Role of MHC class II on memory B cells in post-germinal center B cell homeostasis and memory response. *J Immunol* **176**, 2122-2133 (2006).
181 Janeway, C. A., Travers, P., Walport, M. & Shlomchik, M. *Immunobiology: The immune System in Health and Disease, 5th edition*. (2001).
182 Tarlinton, D. B-cell memory: are subsets necessary? *Nat Rev Immunol* **6**, 785-790, doi:10.1038/nri1938 (2006).
183 Cerutti, A. The regulation of IgA class switching. *Nat Rev Immunol* **8**, 421-434, doi:10.1038/nri2322 (2008).
184 Spencer, J. & Sollid, L. M. The human intestinal B-cell response. *Mucosal Immunol* **9**, 1113-1124, doi:10.1038/mi.2016.59 (2016).
185 Honda, K. & Littman, D. R. The microbiota in adaptive immune homeostasis and disease. *Nature* **535**, 75-84, doi:10.1038/nature18848 (2016).
186 Macpherson, A. J., Yilmaz, B., Limenitakis, J. P. & Ganal-Vonarburg, S. C. IgA Function in Relation to the Intestinal Microbiota. *Annu Rev Immunol* **36**, 359-381, doi:10.1146/annurev-immunol-042617-053238 (2018).
187 Bunker, J. J. & Bendelac, A. IgA Responses to Microbiota. *Immunity* **49**, 211-224, doi:10.1016/j.immuni.2018.08.011 (2018).
188 Macpherson, A. J. *et al.* A primitive T cell-independent mechanism of intestinal mucosal IgA responses to commensal bacteria. *Science* **288**, 2222-2226 (2000).
189 Takahashi, Y. & Fukusato, T. Histopathology of nonalcoholic fatty liver disease/nonalcoholic steatohepatitis. *World J Gastroenterol* **20**, 15539-15548, doi:10.3748/wjg.v20.i42.15539 (2014).
190 Chen, J. *et al.* Immunoglobulin gene rearrangement in B cell deficient mice generated by targeted deletion of the JH locus. *Int Immunol* **5**, 647-656 (1993).
191 Macpherson, A. J. *et al.* IgA production without mu or delta chain expression in developing B cells. *Nat Immunol* **2**, 625-631, doi:10.1038/89775 (2001).
192 Muramatsu, M. *et al.* Class switch recombination and hypermutation require activation-induced cytidine deaminase (AID), a potential RNA editing enzyme. *Cell* **102**, 553-563 (2000).
193 Wei, M. *et al.* Mice carrying a knock-in mutation of Aicda resulting in a defect in somatic hypermutation have impaired gut homeostasis and compromised mucosal defense. *Nat Immunol* **12**, 264-270, doi:10.1038/ni.1991 (2011).
194 Waisman, A. *et al.* IgG1 B cell receptor signaling is inhibited by CD22 and promotes the development of B cells whose survival is less dependent on Ig alpha/beta. *J Exp Med* **204**, 747-758, doi:10.1084/jem.20062024 (2007).
195 Randall, T. D., Carragher, D. M. & Rangel-Moreno, J. Development of secondary lymphoid organs. *Annu Rev Immunol* **26**, 627-650, doi:10.1146/annurev.immunol.26.021607.090257 (2008).
196 Bergqvist, P., Gärdby, E., Stensson, A., Bemark, M. & Lycke, N. Y. Gut IgA class switch recombination in the absence of CD40 does not occur in the lamina propria and is independent of germinal centers. *J Immunol* **177**, 7772-7783 (2006).
197 Fagarasan, S., Kinoshita, K., Muramatsu, M., Ikuta, K. & Honjo, T. In situ class switching and differentiation to IgA-producing cells in the gut lamina propria. *Nature* **413**, 639-643, doi:10.1038/35098100 (2001).
198 Kang, H. S. *et al.* Signaling via LTbetaR on the lamina propria stromal cells of the gut is required for IgA production. *Nat Immunol* **3**, 576-582, doi:10.1038/ni795 (2002).
199 Newberry, R. D., McDonough, J. S., McDonald, K. G. & Lorenz, R. G. Postgestational lymphotoxin/lymphotoxin beta receptor interactions are essential for the presence of intestinal B lymphocytes. *J Immunol* **168**, 4988-4997 (2002).

200 Elgueta, R. *et al.* Molecular mechanism and function of CD40/CD40L engagement in the immune system. *Immunol Rev* **229**, 152-172, doi:10.1111/j.1600-065X.2009.00782.x (2009).
201 Stephenson, K. *et al.* Updates on Dietary Models of Nonalcoholic Fatty Liver Disease: Current Studies and Insights. *Gene Expr* **18**, 5-17, doi:10.3727/105221617X15093707969658 (2018).
202 Warr, G. W., Magor, K. E. & Higgins, D. A. IgY: clues to the origins of modern antibodies. *Immunol Today* **16**, 392-398, doi:10.1016/0167-5699(95)80008-5 (1995).
203 Kroese, F. G. *et al.* Many of the IgA producing plasma cells in murine gut are derived from self-replenishing precursors in the peritoneal cavity. *Int Immunol* **1**, 75-84 (1989).
204 Bos, N. A. *et al.* Monoclonal immunoglobulin A derived from peritoneal B cells is encoded by both germ line and somatically mutated VH genes and is reactive with commensal bacteria. *Infect Immun* **64**, 616-623 (1996).
205 Pinto, D. *et al.* A functional BCR in human IgA and IgM plasma cells. *Blood* **121**, 4110-4114, doi:10.1182/blood-2012-09-459289 (2013).
206 Winer, D. A. *et al.* B cells promote insulin resistance through modulation of T cells and production of pathogenic IgG antibodies. *Nat Med* **17**, 610-617, doi:10.1038/nm.2353 (2011).
207 Duffaut, C., Galitzky, J., Lafontan, M. & Bouloumié, A. Unexpected trafficking of immune cells within the adipose tissue during the onset of obesity. *Biochem Biophys Res Commun* **384**, 482-485, doi:10.1016/j.bbrc.2009.05.002 (2009).
208 Palming, J. *et al.* Plasma cells and Fc receptors in human adipose tissue--lipogenic and anti-inflammatory effects of immunoglobulins on adipocytes. *Biochem Biophys Res Commun* **343**, 43-48, doi:10.1016/j.bbrc.2006.02.114 (2006).
209 McDonnell, M. E. *et al.* B lymphocytes in human subcutaneous adipose crown-like structures. *Obesity (Silver Spring)* **20**, 1372-1378, doi:10.1038/oby.2012.54 (2012).
210 Ley, R. E., Turnbaugh, P. J., Klein, S. & Gordon, J. I. Microbial ecology: human gut microbes associated with obesity. *Nature* **444**, 1022-1023, doi:10.1038/4441022a (2006).
211 Indiani, C. M. D. S. *et al.* Childhood Obesity and Firmicutes/Bacteroidetes Ratio in the Gut Microbiota: A Systematic Review. *Child Obes* **14**, 501-509, doi:10.1089/chi.2018.0040 (2018).
212 Savcheniuk, O. *et al.* Short-term periodic consumption of multiprobiotic from childhood improves insulin sensitivity, prevents development of non-alcoholic fatty liver disease and adiposity in adult rats with glutamate-induced obesity. *BMC Complement Altern Med* **14**, 247, doi:10.1186/1472-6882-14-247 (2014).
213 Kobyliak, N. *et al.* Comparative experimental investigation on the efficacy of mono- and multiprobiotic strains in non-alcoholic fatty liver disease prevention. *BMC Gastroenterol* **16**, 34, doi:10.1186/s12876-016-0451-2 (2016).
214 Kobyliak, N. *et al.* A Multi-strain Probiotic Reduces the Fatty Liver Index, Cytokines and Aminotransferase levels in NAFLD Patients: Evidence from a Randomized Clinical Trial. *J Gastrointestin Liver Dis* **27**, 41-49, doi:10.15403/jgld.2014.1121.271.kby (2018).
215 Bäckhed, F. *et al.* The gut microbiota as an environmental factor that regulates fat storage. *Proc Natl Acad Sci U S A* **101**, 15718-15723, doi:10.1073/pnas.0407076101 (2004).
216 Bäckhed, F., Manchester, J. K., Semenkovich, C. F. & Gordon, J. I. Mechanisms underlying the resistance to diet-induced obesity in germ-free mice. *Proc Natl Acad Sci U S A* **104**, 979-984, doi:10.1073/pnas.0605374104 (2007).
217 Rabot, S. *et al.* Germ-free C57BL/6J mice are resistant to high-fat-diet-induced insulin resistance and have altered cholesterol metabolism. *FASEB J* **24**, 4948-4959, doi:10.1096/fj.10-164921 (2010).
218 Bindels, L. B. *et al.* Resistant starch can improve insulin sensitivity independently of the gut microbiota. *Microbiome* **5**, 12, doi:10.1186/s40168-017-0230-5 (2017).
219 Llorente, C. & Schnabl, B. The gut microbiota and liver disease. *Cell Mol Gastroenterol Hepatol* **1**, 275-284, doi:10.1016/j.jcmgh.2015.04.003 (2015).
220 Hooper, L. V., Littman, D. R. & Macpherson, A. J. Interactions between the microbiota and the immune system. *Science* **336**, 1268-1273, doi:10.1126/science.1223490 (2012).
221 Teixeira, T. F. *et al.* Intestinal permeability parameters in obese patients are correlated with metabolic syndrome risk factors. *Clin Nutr* **31**, 735-740, doi:10.1016/j.clnu.2012.02.009 (2012).
222 Miele, L. *et al.* Increased intestinal permeability and tight junction alterations in nonalcoholic fatty liver disease. *Hepatology* **49**, 1877-1887, doi:10.1002/hep.22848 (2009).
223 Hayes, C. L. *et al.* Commensal microbiota induces colonic barrier structure and functions that contribute to homeostasis. *Sci Rep* **8**, 14184, doi:10.1038/s41598-018-32366-6 (2018).
224 Ukena, S. N. *et al.* Probiotic Escherichia coli Nissle 1917 inhibits leaky gut by enhancing mucosal integrity. *PLoS One* **2**, e1308, doi:10.1371/journal.pone.0001308 (2007).

225 Rooks, M. G. & Garrett, W. S. Gut microbiota, metabolites and host immunity. *Nat Rev Immunol* **16**, 341-352, doi:10.1038/nri.2016.42 (2016).
226 Deplancke, B. & Gaskins, H. R. Microbial modulation of innate defense: goblet cells and the intestinal mucus layer. *Am J Clin Nutr* **73**, 1131S-1141S, doi:10.1093/ajcn/73.6.1131S (2001).
227 Smith, K., McCoy, K. D. & Macpherson, A. J. Use of axenic animals in studying the adaptation of mammals to their commensal intestinal microbiota. *Semin Immunol* **19**, 59-69, doi:10.1016/j.smim.2006.10.002 (2007).
228 Pabst, O. New concepts in the generation and functions of IgA. *Nat Rev Immunol* **12**, 821-832, doi:10.1038/nri3322 (2012).
229 Mazmanian, S. K., Liu, C. H., Tzianabos, A. O. & Kasper, D. L. An immunomodulatory molecule of symbiotic bacteria directs maturation of the host immune system. *Cell* **122**, 107-118, doi:10.1016/j.cell.2005.05.007 (2005).
230 Ivanov, I. I. *et al.* Specific microbiota direct the differentiation of IL-17-producing T-helper cells in the mucosa of the small intestine. *Cell Host Microbe* **4**, 337-349, doi:10.1016/j.chom.2008.09.009 (2008).
231 Strauch, U. G. *et al.* Influence of intestinal bacteria on induction of regulatory T cells: lessons from a transfer model of colitis. *Gut* **54**, 1546-1552, doi:10.1136/gut.2004.059451 (2005).
232 Liu, Y. J., Oldfield, S. & MacLennan, I. C. Memory B cells in T cell-dependent antibody responses colonize the splenic marginal zones. *Eur J Immunol* **18**, 355-362, doi:10.1002/eji.1830180306 (1988).
233 Jacob, J., Kassir, R. & Kelsoe, G. In situ studies of the primary immune response to (4-hydroxy-3-nitrophenyl)acetyl. I. The architecture and dynamics of responding cell populations. *J Exp Med* **173**, 1165-1175 (1991).
234 Blink, E. J. *et al.* Early appearance of germinal center-derived memory B cells and plasma cells in blood after primary immunization. *J Exp Med* **201**, 545-554, doi:10.1084/jem.20042060 (2005).
235 Ochsenbein, A. F. *et al.* Protective long-term antibody memory by antigen-driven and T help-dependent differentiation of long-lived memory B cells to short-lived plasma cells independent of secondary lymphoid organs. *Proc Natl Acad Sci U S A* **97**, 13263-13268, doi:10.1073/pnas.230417497 (2000).
236 Tripathi, A. *et al.* The gut-liver axis and the intersection with the microbiome. *Nat Rev Gastroenterol Hepatol* **15**, 397-411, doi:10.1038/s41575-018-0011-z (2018).

9. Acknowledgments

I would like to thank my supervisor Prof. Dr. Heikenwälder Mathias for trusting me with this very ambitious and demanding project. During my PhD studies I have grown as a person and as a scientist and a lot of this development I owe it my supervisor who gave me the freedom to develop and to carve my own path. Thank you Mathias because through your guidance I became more confident and much more competitive.

I want to thank my colleague and friend for life, Valentina Leone. You were a strong presence of support in every step I took. Thank you for our scientific discussions, thank you for your help on the bench, and most importantly thank you for being a friend through the good and the bad. Thank you for our laughs, our jokes, and for all the beautiful memories.

Special thanks to Dr. Tracy O' Connor. Tracy, thank you for taking me under your wings; there was not a single moment that I've asked for your help and you weren't there for me. Thank you for helping me obtain clarity in my scientific thinking and thank you for your kindness and your sense of humor that made things shine under a different light.

Thank you, Dominik Pfister and Paul Becker for our scientific discussions and for creating such a pleasant working atmosphere. Especially you Dominik that we have spent long hours on the bench, working together, tolerating each other and making fun of each other.

I would to thank all the members of our lab, past and present, for their team spirit and strong technical and scientific support.

I would like to thank my best friends Maria and Michalis for taking care of me at my most emotional moments during these years. Thank you for always reminding me who I am and where I am coming from.

Finally, I would like to thank my family: my father, Savvas, who taught me to always stand up regardless what life throws at you; my sister, Evie, who taught me to never give up, and for her constant and unconditional love, and my husband, Antonios, for being my rock, my home and my everything. Αντώνη μου, you are the best human I know and without you I would have been lost.